Influence of Protein Aggregation and Macromolecular Crowding on the Dynamics and Function of Proteins Respectively

A Thesis Submitted
in Partial Fulfillment of the
Requirements for the Degree of

Doctor of Philosophy

By

Lopamudra Homchaudhuri

Department of Chemistry
Indian Institute of Technology Guwahati
Guwahati -78109, Assam, India

December 2005

INDIAN INSTITUTE OF TECHNOLOGY, GUWAHATI

Department of Chemistry

STATEMENT

I hereby declare that the matter embodied in this thesis is the result of investigations carried out by me in the Department of Chemistry, Indian Institute of Technology Guwahati, India under the supervision of Dr. R. Swaminathan.

In keeping with the general practice of reporting observations, due acknowledgements have been made wherever the work described is based on the findings of other investigators.

I.I.T. Guwahati,
December 2005

Lopamudra Homchaudhuri

TH-265_004703

INDIAN INSTITUTE OF TECHNOLOGY, GUWAHATI

Department of Chemistry

CERTIFICATE

This is to certify that the work contained in the thesis entitled "Influence of Protein Aggregation and Macromolecular Crowding on the Dynamics and Function of Proteins Respectively" by Ms. Lopamudra Homchaudhuri, a student of the Department of Chemistry, Indian Institute of Technology, Guwahati, for the award of the degree of Doctor of Philosophy, has been carried out under my guidance and that this work has not been submitted elsewhere for a degree.

I. I. T. Guwahati,
December 2005

Dr. R. Swaminathan,
Associate Professor,
Department of Biotechnology,
IIT Guwahati

TH-265_004703

INDIAN INSTITUTE OF TECHNOLOGY, GUWAHATI

Department of Chemistry

COURSE CERTIFICATE

This is to certify that Ms. Lopamudra Homchaudhuri has satisfactorily completed all the courses required for the Ph. D. degree programme.

The courses include:

CH 630	A Fundamental Approach to Physical Chemistry
CH 621	Newer Reagents in Organic Synthesis
CH 611	Bio-inorganic Chemistry
CH 631	Experimental Spectroscopy

Ms. Lopamudra Homchaudhuri has successfully completed her Ph. D qualifying examination in February 2001.

Professor Jubaraj B. Baruah
Head
Department of Chemistry
I. I. T. Guwahati

Dr. Anil Kumar Saikia
Secretary
Departmental Post Graduate Program Committee
Department of Chemistry
I. I. T. Guwahati

TH-265_004703

ACKNOWLEDGEMENT

At the very outset I wish to express my sincerest gratitude to my supervisor for his untiring and ceaseless guidance throughout my Ph. D. program. I have learnt whatever I have in this period solely through the way he guided me. Whenever I had problems he was always available to hear me through and advise me and encourage me. I am indeed very grateful to him.

As I look back and recall all the experiences I have had in the last five years here as a Ph. D. student, I feel I couldn't have had a better time in a million years. There were difficult times no doubt, indeed, life is fraught with difficulties. However, once they are over one realizes how much one has learnt from them.

I would next like to express my most heartfelt gratitude to my parents and brother for perpetually encouraging me. They have been perfect bricks right through!

I also wish to thank Prof. J. B. Baruah, Head of the Department of Chemistry for enabling me to carry on my work in the department smoothly.

Finally, I thank all my colleagues and friends and all the members of the department of chemistry for their support.

TH-265_004703

ABSTRACT

The phenomenon of macromolecular crowding is ubiquitous in cells. It is reported to affect equilibria and kinetics of processes taking place in cells and is also hypothesized to affect enzyme catalyzed reactions. A part of this doctoral work was directed towards ascertaining the effect of crowding on an enzyme catalyzed reaction in an environment crowded with synthetic crowding agents viz., dextran (15-500 kDa) and Ficoll (70 and 400 kDa). The hydrolysis of p-nitrophenyl phosphate by alkaline phosphatase was used as the model reaction for the purpose.

We observed that macromolecular crowding affects the catalytic rate of hydrolysis of p-nitro phenyl phosphate in a size dependent manner. In the presence of increasing concentrations of 15-70 kDa dextrans, the rates were observed to be partly transition rate limited and partly diffusion controlled. However, in the presence of the larger dextrans, viz., 200 and 500 kDa dextrans, the rates appeared to be limited by the encounter rate of substrate with enzyme. Ficolls were observed to affect the rates to a lesser extent compared to the dextrans. In the presence of 20 % w/w 40, 200 and 500 kDa dextrans, the profile of initial rate vs. substrate concentration appeared to deviate from the hyperbolic curve observed in their absence. Thus, the validity of Michaelis-Menten kinetics in crowded media needs to be examined.

The remaining part of the thesis was devoted to the study of protein aggregation. Insoluble protein aggregates are associated with neurodegenerative diseases like Alzheimer's and Prion diseases. A couple of findings in the last few years indicate that soluble aggregates are more harmful than the insoluble deposits. It is thus important to detect these soluble aggregates. Moreover, it is reported that the insoluble aggregates actually arise from soluble precursors, viz., these soluble aggregates. The remainder of the thesis is thus dedicated to explore methods to track the formation and growth of these soluble aggregates.

There are two sections here. In the first section is reported the observations of novel absorbance and luminescence features of L-lysine.HCl in aqueous solution. These features could not be accounted for by any chromophore present in the lysine molecule and so based on experiments with pyrene we concluded that intermolecular interactions

TH-265_004703

among lysine molecules give rise to the absorbance and luminescence features. Absorbance features were also observed by us in proteins rich in lysine residues and in poly-L-lysine.HBr at concentrations much lower than that at which they were observed in aqueous solutions of L-lysine.HCl. These observations led us to conclude that the lysine-lysine interactions take place intramolecularly among proximal lysine residues in the proteins and in poly-L-lysine. These interactions among the proximal lysine residues were then used to monitor unfolding and aggregation of histone, which is a protein that abounds in lysine residues.

In the second section, fluorescence anisotropy was used to track the formation of soluble aggregates of dansyl-labeled lysozyme at the alkaline pH of 12.2. Lysozyme was observed to have a propensity to aggregate at the alkaline pH of 12.2. Both steady-state and time-resolved fluorescence anisotropies were used to track the growth of aggregates. Time-resolved anisotropy decay analysis yielded a slow correlation time in the range 39-44 ns that can arise from a molecular aggregate consisting of ten or more lysozyme monomers. The growth of aggregates took place rather slowly and could be arrested on addition of 0.9 M L-Arginine.HCl. The aggregation was reversible at the initial stages (~60 minutes) but irreversible beyond this period. Moreover, the aggregates once formed were rather stable. Overnight incubation of day old aggregates (formed at pH 12.2) in 6 M guanidine chloride at room temperature had no effect on the steady-state anisotropy of the aggregates.

In this thesis, we have looked into two phenomena that are not unrelated, viz., macromolecular crowding and protein aggregation. We have examined the effect of macromolecular crowding on the kinetics of enzyme catalyzed reactions and measured the growth of soluble aggregates of proteins. Our investigations have led to the following observations:

1. The effect of macromolecular crowding on the kinetics of enzyme catalyzed reactions is dependent on the size and nature of the crowding agents.
2. The initial rates of enzyme catalyzed reactions appeared to deviate from typical Michaelis-Menten behavior

TH-265_004703

3. We discovered novel absorbance features of L-lysine and were able to track the unfolding and aggregation of the protein histone using the afore-mentioned features.
4. Using fluorescence anisotropy we were able to track the slow growth of soluble aggregates of lysozyme at the alkaline pH 12.2.

TH-265_004703

Table of Contents

TH-265_004703

TH-265_004703

TH-265_004703

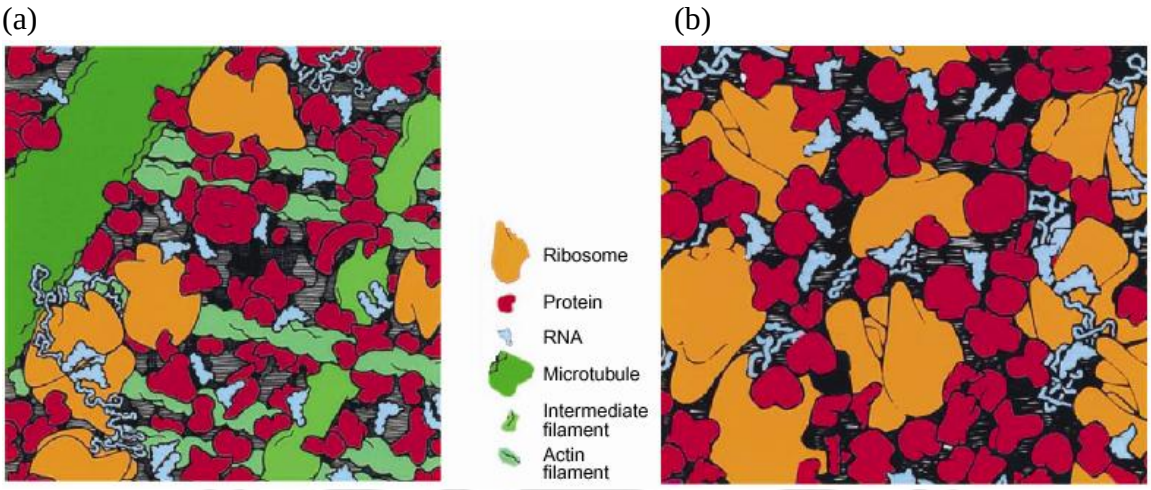

Figure 1.1 The crowded state of the cytoplasm in (a) eukaryotic and (b) E. coli cells. Each square illustrates the face of a cube with an edge 100 nm in length. The sizes, shapes and numbers of macromolecules are approximately correct. Small molecules are not shown. (Adapted from Ellis, R. J., Curr. Opin. Structr. Biol. 2001, 11:114-119)

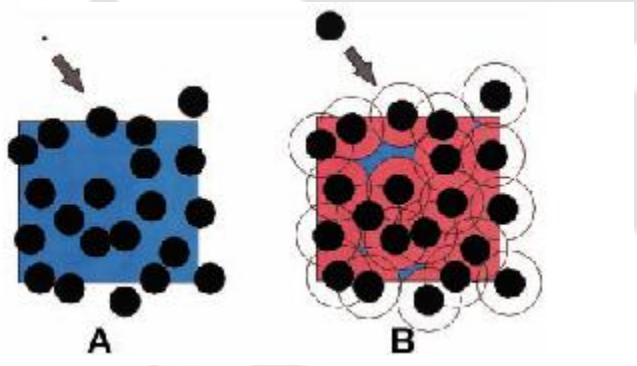

Figure 1.2 The importance of size in volume exclusion. The squares in the figure have 30% of their volumes occupied by spherical macromolecules.(A) almost all of the of the free volume is available to the centre of an infinitesimally small probe (B) almost no volume is available to the centre of a molecule whose size is comparable to that of the background molecule. (Adapted from Minton, A. P., J. Biol. Chem. 2001, 276: 10577-10580)

TH-265_004703

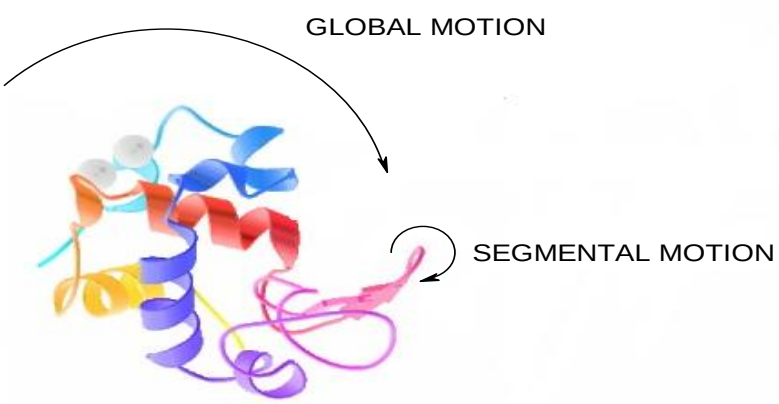

Figure 2.3 The figure above depicts global and segmental motion.

TH-265_004703

Figure 3.3.1 A PDB structure of hen egg white lysozyme (PDB: 2LYZ) is shown below. The residues that are represented by the ball and stick model indicate the 6 lysine residues present in lysozyme.

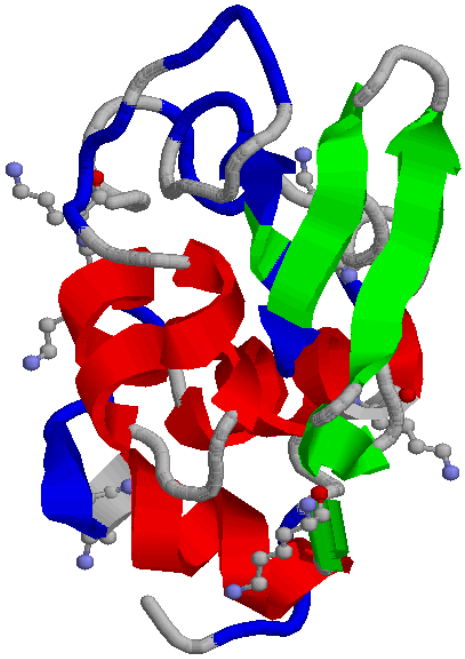

Indian Institute of Technology Guwahati

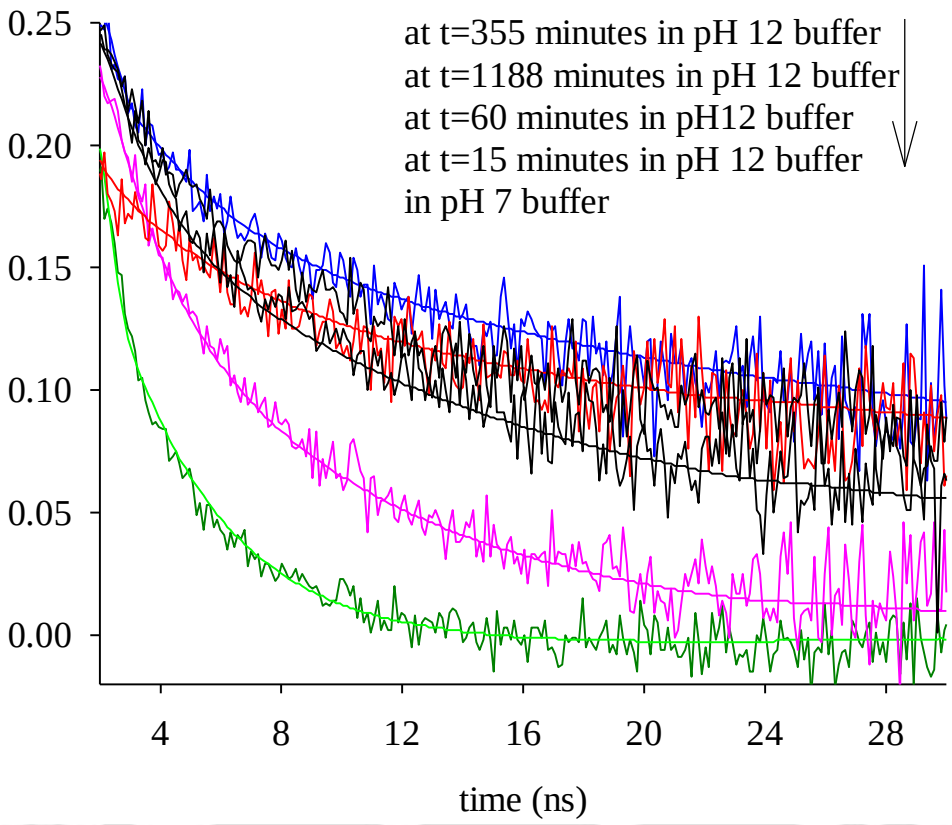

Figure 6.4 Overlay of anisotropy decay profiles of 40 μM lysozyme in pH 7 buffer (in green) and in pH 12 buffers respectively. The profiles in pH12 buffer show a gradually increasing residual anisotropy at t=30 s with increasing time as indicated in the figure.

TH-265_004703

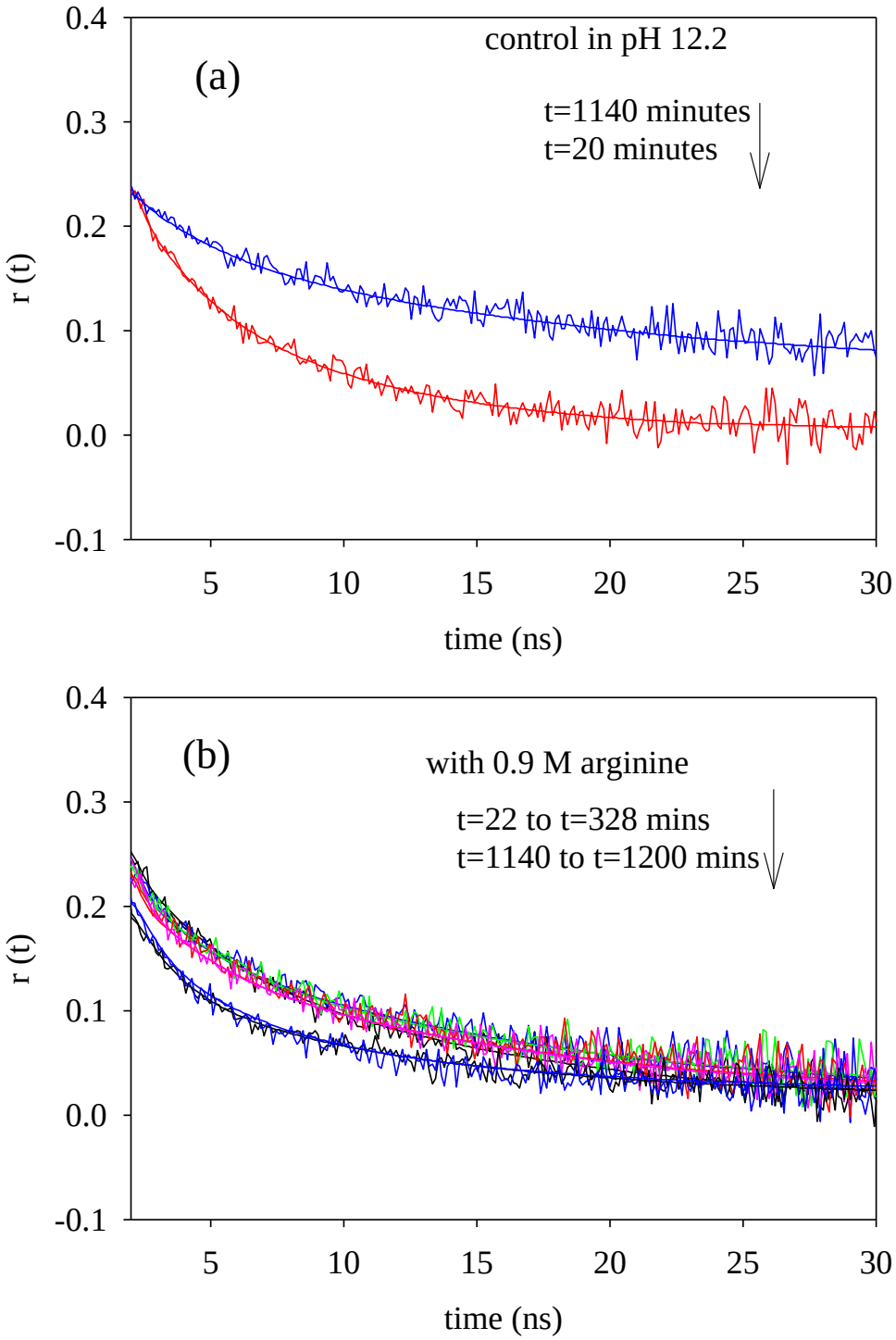

Figure 6.5 Anisotropy decay profiles in pH 12.2 buffer in (a) the absence of 0.9 M L-Arg HCl and (b)0.9 M L-Arg. HCl . The decay profiles were collected with increasing time.

The figures obtained in the process of analyzing the anisotropy decays are given below.

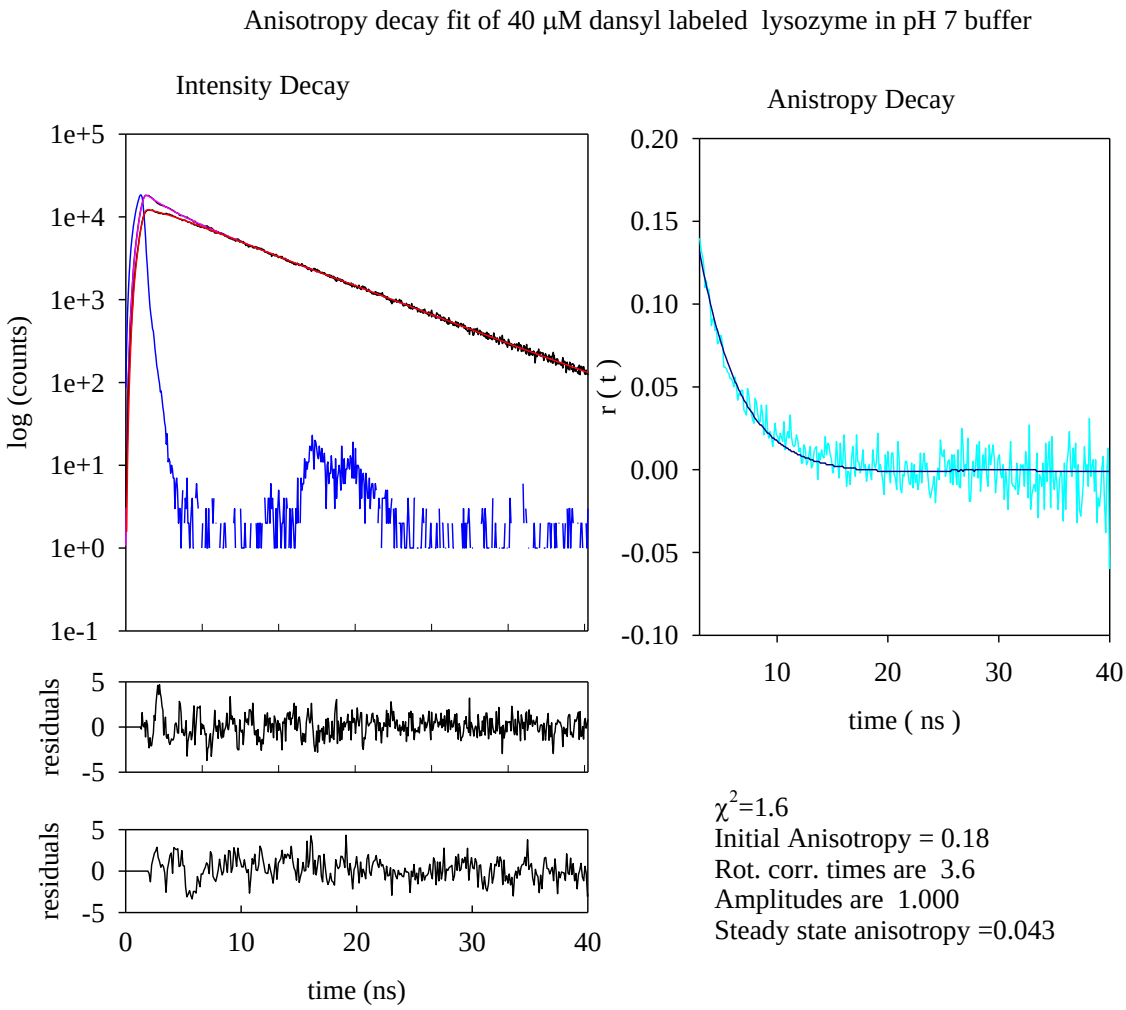

Figure 6.8 The plots shown above correspond to (i) IRF (blue); (ii) measured I_{par} (black); (iii) fitted I_{par} (pink); (iv) measured I_{per} (black); (v) fitted I_{per} (red) . The corresponding residuals are depicted in black below the intensity decay plots.
The measured anisotropy decay is shown in cyan and the fitted anisotropy decay is depicted by the dark blue curve

Anisotropy decay fit of 40 μM dansyl labeled lysozyme at t= 15 minutes in pH 12.2 buffer

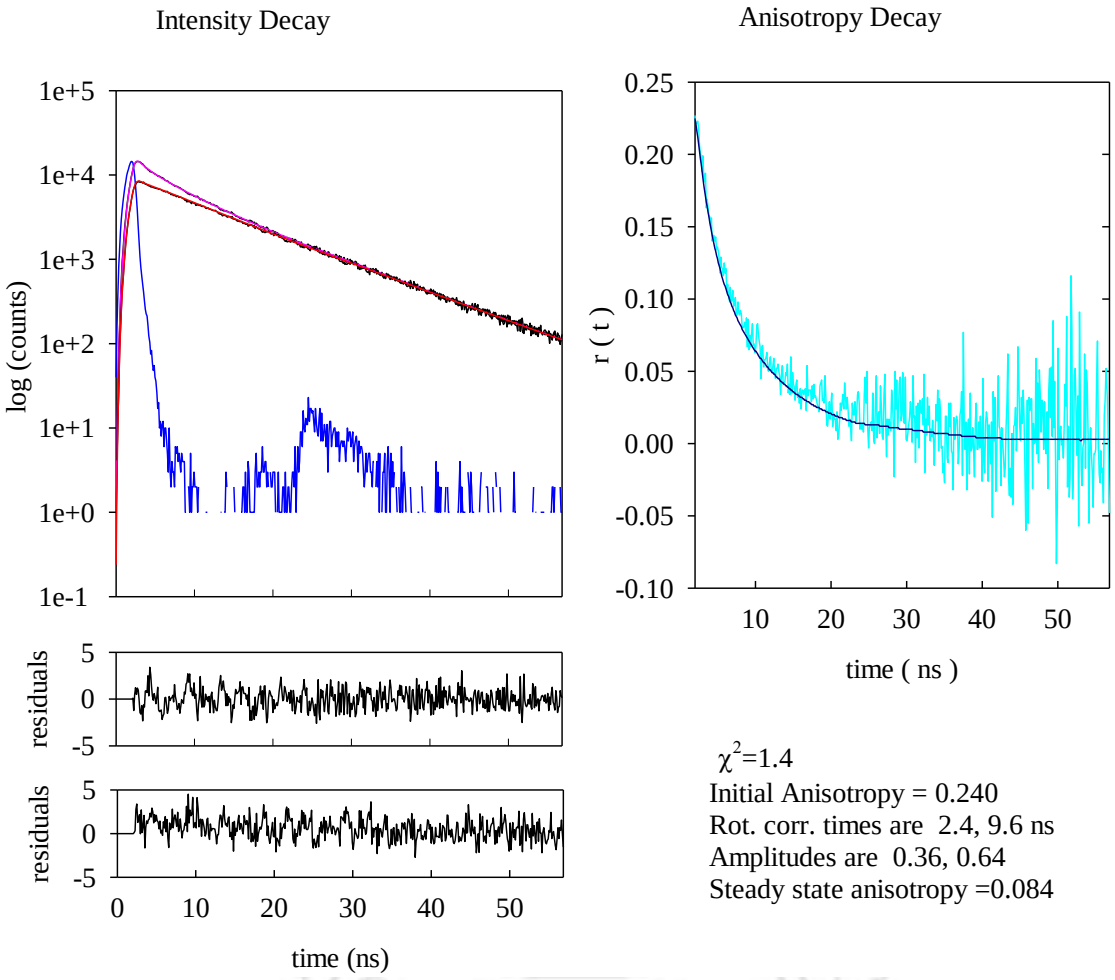

Figure 6.9: The curves are the same as in figure 6.8. The residuals are shown in black.

Anisotropy decay of 40 μM dansyl labeled lysozyme in pH 12.2 buffer at t = 60 minutes

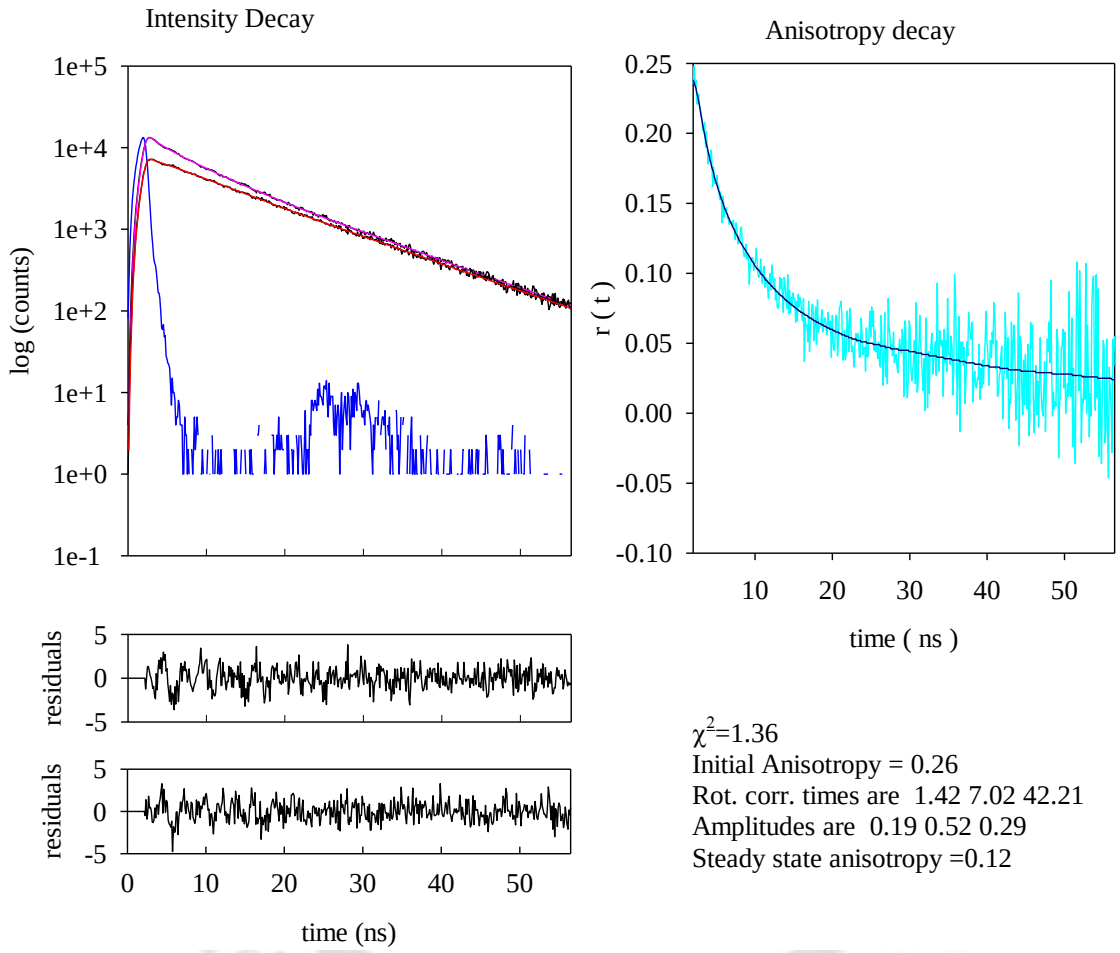

Figure 6.10: Anisotropy Decay Analysis profiles. The curves depicted above are the same as in the previous figures

TH-265_004703

Anisotropy decay fit of 40 μM lysozyme in pH 12.2 buffer at t=355 minutes

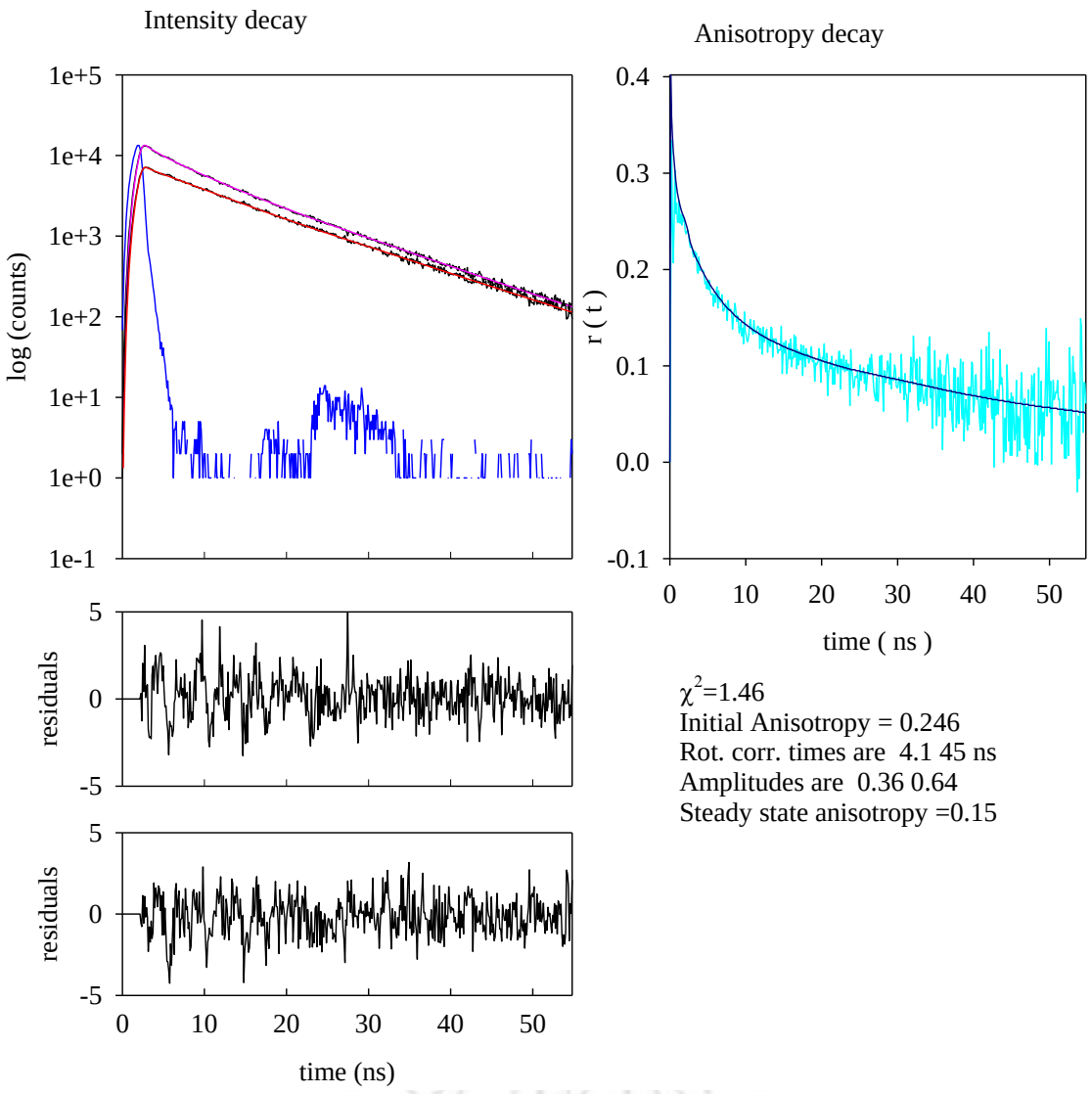

Figure 6.11 Anisotropy Decay Analysis profiles

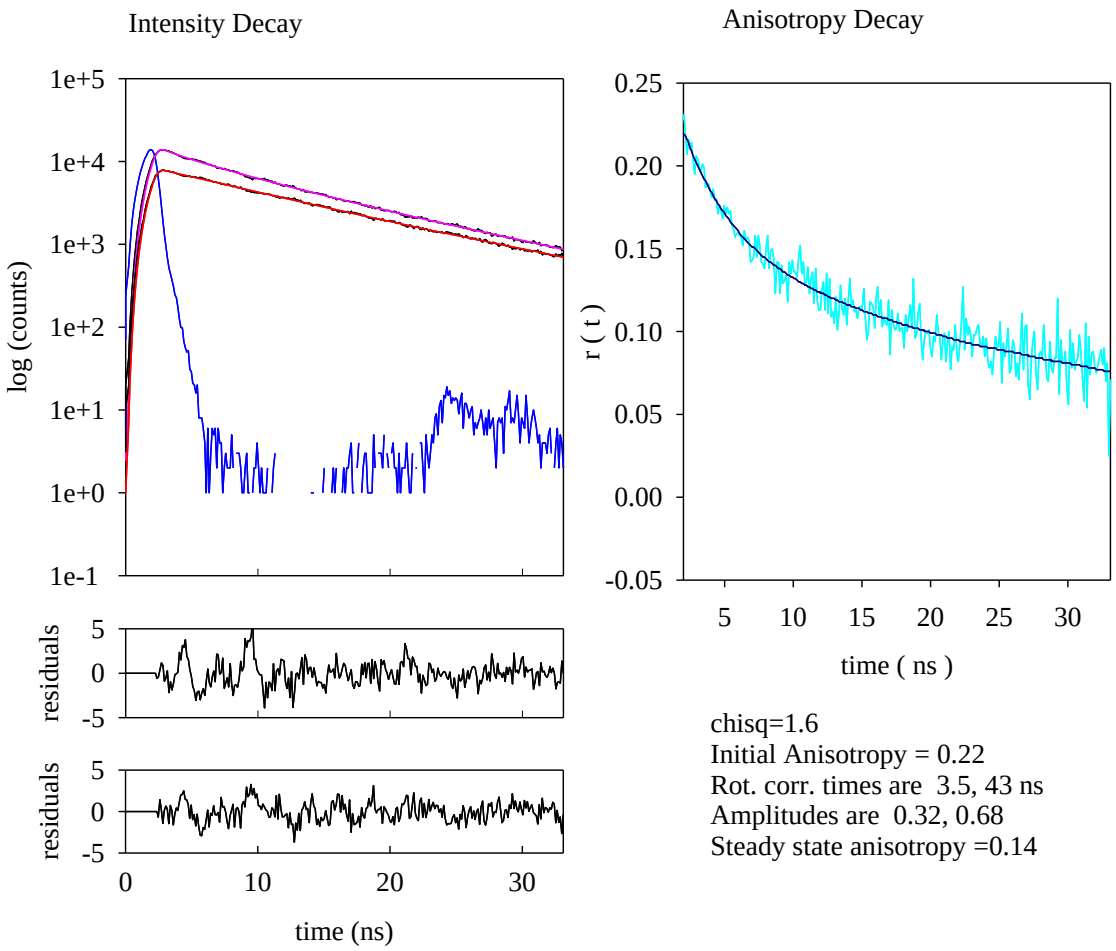

Figure 6.12: Anisotropy decay analysis curves

TH-265_004703

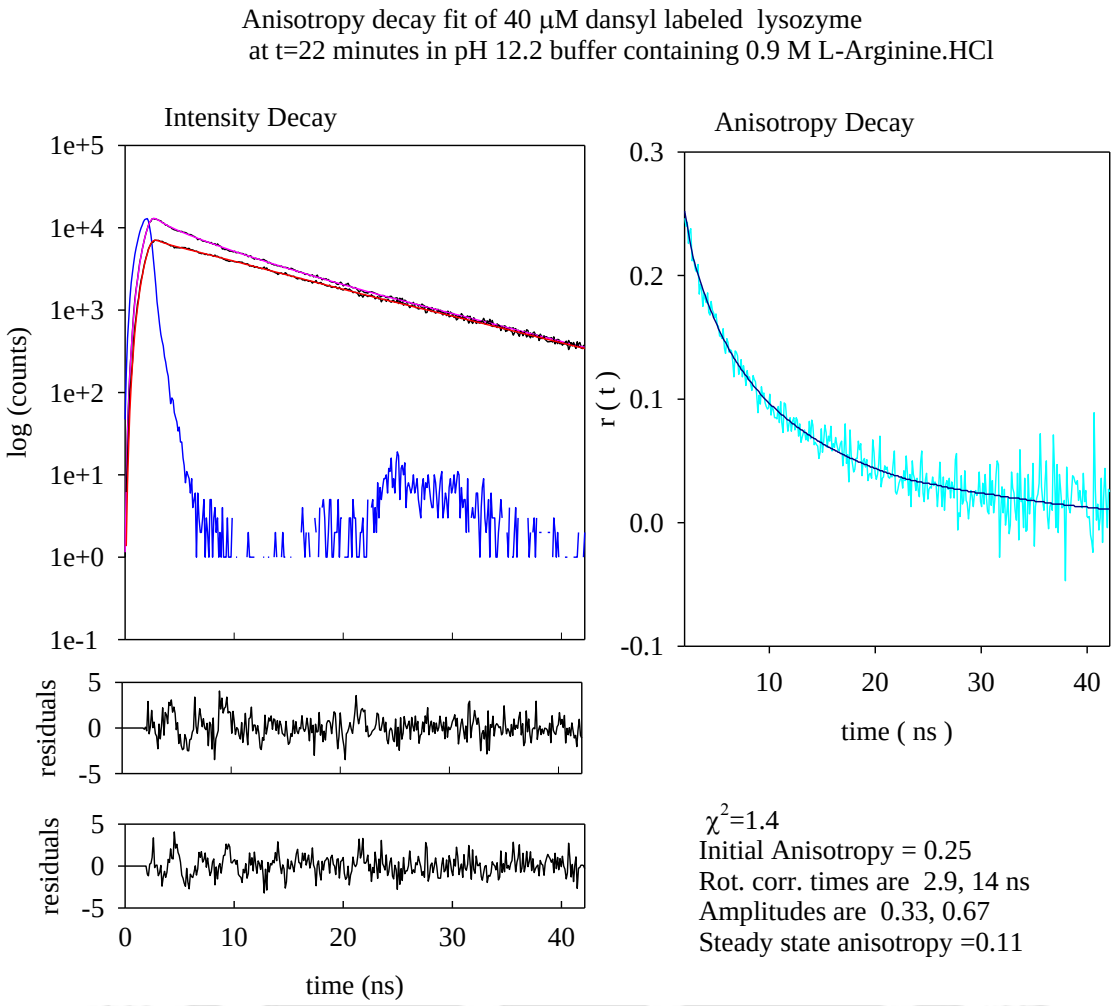

Figure 6.13: Anisotropy Decay Analysis profiles

TH-265_004703

Anisotropy Decay of 40 μM dansyl labeled lysozyme in pH 12.2 buffer containing 0.9 M L-Arginine.HCl at t=135 minutes

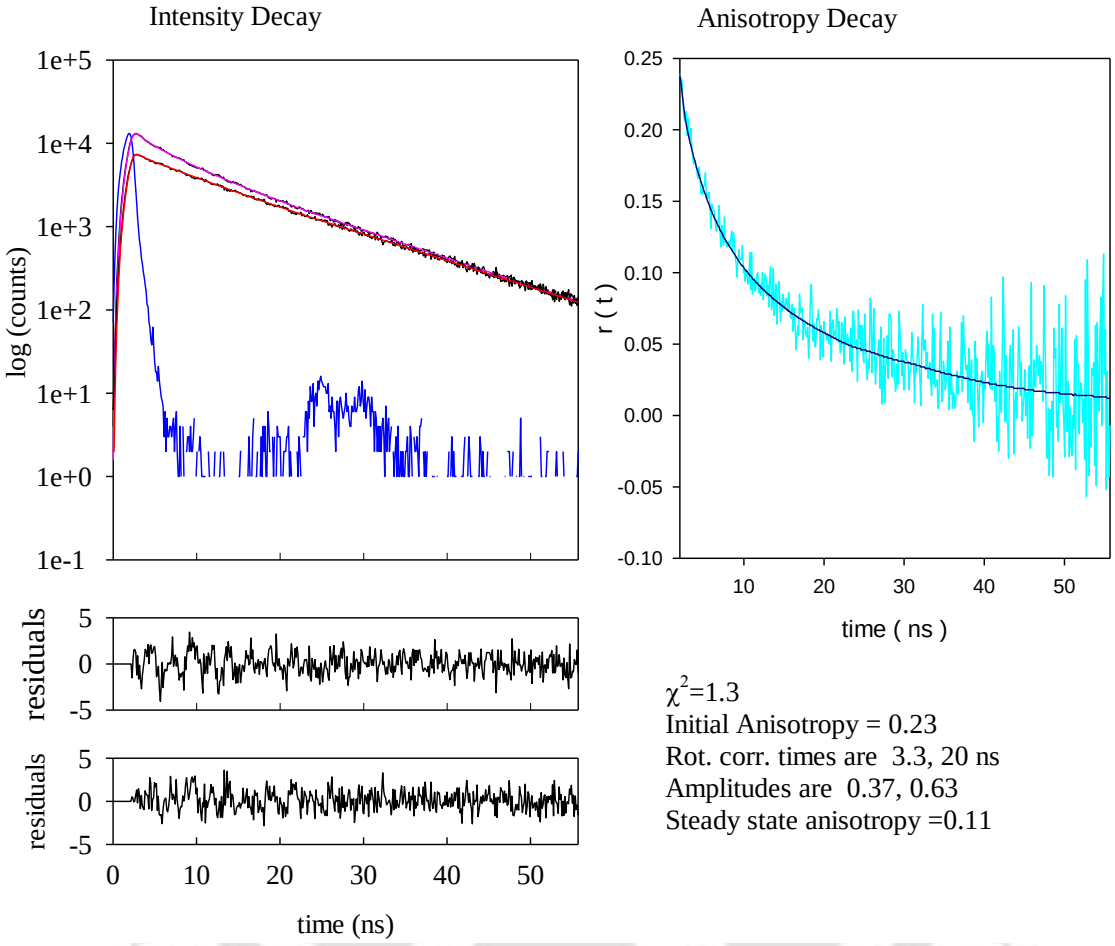

Figure 6.14: Anisotropy decay analysis figures

Anisotropy Decay fit of 40 μM dansyl labeled lysozyme in pH 12.2 buffer containing 0.9 M L-Arginine.HCl at t=1140 minutes

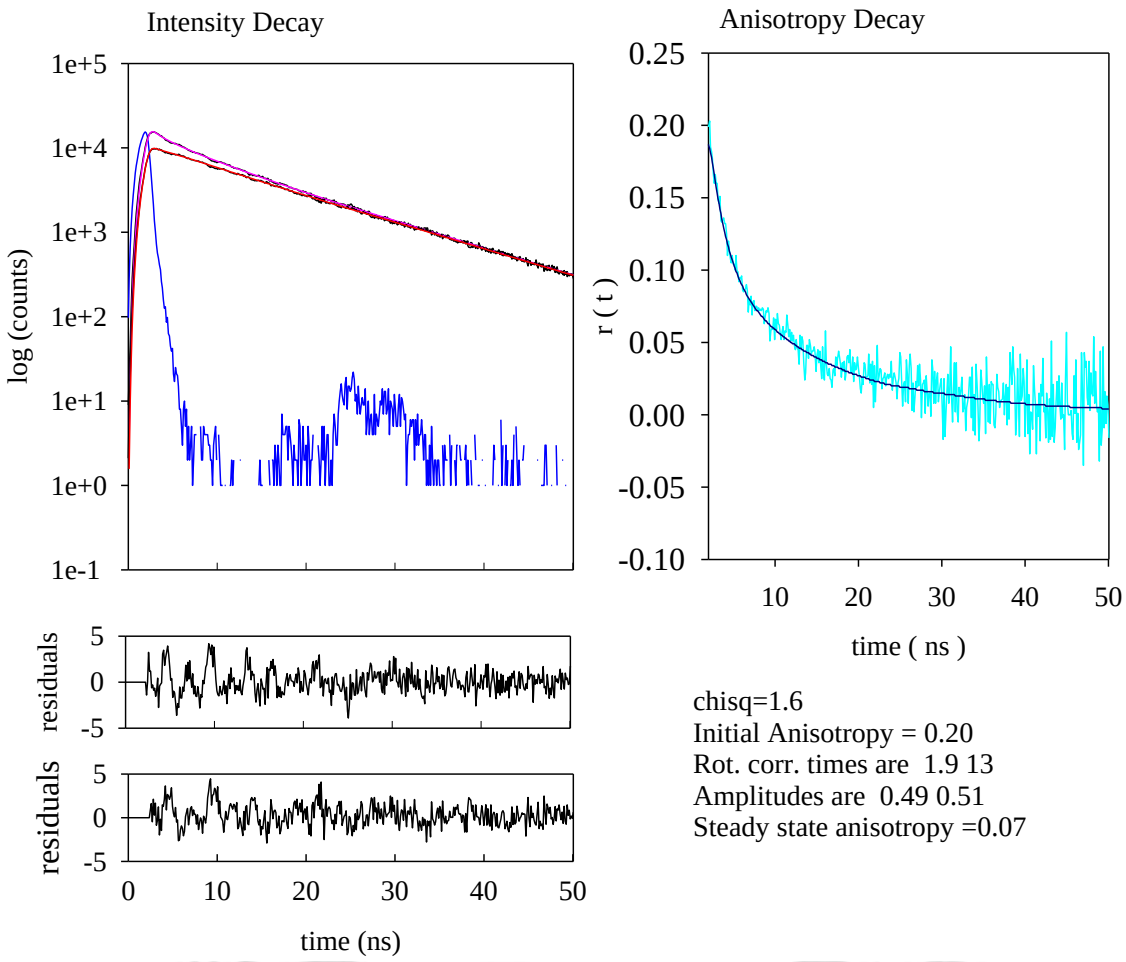

Figure 6.15: Anisotropy Decay Analysis profiles

TH-265_004703

CHAPTER 1

INTRODUCTION

A few aspects of the phenomena of protein aggregation and macromolecular crowding are discussed here. The phenomenon of protein aggregation has, in recent years, attracted a great deal of attention. Occurrence of protein aggregates in the neurons of people affected with neurodegenerative diseases has led to extensive studies of the phenomenon. Macromolecular crowding which is a phenomenon that is ubiquitous in cells is generally ignored. *In vitro* studies of cellular processes are generally carried out in conditions which do not represent the crowded ambience of cells and tissues. However, in recent years a number of reports in literature have appeared, indicating that the importance of the phenomenon is gradually being recognized.

A brief review of the two areas is presented below, highlighting their respective importance and applications. The current status of research in these two areas is also reviewed briefly along with the problems that we have attempted to address.

Macromolecular Crowding

The term macromolecular crowding was coined to describe the presence of high concentrations of proteins and nucleic acids in the cells and tissues of living organisms. The figure 1.1 below depicts crowding in the cytoplasm of a eukaryotic and a prokaryotic cell respectively (Ellis, 2001b; Goodsell, 1992).

Concentrations of macromolecules in cells are of the order of 200-300 g/l (Zimmerman, and Trach, 1991; Ellis, 2001a). A typical cell is reported to contain about 20-30% proteins (Han and Herzfeld, 1993). Muscle cells contain ~23% protein by weight and hemoglobin in red blood cells occupies approximately 30-35% (w/v) of the erythrocyte cytosol (Ralston, 1990). This is a case in which a single macromolecule is present at a high concentration. In most cells however, the medium contains a variety of macromolecules, none of which may be individually present at a high concentration, but which taken together occupy a significant fraction of the total volume of the medium e.g. the cytoplasm of Escherichia coli contains ~340 g/l of total RNA and protein (Zimmerman and Trach, 1991; Cayley, 1991; Fulton, 1982; Zimmerman and Minton, 1993). Such media are called crowded or confining (Minton and Wilf, 1981; Minton,

1992, 2001). The volume occupied by these macromolecules is excluded to other species present in the cells and the phenomenon is also called the exclusion volume effect. The theory of volume exclusion was propounded by Ogston and Laurent (Ogston, 1962; Laurent and Ogston, 1963; Edmond and Ogston, 1968). They observed that chemical potential of proteins increase on addition of a macromolecular agent to its solution (Schnell and Turner, 2004; Turner et al., 2004). The figure 1.2 below shows how the volume that is excluded to a particular species depends on the volume of that species. An infinitesimally small molecule will hardly experience any volume exclusion as compared to a molecule whose size is comparable to that of the background macromolecule which will be almost completely excluded from the cube. This happens because the volume available to an incoming molecule is actually the volume available to the centre of that molecule (Minton, 2001).

This exclusion arises because of the mutual impenetrability of macromolecules with probe species; molecules are spatially constrained on the microscopic level by force fields such as steric repulsion and electrostatic interactions (Minton, 1990; Zimmerman and Minton, 1993; Schnell and Turner, 2004)

There are various implications of macromolecular crowding. A reduction in diffusion rates is one of the consequences (Zimmerman and Minton, 1993; Luby-Phelps, 2000). A decrease in the values of diffusion coefficient was observed both in the cases of small and large molecules in the presence of crowding compared with the values in dilute solution e. g. the translational diffusion coefficient of carboxyfluorescein showed a 3-fold decrease in 3T3 fibroblast cytoplasm as compared to the value obtained in water (Ellis, 2001a, 2001b; Kao, et al., 1993) and GFP showed an11- fold decrease in its translational diffusion coefficient in E. coli cytoplasm as compared to its value in water (Ellis, 2001a, 2001b; Elowitz, 2001). If both the probe species and background species are macromolecules, the repulsive interactions between them may affect the activity of the probe species (Ralston, 1990; Minton, 1997) ---- the probe species may undergo a change in conformation or it might undergo association to assume a more compact state, since compact states are favored (Zimmerman, 1993; Minton, 1997; Zimmerman, 1993; Lindner and Ralston, 1997; Poon et al., 1997). For example, van den Berg et al. (van den Berg et al., 1999; 2000) showed that presence of high concentrations of crowding agents

like dextran, ficoll and BSA disrupts the refolding of reduced hen egg white lysozyme leading to the formation of aggregates whereas the refolding of oxidized lysozyme is not affected. van den Berg also showed that the rate of correct refolding of reduced lysozyme can be increased upto fivefold compared with rates in uncrowded buffers (van den Berg et al., 2000). There are also reports showing that the proteins dihydrofolate reductase, enolase and green fluorescent protein lose the ability to fold spontaneously in crowded solutions (Martin, 2002). Recently it was shown that the unfolded states of ribonuclease A were changed to native states in 2.4 M urea solution at pH 3 on addition of 35% PEG 20000 or Ficoll 70 (Tokuriki et al., 2002). Some examples of association in the presence of crowding agents are formation of amyloid by human apolipoprotein C-II (Hatters et al., 2002) and *in vitro* fibril formation by α-synuclein (Uversky et al., 2003). According to Minton (Hatters et al., 2002), this observation might also provide a link between up to now two unrelated observations. The first is the observation that amyloid-associated diseases occur most frequently in the aged and the second is that cellular and tissue hydration decreases substantially with age (Naber et al., 1979; Nagy, et al., 1981; 1982; Barber et al., 1995). Because loss of cellular and tissue water is equivalent to an increase in the fraction of cellular or tissue volume occupied by macrosolutes, one would expect aggregation processes to be accelerated with advancing age due to the increased influence of macromolecular crowding.

Various expressions have been suggested to explain the effect of crowding on the thermodynamic properties of solutions. The general theory of the effects of volume exclusion on the thermodynamics of globular macromolecules and macromolecular complexes in solution was developed by Minton in 1981 (Minton, 1981) assuming the law of mass action and using the hard particle approximation.

Here is a brief discussion of the effect of excluded volume on equilibria and kinetics (Zimmerman and Minton, 1993; Minton, 1981).

Effect on equilibria

Consider a system containing N molecular species in thermodynamic equilibrium as indicated in the following scheme:

$$n_1X_1 + n_2X_2 + \cdots n_jX_j \Leftrightarrow n_{j+1}X_{j+1} + n_{j+2}X_{j+2} + \cdots + n_NX_N \qquad 1.1$$

Where n_i represents the stoichiometric coefficient of species X_i. The chemical potential μ_i of species X_i as

$$\mu_i = \mu_i^o + RT \ln a_i = \mu_i^o + RT \ln \gamma_i c_i = \mu_i^O + RT \ln \gamma_i + RT \ln c_i \qquad 1.2$$

R the molar gas constant, T the absolute temperature and a_i, γ_i and c_i the activity, activity coefficient and the concentration of species X_i respectively. In the ideal standard state when the interactions between all solute species have been assumed absent, $\gamma_i = 1$. Such a state is the solution equivalent of an ideal gas. Thus, $\mu_i^o + RT \ln c_i$ may be called the ideal part of the chemical potential denoted by μ_i^I, and $RT \ln \gamma_i$ the nonideal part, μ_i^{NI}.

At equilibrium,

$$\sum_{i=1}^{j} n_i \mu_i = \sum_{i=j+1}^{N} n_i \mu_i \qquad 1.3$$

Incorporating equation 1.2 in equation 1.3 we have

$$\sum_{i=1}^{j} n_i (\mu_i^o + RT \ln \gamma_i c_i) = \sum_{i=j+1}^{N} n_i (\mu_i^o + RT \ln \gamma_i c_i)$$

Rearrangin g the above equation leads to

$$\sum_{i=j+1}^{N} n_i \mu_i^o - \sum_{i=1}^{j} n_i \mu_i^o = -\sum_{i=j+1}^{N} n_i RT (\ln \gamma_i + \ln c_i) + \sum_{i=1}^{j} n_i RT (\ln \gamma_i + \ln c_i) \qquad 1.4$$

$$= -\sum_{i=j+1}^{N} RT (\ln \gamma_i^{n_i} + \ln c_i^{n_i}) + \sum_{i=1}^{j} RT (\ln \gamma_i^{n_i} + \ln c_i^{n_i})$$

$$= RT \ln \frac{\prod_{i=i}^{j} \gamma_i^{n_i}}{\prod_{i=j+1}^{N} \gamma_i^{n_i}} - RT \ln \frac{\prod_{i=j+1}^{N} c_i^{n_i}}{\prod_{i=1}^{j} c_i^{n_i}},$$

Now, the ratio $\dfrac{\prod_{i=1}^{j} \gamma_i^{n_i}}{\prod_{i=j+1}^{N} \gamma_i^{n_i}}$ is called the non - ideal correction factor and is denoted by Γ while,

the ratio $\frac{\prod_{i=j+1}^{N} c_i^{n_i}}{\prod_{i=1}^{j} c_i^{n_i}}$ gives the apparent equilibrium constant, K_c.

Now, we know that μ_i^o is the ideal standard state chemical potential and we also know that chemical potential is actually the free energy per mole. So , the left hand side of equation 1.4 gives us the change in ideal standard state free energy and may be written as

$$\Delta G_I^0 = RT \ln \Gamma - RT \ln K_c \qquad 1.5$$

Equation 1.5 shows that the ideal standard state free energy change may be conveniently expressed as the difference between a total standard state free energy change $\Delta G^0_T \equiv -RT \ln K_c$ and a nonideal contribution $\Delta G_{NI} \equiv -RT \ln \Gamma$. Equation 1.5 may be rewritten in the form

$$K_c = \exp(-\Delta G_I^0 / RT)\Gamma = K_c^0 \Gamma \qquad 1.6$$

Thus, the apparent equilibrium constant K_c is increased or decreased relative to the ideal equilibrium constant by a factor that reflects the difference between the free energies of nonspecific interaction of molecules of products with all solute species and molecules of reactants with all solute species (Minton, 1983).

The logarithm of the activity coefficient may be expanded in powers of the concentration of solute:

$$\ln \gamma_i = \sum_j B_{ij} c_j + \sum_j \sum_k B_{ijk} c_j c_k + ..., \qquad 1.7$$

where the indices j, k … can have any value from 1 to q. The terms B_{ij}, B_{ijk} … are referred to as two-body, three-body … interaction (or virial) coefficients, respectively.

These virial coefficients are represented as functions of effective potential of interactions between two or more molecules of solute (Zimmerman and Minton, 1993). In practice, evaluation of the values of these potentials is possible only for small numbers of particles interacting via very simple interaction potentials. The simplest among these is the hard particle potential, which is equal to zero when the distance between the interacting particles is greater than their contact distance with reference to the centers of the particles. The inter-particle potential is infinite for inter-particle distances equal to or less than the contact distances. Macromolecules are therefore, for mathematical simplicity,

referred to as rigid hard particles with simple shapes for determining the virial coefficients.

Two approximate methods are normally used to calculate the effect of excluded volumes on thermodynamic equilibria. They are (a) the scaled particle approximation (Lebowitz et al., 1965; Gibbons, 1969) and (b) the lattice theory (Minton, 1981).

The scaled particle theory is used to calculate the non-ideal part of the chemical potential of convex hard particles (for example spheres, cylinders, etc) in an environment of similarly shaped but arbitrarily sized hard particles. Using the lattice theory, the activity coefficients of probe particles having planar surfaces (like rods, cubes, parallelepipeds etc) are calculated in an environment of cubes of arbitrary size. In the lattice treatment the planar surfaces are constrained to be parallel or perpendicular to each other. This constraint results in excluded volumes and activity coefficients calculated using the lattice theory to have lower values as compared with values obtained using the scaled particle theory.

Effect on Kinetics: A bimolecular reaction may be written as

$$A + B \rightarrow (AB)^* \rightarrow products$$

In the above reaction, (AB)*, represents the activated complex or transition state, that forms when the reactants A and B come together.

The expression for the rate of the above reaction when it takes place in solution was suggested by Bronsted (Bronsted, 1922; Laidler, 1987) and is given by

$$v = k_0[A][B]\frac{\gamma_A \gamma_B}{\gamma_{AB^*}} \qquad 1.8$$

where k_0 is a constant at a given temperature, γ_A and γ_B are the activity coefficients of the reactants, and γ_{AB^*} is the activity coefficient of the collision complex .

Bronsted referred to the ratio $\frac{\gamma_A \gamma_B}{\gamma_{AB^*}}$ as the kinetic activity factor and it may be written as Γ^*. The use of the activity factor results in data that agree with experimental measurements.

Now, the second-order rate constant for the above reaction may be written as

$$k = \frac{\mathrm{v}}{[A][B]}$$

Substituting this in equation (1.8) gives

$$k = k_0 \Gamma^* \qquad 1.9$$

The terms γ_A, γ_A, γ_{AB}, k and Γ^* respectively are functions of the concentrations of all the species present.

Therefore, according to Minton's theory, if a reaction occurs in an ideal and homogeneous medium, $\Gamma^*=1$, and no correction factor is necessary. However, a correction factor is required if the reaction occurs in a macromolecularly crowded environment and one or more of the reactants is a macromolecule (Schnell and Turner, 2004)

We will now focus on the effect of crowding on enzyme catalyzed reactions. Enzyme catalysis plays a very important role in all living systems. In fact, "life depends on the existence of these powerful and specific catalysts. Under biologically relevant conditions, un-catalyzed reactions tend to be slow – most biological molecules are quite stable in the neutral pH and mild temperatures prevalent in living tissues. Furthermore, many common reactions in biochemistry entail chemical events that are unfavorable or unlikely in the cellular environments, such as the transient formation of unstable charged intermediates or the collision of molecules in the right orientation required for reaction. Reactions required to digest food, send nerve signals or control muscles simply do not occur at a useful rate without catalysis. An enzyme circumvents these problems by providing a specific environment within which a given reaction can occur more rapidly." (Nelson and Cox, 4th Edn.) These enzyme catalyzed reactions take place in living systems within the crowded environment of the various cellular organs and tissues and hence the rates at which they occur may be quite different from the rates observed in the dilute solution conditions which are generally used in the laboratory (Goodsell, 1992). Macromolecular crowding and its influence on both thermodynamic and kinetic rates have been recognized since the early 1960s by the pioneering investigations of A. G. Ogston and T. C. Laurent (Ogston and Phelps, 1960; Laurent 1963; Laurent and Ogston,

1963; Edmond and Ogston, 1968). However, a majority of researchers discuss the physiological or biochemical relevance of their *in vitro* experiments in dilute solutions (Ellis, 2001b). "There have been a number of reviews on the qualitative and quantitative thermodynamic aspects of macromolecular crowding (Minton 2000, 2001; Ellis 2001a, b), its role in the regulation of cell volume (Al-Habori, 2001) and the physical properties of the cytoplasm (Luby-Phelps, 2000).However the literature remains inadequately understood for the biochemical reaction kinetics in intracellular environments." (Schnell and Turner, 2004)

Most of the available literature deals with effects of crowding on enzyme activity. There are more than 30 biochemical systems in which protein-protein, protein-nucleic acid and nucleic acid-nucleic acid interactions increase their activity in solution (Zimmerman and Pheiffer, 1983; Zimmerman and Minton, 1993; Minton, 2001; Hall and Minton, 2003). Laurent in 1971 (Laurent, 1971) made the important discovery that the Michaelis-Menten coefficient decreases in the presence of a macromolecular crowding agent in the single enzyme- substrate and other enzymatic reactions like two substrate-enzyme reaction and competitive inhibitions. The exact nature of the effect of crowding on enzyme catalyzed reactions depends upon the rate-determining steps of the reactions involved (Minton, 1981). The various steps in an enzyme catalyzed reaction are: (a) the binding of substrate to an enzyme; (b) the reaction of enzyme bound substrates to form enzyme bound products; and (c) the dissociation of enzyme bound products from the enzyme.

Depicted below is a schematic of the different steps involved, where E, S and P respectively denotes enzyme, substrate and product and [ES] denotes the enzyme-substrate complex formed on encounter of enzyme with substrate

$$E + S \rightleftharpoons [ES] \longrightarrow P \qquad 1.10$$

The rate of the reaction may depend on either of these steps. If the rate at which E and S encounter each other in solution is less than the rate at which the activated complex decays, then the encounter rate will be rate limiting. This is one of the assumptions for calculating rate laws. It means that all the species present in the step preceding the rate determining step will be present at steady state concentrations and all the species

involved after the rate determining step will be present in negligible concentrations and will not appear in the rate law. Molecular diffusion of substrates to enzymes is important in metabolic processes where the encounter of free substrates with the active site of an enzyme is the rate-determining step. One example is the hydration of CO_2 by carbonic anhydrase. The k_{cat}/K_m for this reaction is 1.6×10^8 M^{-1} s^{-1}, which is close to the diffusion controlled rate. The influence of macromolecular crowding on such bimolecular encounters has not been examined very exhaustively.

The effects of excluded volume on enzyme-catalyzed reactions were summarized by Minton (Minton, 1981) as follows:

(1) The conformation of the enzyme may be altered, if the enzyme exists in two or more conformations with different enzymatic activities. The presence of macromolecules shifts the equilibrium between the different conformations, favoring the more compact conformation and thereby alters the catalytic activity of the enzyme.

(2) The enzymes might self-associate in volume occupied media, leading to a change in catalytic activity. This change will depend upon the extent of self-association (Minton, 1981).

(3) If the reaction is encounter rate controlled, the presence of macromolecules will lead to a decrease in the rate of the reaction. Minton studied the effect of crowding on the rate of encounter and suggested the following relation:

$$k_e = k_e^0 e^{-g\varphi}, \qquad 1.11$$

where, k_e is the encounter rate in the presence of background molecules, k_e^0 is the encounter rate constant in the absence of background molecules,

g is a constant whose magnitude is a function of the relative sizes and shapes of enzyme, substrate and background molecules and ϕ is the fractional volume occupancy.

He predicts that under the conditions where the encounter between the substrate and enzyme is rate limiting, the rate of an enzyme-catalyzed reaction will experience a monotonic decrease with increase in the fractional volume occupancy (ϕ) of the crowding agent.

There have been other approaches directed towards determining the effects of crowding on biochemical reactions e. g. stochastic modeling, which is based on the randomness of molecular reactions (Gillespie, 1992; Kepler and Elston, 2001); the power law approach

developed by Savageau (Savageau, 1969, 1976) to describe non-ideal kinetics in crowded systems. Kopelman (Kopelman, 1986) discovered that chemical reactions occurring in heterogeneous media where reactants are spatially constrained follow fractal like kinetics. The Monte Carlo method was used by Berry in 2002 to study the effect of fractional volume occupancy (ϕ) on enzyme kinetics (Berry, 2002). According to his investigations, conventional equations (steady-state equations) for enzyme-kinetics fail when the reactions take place in crowded media due to the occurrence of anomalous diffusion of the reactants. He did Monte Carlo simulations to study the evolution of a system containing enzyme, substrate, enzyme-substrate complex and product molecules respectively on a 2-D lattice. The Monte Carlo (MC) technique is a statistical method in which a problem is studied based on the use of random numbers and is very useful for studying kinetics, as molecular motions are essentially random in nature. Each of the molecules on the lattice was free to diffuse throughout the lattice by carrying out a random walk. Immobile (non-reactive) point obstacles were introduced in the lattice and at any given time any point on the lattice could be occupied by only one molecule, except in the case when a substrate molecule wandered into a point occupied by an enzyme, in which case, depending on the reaction probability an E-S complex would form. The reactions took place in accordance with Michaelis-Menten kinetics. A time unit in these simulations corresponds to the time required by each molecule to move once. Now earlier, various bimolecular diffusions of the type A + B $\longrightarrow$ P, were studied in low-dimensional systems. In those cases however, the reactions involved identical concentrations or densities of the reactants A and B. Simulation of enzyme-kinetics is different from the above cases because a Michaelis-Menten type reaction involves three elementary reaction steps and also the ratio $\rho_E/\rho_S<<1$. In no biological systems, is this ratio equal to one. The results obtained from these studies showed that the bimolecular rate constant k_1 displays a power law dependence of time i.e., $k_1 \propto t^{-h}$, h is a parameter called the fractal exponent. So, k_1 did not remain constant throughout the reaction course, contrary to classical chemical kinetics. It remained constant at short times but decreased at longer ones. Since the formation of the complex itself showed anomalous behaviour the entire reaction kinetics may be expected to be anomalous. Anomalous diffusion is

said to occur when the mean square displacement shows a power law dependence on time i.e. $< R >^2 \propto t^{\alpha}$ where α is called the anomalous diffusion coefficient. α <1 in low-dimensional media and equals one in normal diffusion. However, the rate constants k_{-1} and k_2 displayed no change over time, being first order rate constants, showing agreement with classical chemical kinetics. Also, evolution of complex formation and enzyme densities showed agreement with the classical model only at very short times but showed marked deviation at longer times. It was also observed that the quasi-stationary state hypothesis which is followed by biochemists and according to which the concentration or density of the enzyme-substrate complex remains steady over the entire course of the reaction beyond a pre-stationary state, is valid only at very high ratios of initial substrate –to-enzyme density ratios. For calculation time reasons, such high ρ_E / ρ_S values are difficult to study in MC simulations. Another peculiarity observed using the MC simulation was the segregation of products and substrates at obstacle densities comparable with in vivo conditions. This phenomenon of segregation was reported earlier by Argyrakis and Kopelman in 1990 (Argyrakis and Kopelman, 1990), and were thought to occur because of spatial self-organisation of reactants as a result of the compact properties of diffusion (In compact diffusion, the molecule remains in the vicinity of its initial position with a probability P=1 as a result of which mixing is not uniform. In normal diffusion, however, the particle explores only a low fraction of the volume available to it and the particle always escapes from its initial position). It is also called the Zeldovich effect (Ovchinnikov and Zeldovich, 1978; Toussaint and Wilczek, 1983). Conventional mass-action laws failed to account for the spatial segregation that occurs because the classical hypotheses are based on continuum approximations and do not take spatial fluctuations into account. On the whole one can conclude from the paper that enzyme-catalyzed reactions occurring in low-dimensional media are not governed by the conventional mean-field equations of classical kinetics, because the reactions are essentially fractal in nature.

The diffusion of probes in dilute solutions, also called normal diffusion follows the equation:

$\Delta x^2 = 4Dt,$ for diffusion in $2-D$

where, Δx = displacement of the probe,

D = diffusion coefficient of the probe,

and t = time

for diffusion in 3 - D space

$\Delta x^2 = 6Dt$

In the presence of obstacles, however, the linear relationship between the square of displacement and time does not exist as explained earlier, and the probe is believed to undergo anomalous diffusion. For the 2-D case

$\Delta x^2 = 4Dt^{\frac{2}{d_w}}$,

where, d_w is the anomalous diffusion exponent.

while for the 3 - D situation, the equation is

$\Delta x^2 = 6Dt^{\frac{2}{d_w}}$

The ratio $2/d_w$ which is also denoted by α, can be either less than or greater than unity in the case of anomalous diffusion.

The influence of background molecules on the diffusive motion of a probe molecule is a phenomenon that is extremely complex to analyze theoretically, and is far more difficult to solve than the phenomenon of the influence of background particles on the thermodynamic activity of a probe molecule. The reduced tracer diffusion coefficient (the diffusion coefficient at high fractional volume-occupancy) may be expressed in terms of a power series of concentrations of solute molecules

$$D_i^R \equiv \frac{D_i^{tr}}{D_i^0} = 1 + \sum_j Q_{ij} + \sum_j \sum_k Q_{ijk} c_j c_k + ..., \qquad 1.12$$

Where D_i^{tr} and D_i^0 respectively denote the tracer and intrinsic diffusion of the solute species i, and the coefficients Q_{ij}, $Q_{ijk,}$...are measures of two-body, three-body, and higher-order interactions. These coefficients reflect contributions from direct interactions between solute molecules and from hydrodynamic interactions (Zimmerman and Minton, 1993).

However, though a number of theoretical approaches exist for describing the effects of crowding on the kinetics of biochemical reactions, yet, few of them have been experimentally verified. Recently, in a study carried out by Wenner and Bloomfield (Wenner and Bloomfield, 1999), they attempted to study the effects of ficoll on the binding affinity and catalytic rate of of EcoRV catalysed cleavage of pBR322. EcoRV is a restriction endonuclease and is prevalent in the cytoplasms of archea and bacteria, where they cleave viral DNA. The addition of ficoll was expected to increase non-specific binding and raise the maximum velocity,V_{max} due to crowding effects. Earlier work by Minton (Minton, 1983) with small cosolvents showed that increasing viscosity raised the value of K_m and the large size of ficoll was bound to increase the viscosity of the medium. Thus the net result of ficoll addition was expected to give rise to opposing effects. It was observed that the reaction rate in the presence of ficoll did not differ from that obtained in the absence of ficoll. This was because in the presence of ficoll there was a 44% increase in V_{max}, the K_m value doubled and there was a fourfold decrease in non-specific binding as indicated by $K_{d,ns}$.

The influence of PEG 8000 on the kinetics of trypsin catalyzed hydrolysis of p-nitrophenyl acetate was investigated recently by Asaad and Engberts (Asaad and Engberts, 2003). They also used the solute N-tert-butyl acetoacetamide (NBAA) to compare its effect on the kinetics of the hydrolysis with that of PEG 8000. They observed that the K_m remained invariant (mean $K_m=5.57x10^{-4}M$). The added PEG was however, observed to cause a ~2.7 fold decrease in k_{cat} in the concentration range 0-395gL^{-1}. A greater decline in k_{cat} was observed with NBAA. They concluded from their study that since addition of solutes affects both polarity and water activity, that the observed kinetics indicate an influence of the environment on enzyme activity. Minton and Wilf in 1981, studied the effect of addition of the proteins ribonuclease A, β-lactoglobulin, bovine serum albumin and poly-ethylene glycol (20 kDa) on the structure and function of rabbit muscle glyceraldehyde-3-phosphate dehydrogenase (Minton and Wilf, 1981). They observed that the enzyme glyceraldehyde-3-phosphate dehydrogenase exists as an equilibrium mixture of monomer and tetramer in solution and that on addition of the globular proteins the equilibrium is shifted towards the tetrameric form. The tetrameric form having a lower specific activity as compared to the monomeric form, overall, a

decrease in activity of the enzyme was observed on adiition of globular proteins to the reaction medium. Several other studies in the past have also reported only a moderate influence of high concentration of neutral polymers on enzyme reactions (Laurent, 1971). However, the fact remains that, though the effect of obstacles on reactions including enzyme catalyzed reactions has been studied *in silico*, there are very few reported experimental observations of crowding on the kinetics of enzyme catalyzed reactions. Notably effect of crowding agents in a range of molecular weights is necessary.

Scope of my work

We have attempted to study the influence of macromolecular crowding on the kinetics of an enzyme catalyzed reaction involving the encounter of a freely diffusing substrate with the active site of a freely diffusing enzyme. The enzyme chosen for our study was alkaline phosphatase with p-nitrophenyl phosphate as the substrate. Crowding agents were added to mimic cellular conditions where numerous such enzyme catalyzed reactions take place.

In most of the *in vitro* studies carried out earlier, the crowding agents used, do not reflect the size distribution that is actually present in cells. It is well known that physiological media contain macromolecules having a spectrum of molecular masses, often approaching several hundred kilodaltons in the upper limit. It is thus imperative to know the influence of crowding exerted by macromolecules of vastly different sizes, and shapes. We have used crowding agents in the molecular mass range of 15-500 kDa. The crowding agents used for our investigations were dextrans (15-500 kDa) and Ficoll (70and 400 kDa).

Using these crowding agents we tried to monitor the kinetics of alkaline phosphatase catalysed hydrolysis of para nitrophenyl phosphate. The product of the reaction being colored, the reaction could be monitored conveniently using uv-visible spectroscopy. We studied the enzyme hydrolysis reaction varying (1) the concentration of the crowding species and (2) the size of the crowding species as well as (3) the *shape/nature* of the crowding species.

There are a number of reports in literature where the applicability of the law of mass action to reactions occurring in disordered systems, like macromolecularly crowded systems, has been questioned. In such crowded systems, presence of the background

molecules impedes the normal diffusion of the reactants and causes them to be non-uniformly distributed. The law of mass action may actually be stated as follows "For a reaction in a homogeneous, free medium, the reaction rate will be proportional to the concentrations of the individual reactants involved". Therefore, the law of mass action may not exactly be applicable in disordered systems. The Michaelis-Menten formalism in enzyme-kinetics, which is based on the law of mass action, therefore, may not be valid in enzyme-catalysed reactions occurring in crowded systems. In his paper in 2002, Berry simulated a single enzyme-substrate system with varying densities of obstacles in a 2-dimensional lattice using the Monte-Carlo technique (Berry, 2002). The model predicted that as a result of anomalous diffusion, the kinetics is fractal in nature and therefore, the conventional equations of enzyme-kinetics fail to describe the reaction. There have been no reports verifying the above observations experimentally. We have attempted to examine the validity of the Michaelis-Menten formalism, by monitoring the change in initial rate of the reaction on varying the concentrations of substrate in the presence of 20 % w/w concentrations of 40, 200 and 500 kDa dextrans.

PROTEIN AGGREGATION

Protein aggregates are associated with a large number of pathologies like Alzheimer's disease, Parkinson's disease, Huntington's disease and prion diseases (Ross and Poirier, 2004; Caughey and Lansbury, 2003; Perutz, 1999; Taylor and Fischbeck, 2002; Bates, 2003; Berke and Paulson, 2003; Ross and Pickart, 2004; Nussbaum and Ellis, 2003; Wong et al., 2002; Ross, 1995; Selkoe, 2003; Stefani, 2004). These diseases are responsible for the degeneration of nerve cells leading to dementia or memory loss in patients suffering from Alzheimer's disease, uncontrolled movements in Huntington's disease, inability to initiate movement in Parkinson's disease etc. There are a whole host of problems resulting from these neurodegenerative diseases; however, all of them have not been listed here. Occurrence of amyloid deposits are not confined to neurons alone, there are other organs where amyloid deposition results in disruption of normal cellular activity e. g. diabetes mellitus type 2 that is caused by the deposition of insoluble amyloids called amylin in the pancreas. This disease is caused by impaired islet functions in the pancreas (Selkoe, 2003; Stefani, 2004; Cooper et al., 1987; Hull et al., 2004; Opie,

1901; Westermark and Wilander, 1978; Janson et al., 1999; Roberts et al., 1989; Hanabusa, 1992; Kahn, 1999).

Protein aggregates are also responsible for problems encountered in storing and transporting large quantities of proteins (Young et al., 1993). Concentration dependent aggregation is the greatest challenge to developing protein formulations at high concentration (Shire et al., 2004). This is one reason why proteins in liquid formulations can be unstable. For this reason many protein products are stored frozen or freeze dried. However, if drug activity can be maintained in solution, liquid formulation is preferred, owing to the reduced costs of manufacture and convenience to the end user (Tatford et al., 2004; Cleland, 1993; Ring et al., 1979; Katakam and Banga, 1995).

Aggregates associated with most of the diseases mentioned above occur in the form of insoluble fibrillar extracellular plaques or intracellular inclusions and are called amyloids (Stefani, 2004). The term amyloid was used by Virchow in 1855 to describe waxy eosinophilic deposits in tissues that he then thought to be composed of carbohydrates based on blue-iodine staining experiments and called them amyloid (Virchow, 1855). However, it was discovered 10 years later that proteins are the actual constituents of these deposits. In 1959 electron microscopy studies revealed these deposits to be fibrillar (Cohen and Calkins, 1959). Diseases accompanied by the deposits of amyloids in the different tissues and organs are called amyloidosis. Currently, there are roughly 20 amyloidoses known (Stefani, 2004).

Amyloids are observed to have common structural characteristics irrespective of the polypeptides or proteins that are involved in their formation. Typically, amyloid fibrils are straight, unbranched, 6-12 nm wide (larger in some cases) formed by a variable number of elementary filaments (protofilaments) approximately 1.5-2.0 nm in diameter, twisted around each other in a rope like structure (Stefani, 2004). A defining test of amyloid formation is Congo red birefringence. It requires that the binding site be ordered with respect to one another. This way ordered aggregates like amyloid may be distinguished from amorphous aggregates (Harper and Lansbury, 1997; Le Vine, 1993; Naiki et al., 1989). Thioflavin T fluorescence is also used as an indicator of aggregate formation and is widely employed to study amyloid fibril formation (Harper and Lansbury, 1997; Wood et al., 1996a; 1996b; Lansbury, 1992).

There are many factors responsible for the formation of protein aggregates. Aggregates can be either ordered or disordered. Ordered aggregates have a well defined intermolecular packing arrangement and a single protein conformation e.g. amyloids which have a crossed beta-sheet structure. Aggregates which do not have well defined intermolecular interactions and multiple conformations are called amorphous aggregates. Amorphous aggregates form rapidly at high protein concentrations whereas ordered aggregates require a critical concentration and they also require time owing to the kinetic barrier imposed by nucleus formation. Nucleus formation requires a series of steps that are thermodynamically unfavorable $K_a<<1$ because the resultant intermolecular interactions do not outweigh the entropic cost of association. Once the nuclei are formed, the association process becomes thermodynamically favored because the already formed nuclei present multiple sites for the addition of further monomers. The energy gained by this multiple site interaction outweighs the loss in energy and entropy during aggregation growth (Chothia and Janin, 1975; Li et al., 2001).

In vitro, aggregates form by iso-electric precipitation (i.e., at the pI of the proteins), by the process of salting out, by subjecting proteins to extremes of pH and temperature and also in the presence of high concentration of background macromolecules (Chi et al., 2003). There are also reports suggesting that induction of non-native beta-sheet conformation favors protein aggregation (Srisailam, 2001). Aggregates in physiological conditions arise mostly due to mutations in one or more of the amino acid residues that comprise the primary sequence of the protein. These mutations result in reduced stability of the native conformation, causing the protein to unfold partially, exposing hydrophobic patches and thereby resulting in aggregates when there is a high concentration of such partly folded species in the medium. These aggregates once formed have also been reported to trap normally folded proteins, thereby, leading to loss of functional proteins. Mostly, the aggregates that occur in diseased tissues are found to be ordered aggregates. An example of fibril formation due to mutations is the E22Q 'Dutch' peptide, where a charged species, glutamate (E), is replaced by an uncharged/ neutral species glutamine (Q). This peptide is observed to undergo fibril formation at an enhanced rate as compared with the wild type peptide for both the full length (1-40) peptide and the truncated (10-35) variants (Esler et al., 2000; Sian et al., 2000). Aggregation times have also been

observed to vary greatly for wild type transthyretin and its mutants under similar conditions (Hammarström et al., 2002). In the case of Amyloid-beta (1-42) peptide, truncation of the two terminal hydrophobic residues to Amyloid-beta (1-40) peptide results in considerable differences in the time of plaque formation between the two peptides (Thirumalai et al., 2003). Mutations in genes encoding proteins as for example in Huntington's disease, where expansion of the CAG codon results in expanded polyglutamine tracts are also known to render the protein unstable under physiological conditions (Perutz, 1999). Two known natural mutations in the genes encoding human lysozyme are responsible for fatal amyloidoses. These mutations in the genes, lead to amino acid substitutions Ile56Thr and Asp67His respectively, and the amyloid fibrils are found to consist of these variants (Pepys et al., 1993; Booth et al., 1995).

However, not in all cases does misfolding arise due to mutations. It has been observed in prion diseases (Creutzfeldt Jakob's disease, Bovine Spongiform Encephalopathy) that natively folded prions (PrP^{c}) misfold and aggregate, provided, they meet a suitable template, PrP^{Sc}, favoring a specific conformational modification (Dimcheff et al., 2003; Kocisco et al.; 1994; Saborio et al.., 2001).

Formation of aggregates is also favored under conditions in which the molecular machinery responsible for the quality control of protein folding get impaired or overwhelmed. The molecular machinery responsible for quality control of protein folding comprise the molecular chaperones in the cellular cytosol (heat-shock proteins, crystallins, prefoldin, heat shock cognate protein 70) and in the lumen of the endoplasmic reticulum(immunoglobulin binding protein, 94 kDa glucose regulated protein, calnexin) which assist the nascent polypeptide chains to fold by avoiding inappropriate interactions, and the ubiquitin-proteasome system which destroys polypeptide chains that have failed to undergo proper folding (Stefani, 2004).

Apart from the proteins involved in the various diseases, it has been observed recently, that there is an inherent tendency for most proteins and polypeptide chains to aggregate under suitable destabilizing conditions. This inherent tendency of polypeptide chains to aggregate may have resulted in the evolution of the elaborate molecular machineries that maintain the quality control of protein folding. Aggregation of proteins leading to the

various diseases occurs mostly at a relatively advanced age possibly because the processes responsible for clearance of these aggregates slow down with age, thereby, leading to the accumulation of misfolded and misassembled proteins (Stefani, 2004; Cohen and Kelly, 2003).

The exact mechanism by which aggregation is prevented or delayed in living organisms is not yet clear. There are a species of proteins present in living beings called molecular chaperones which guide the folding of proteins into their respective native states by binding to the exposed hydrophobic regions of the partly folded proteins (Thirumalai et al., 2003). However, only a very small fraction (e. g. 5-10% in E. coli) of proteins can afford to use chaperones to help them reach the folded state (Lorimer, 1996). Thus, as hypothesized by Anfinsen, most proteins must fold spontaneously without any help from molecular chaperones. Exactly, how this happens has led to a wide range of surmises. One such suggestion has been that proteins use a form of negative design in generating sequences that can only reach the desired structure efficiently avoiding unproductive pathways (Otzen and Oliveberg, 1999). Otzen and Oliveberg use the term "gate keepers" to denote the factors/residues that implement the negative design principle (Otzen et al., 2000). Richardson and Richardson have proposed a set of rules that can identify aggregation blocking mechanisms in beta-sheet proteins as the majority of the mentioned beta-sheet proteins tend to oligomerize (Richardson and Richardson, 2002). The rules are (a) minimizing the number of dangling hydrogen-bonds e. g. in beta-barrels which have very few unsatisfied hydrogen-bonds, (b) presence of inward pointing charged residues on the hydrophobic side of the beta-strands. The presence of unsatisfied hydrogen-bonds promotes intermolecular association that stabilizes beta-sheet proteins e.g. the percentages of unsatisfied hydrogen bonds are 14, 14 and 9 in mouse PrP^c, Syrian hamster PrP^c and $h1PrP^c$ respectively, which are larger than the average fraction of 6% of residues in normal proteins that possess unsatisfied buried hydrogen-bond donors and acceptors, and thereby makes the former susceptible to aggregation (Duma and Thirumalai, 2002; McDonald and Thornton, 1994).

It has been observed that there is a high degree of specificity in protein aggregation. In vivo studies carried out have shown that non-specific aggregation between hydrophobic, or hydrophobic and hydrophilic proteins does not occur even in mammalian cells. It has

been reported that early multimeric intermediates identified along the aggregation pathway for P22 tailspike and P22 coat proteins do not aggregate with each other but only among themselves in a mixture of the proteins folding in vitro (Juneja et al., 2002; Speed et al., 1995; 1996).

In addition to the formation of aggregates, which result in a toxic gain of function, misfolded proteins are also responsible for loss of function diseases like Cystic Fibrosis, hemophilia and cancer which arise due to loss of functional proteins (Lindgren et al., 2005; Bullock and Fersht, 2001). Cystic fibrosis for example is caused by the chaperone mediated retention in the endoplasmic reticulum of the ΔF508 mutated Cl^{-1} ion channel protein followed by its subsequent degradation by the proteasome (Dobson, 2003; Cohen and Kelly, 2003; Howard and Welch, 2002; Powell and Zeitlin, 2002).

The detailed mechanism of protein aggregation is still unclear. A number of intermediate conformations have been suggested, viz., transiently expanded species within the native state ensemble, a molten globule structure and even a fully unfolded molecule (Lumry and Eyring, 1954; Georgiou et al., 1994; De Young et al., 1993; Goldberg et al., 1991; Bam et al., 1995; Ikeguchi et al., 1997). Usually the aggregation pathway is modeled as shown in scheme1 by using the Lumry-Eyring Framework (Minton, 1982; Lumry and Eyring, 1954). The model involves a first order reversible unfolding of the protein and subsequent aggregation of nonnative species in a higher order process (Minton, 1982; Lumry and Eyring, 1954; Mulkerrin and Wetzel, 1989; Georgiou et al., 1994; Kendrick, et al., 1998).

Scheme 1

(a) $N \underset{k_{-1}}{\overset{k_1}{\rightleftharpoons}} A$

(b) $A_m + A \xrightarrow[k_m]{} A_{m+1}$

1.13

In this scheme, N refers to native protein, and A refers to an intermediate conformational state preceding aggregation. A_m refers to an aggregated form composed of m protein molecules which is thought to form because of association between hydrophobic residues exposed in A. The rate constants for each reaction, m, are represented by k_m.

The possibility that protein aggregation is a cause rather than an effect of diseases is supported by overwhelming circumstantial evidence from a variety of sources viz.,
(1) pathology- colocalization of cell death and disease (2) genetics-genes linked to familial forms of diseases encode the aggregated protein, (3) animal modeling- over expression of the aggregated protein produce disease associated phenotypes (4) biophysics- disease associated mutations promote *in vitro* aggregation and (5) mathematical modeling- rates of cell death and disease onset and progression are consistent with nucleation dependent aggregation processes (Caughey and Lansbury, 2003; Wong et al., 2002, Jarrett et al., 1993; Clarke et al., 2000; Perutz and Wendle,2001; Eigen, 1996).

Until recently, it was believed that the insoluble fibrillar deposits found in affected tissues are actually responsible for the diseases. However, in most cases where protein aggregates and disease associated phenotypes were separated in time, fibrous proteinacious inclusions were observed much after the earliest occurrence of the behavioral/or neuropathological phenotypes (Caughey and Lansbury, 2003). When the protein aggregation state is assessed using more sensitive biochemical techniques, it is observed that non-fibrillar aggregates precede the occurrence of the behavioral phenotypes. Moreover, combined biophysical and animal modeling studies have been observed to support the notion that ordered prefibrillar aggregates rather than mature fibrils are responsible for cell death and mature fibrils may infact be neuro-protective (Lansbury, 1999; Goldberg and Lansbury, 2000; Haass and Steiner, 2001). Protofibrillar amyloid beta was first produced as an intermediate in the course of in vitro fibril formation. A nonfibrillar and eurotoxic form of Amyloid-β was identified in the course of studies of the effect of clusterin (apolipoprotein J) on in vitro A-beta aggregation (designated ADDL for Aβ derived diffusible ligands) (Lambert, 1998). Moreover, Bucciantini et al have observed in experiments conducted with proteins not associated with diseases, but that form fibrils in vitro, that aggregates formed prior to the appearance

of fibrils were found to be toxic to cells (Bucciantini et al., 2002). Walsh et al (Walsh et al., 2002) have also reported that soluble aggregates derived from Aβ 1-42 (ADDLs) under conditions where fibril formation is inhibited, were found to be neurotoxic. In a recent issue of Nature (Silveira, 2005), Silveira et al reported results of experiments carried out to evaluate systematically the infectivity, converting activity and size of the prion particles. For the purpose they used partially disaggregated protease resistant prions (PrP^{res}). They observed that non-fibrillar particles of the sizes of 17-27 nm (300-500 kDa) containing 14-28 PrP^{res} molecules were more infectious as compared with smaller or larger oligomers. Studies also suggest that globular and protofibrillar intermediates form before mature Huntingtin fibrils and that they might be crucial for toxicity (Ross and Poirier, 2004). Data from these various sources point to the fact therefore that soluble aggregates that form en-route to fibril formation and which therefore represent the prefibrillar stages of fibrils are actually the toxic species.

Methods, therefore, have to be devised to identify and detect these species that occur in the early stages of aggregation, in particular the nature of the structural perturbations that lead to their formation.

There are a number of techniques available for determining insoluble fibrillar aggregates viz., thioflavin T fluorescence, congo-red birefringence, electron microscopy, atomic force microscopy (Le Vine, 1993; Naiki et al., 1989; Wood et al., 1996a; 1996b; Lansbury, 1992; Roher et al., 1996; Stine et al., 1996) etc. However, these aforementioned techniques cannot be used to determine soluble aggregates especially at very low concentrations. A number of commonly used techniques for soluble aggregate detection are far UV CD-to determine secondary structure changes, since in most of the cases the aggregates are observed to have a higher β– sheet content (Boren et al., 1999; Wetzel et al., 1980; Muzammil et al., 1999; Dockal et al., 2000; Greenfield and Fasman, 1969; Peters Jr., 1996; Tatford et al., 2004); the amide I band using FTIR spectroscopy is also useful for detecting changes in secondary structure (Pelton, 2000; Jung, 2000; Jackson and Mantsch, 1995); turbidity measurements-since the formation of protein aggregates or particles in solution leads to an increase in turbidity (Meireles, 1991; Martin, 1964; Tatford et al., 2004); light-scattering techniques (both static and dynamic and especially in conjunction with size-exclusion chromatography) (Sluzky et al., 1991;

McCarthy et al., 1981; Rosenqvist et al.,1987; Oliva et al., 1999; Schuler et al., 1999; Gombotz et al., 1994; Tatford et al., 2004); analytical ultracentrifugation (Sakurai et al., 2001; Smith and Radford et al., 2001; Huang et al., 2000; Tatford et al., 2004) (direct measurement of molecular mass in solution is possible without assumptions concerning shape etc). Covalent labeling of probes to thiol or amine groups of proteins may also be used to study the onset and progress of aggregation using the technique of fluorescence anisotropy. Time-resolved fluorescence anisotropy using extrinsic probes is a useful approach for monitoring the growth of aggregates using probes having sufficient long lifetimes to measure tumbling motions of proteins and larger aggregates e.g. the oligomerization of dansyl labeled hydrophobin SC3 was monitored using time-resolved anisotropy. The rotational correlation time of soluble state SC3 was observed to increase from 19.7 to 61.5 ns at room temperature indicating that larger and larger oligomers were forming in solution (Wand et al., 2002; 2004). Fluorescent probes which bind non-covalently may also be used to detect aggregates for example probes like ANS, bis-ANS etc. which undergo increases in fluorescence intensity on binding to hydrophobic sites may be used for detecting aggregates in solution (Uversky et al., 1996; Tatford et al., 2004; Lai et al., 1996; Semisotnov et al., 1991; Lindgren et al., 2005). Another well known example is thioflavinT which displays a shift in absorption band from 385 to 450 nm and a corresponding shift in the emission band from 445 to 482 nm.

Once these initial aggregates have been detected, the next step is to find ways to stem their further growth. There are a number of methods reported in literature to either break up the prefibrillar aggregates when formed or to arrest their growth in the initial stages and thereby prevent formation of insoluble aggregates. Some of the techniques reported involve adding guanidine hydrochloride which is a strong denaturant. This was observed to unfold PrP^{Sc} to a predominantly random coil conformation (Callahan et al., 2001). When the guanidinium chloride solution was diluted, PrP refolded into a conformation that was high in alpha-helix as measured by CD spectroscopy, similar to the normal cellular isoform (PrP^{c}). There has also been a report where the amyloid beta peptide fragment ($A\beta^{16-20}$) was successful in preventing the assembly of the full length amyloid-beta peptide into fibrils by binding to it (Tjeruberg et al., 1996). A heat shock protein ClpB has also been reported to greatly enhance the recovery of luciferase activity

(following its denaturation in urea) in combination with conventional chaperone systems (DnaK, DnaJ and GrpE) in vitro in the presence of ATP hydrolysis (Zolkiewski, 1999). There have also been widespread reports of the amino acid arginine for its role in preventing aggregation. Inspite of its widespread use as an effective refolding agent, its exact mechanism is still not clearly known (Zolkiewski, 1999). Arakawa and Tsumoto have very recently shown that L-ArgHCl does not appreciably increase the thermal stability of RNaseA or Hen Egg White lysozyme, but improves the reversibility of the respective thermal transitions (Reddy et al., 2005; Arakawa and Tsumoto, 2003).

Scope of my work

The investigations of protein aggregation reported here in this thesis have been done *in vitro*. We have not attempted to compare our work with *in vivo* situations. Protein aggregates formed in the solution phase were subjected to uv-visible absorption and fluorescence spectroscopic analyses.

Serendipitous observations of concentration dependent absorbance features of L-lysine.HCl in aqueous solutions at 270 nm, led to the development of this part of the work. Since the absorbance features observed could not be attributed to any particular chromophoric group, (lysine has none), we concluded that intermolecular interactions among the lysine molecules were responsible for the features. We then checked for similar features in proteins. We observed that the proteins human serum albumin and histone showed features which were comparable to that observed with L-lysine and poly-L-lysine hydrobromide, though in case of the proteins and poly-L-lysine the features were observed at much lower concentrations, indicating that in proteins the putative lysine-lysine interactions were intramolecular in nature. We then used these interactions to monitor unfolding and aggregation of the protein histone.

However, the method used above to track aggregation is a) limited to only lysine rich proteins b) not sensitive enough for dilute protein samples. A more sensitive method is required to monitor the formation and growth of soluble aggregates that can be applicable to any protein. The technique of fluorescence anisotropy was employed, since fluorescence is sensitive to very dilute concentrations of fluorophores and moreover, the rotational correlation time is dependent on the volume of the fluorophore that is being investigated as per the Stoke-Einstein relation

$$\theta = \eta V/RT \quad 1.14$$

Here, θ denotes the rotational correlation time, η denotes the viscosity of the solution, V corresponds to the hydrodynamic volume of the species being examined and T indicates the temperature. The volume dependence of the rotational correlation time could be of great use in detecting the onset of aggregation.

We monitored the growth of soluble aggregates of chicken egg white lysozyme at the alkaline pH of 12.2 using steady-state fluorescence anisotropy and time-resolved fluorescence anisotropy respectively. For this purpose we labeled the protein with dansyl chloride (an amine reactive fluorescent probe). Time-resolved anisotropy decay analysis yielded a slow correlation time of ~44 ns that can arise from a molecular aggregate consisting of ten or more lysozyme monomers. The growth of the aggregates was monitored over a period of ~24hours. Addition of 0.9 M arginine was observed to arrest the growth of aggregates. The aggregates were observed to be reversible in the initial stages (approx. 30 minutes after formation). The aggregates formed were found to be unaffected by 6M guanidine hydrochloride, since solutions incubated overnight at room temperature did not show any significant change in anisotropy. Moreover, the aggregates were observed to form only at the pH of 12.2 as solutions prepared in buffers of pH ranging from 4 to 11 did not show similar behaviour.

CHAPTER 2

EXPERIMENTAL TECHNIQUES

Various spectroscopic techniques were used to carry out the different experiments that have led to the development of this thesis. The principles involved in these techniques have been described here. Most of the theories described here have been extracted from three texts which I found invaluable (Cantor and Schimmel, 1980; Turro, 1991; Lakowicz, 1999). The last section of this chapter comprises a brief discussion on enzyme kinetics.

Absorbance

The interaction of light with molecules leads to the induction of dipoles within the system. In the following equation

$$\mu_{ind} = \underset{\sim}{\alpha} \cdot E \qquad 2.1$$

$\underset{\sim}{\alpha}$ is the polarizability of the molecule, μ_{ind} is the induced dipole moment and E is the electric field of light. Because E is a function that fluctuates with time, μ_{ind} fluctuates too. If a molecule is initially in a state A, interaction with light perturbs the state so that it resembles another state B.

The probability of transition from a state A to a state B is determined by the transition dipole moment integral.

The transition dipole moment integral is also denoted as μ_{ba} and can be calculated by performing the integration

$$\int \psi_b^* \underset{\sim}{\mu} \psi_a \, d\tau$$

The integral may also be written as follows

$$\langle \psi_b | \underset{\sim}{\mu} | \psi_a \rangle$$

The transition dipole for each pair of states is in a fixed orientation relative to the structure of the molecule. It can be represented as a vector in the coordinate system defined by the location of the nuclei.

A molecule is perturbed by light because the distribution of electric charges is altered by the oscillating electric field *E*.

Suppose that a system is initially in a state A denoted by Ψ_a and that it is perturbed by light to a state B denoted by Ψ_b. The wavefunction in the presence of light will be denoted by

$$\psi(t) = C_a(t)\psi_a e^{-iE_a t/\hbar} + C_b(t)\psi_b e^{-iE_b t/\hbar} \qquad 2.2$$

The Hamiltonian in the presence of light may be written as

$$\underset{\sim}{H'} = \underset{\sim}{H} + \underset{\sim}{V}(t) \qquad 2.3$$

The effect of light appears entirely in the function $\underset{\sim}{V}(t)$.

The interaction energy between a molecule and light may be written as

$$\underset{\sim}{V}(t) = \underset{\sim}{\mu} \cdot E_0 e^{i\omega t} \qquad 2.4$$

The probability that a system will undergo a transition from a state A to a state B is given by the equation

$$P_b = |C_b(t)|^2 \qquad 2.5$$

The following equation gives us the condition when $|C_b(t)|^2$ will be maximum.

$$|C_b(t)|^2 = \frac{|<\psi_b | \underset{\sim}{\mu} | \psi_a > \cdot E_0|^2}{\hbar^2} \frac{t^2 \sin^2[(E_b/\hbar - E_a/\hbar - \omega)t/2]}{2[(E_b/\hbar - E_a/\hbar - \omega)t/2]^2} \qquad 2.6$$

In the above expression E_b and E_a correspond to the energies of the states B and A respectively and ω corresponds to the frequency of light incident on the system.

In the above equation when $(E_b - E_a)$ is approximately equal *to* $h\nu = \hbar\omega$, the value of $|C_b(t)|^2$ is large and so the transition from A to B will only take place when the energy of light is approximately equal to the energy separation between the two states. The rate at which energy is taken up by a molecule from the incident light beam will enable us to determine the absorption intensity. This transition rate dP_b/dt may be written as follows

$$dP_b / dt = B_{ab} I(\nu) \qquad 2.7$$

where B_{ab} is the transition rate per unit energy density of radiation and $I(\nu)$ is the energy density incident on the sample at frequency ν.

The term B_{ab} is given by

$$B_{ab} = (2/3)(\pi/\hbar^2) |< \Psi_b | \underset{\sim}{\mu} | \Psi_a >|^2 \qquad 2.8$$

$|\psi_b | \underset{\sim}{\mu} | \psi_a|^2$ is also called the dipole strength and is denoted as D_{ab}. It is a direct measure of the intensity of a spectral absorption.

The rate at which energy is removed from the incident light beam will depend on the number of a to b transitions stimulated by light, on the number of b to a emission transitions and on the energy per transition (E_b-E_a=$h\nu$).

From equation (2.7) the rate is

$$-\frac{dI(\nu)}{dt} = h\nu(N_a B_{ab} - N_b B_{ba}) I(\nu) \qquad 2.9$$

where N_a and N_b are the number of molecules per cm^3 in states a and b, respectively.

Thus light absorption depends on concentration through the factors N_a and N_b. The factors B_{ab} and B_{ba} are called the Einstein coefficients for stimulated absorption and emission respectively.

The most important factor in light absorption is the molar extinction coefficient.

Consider a set up in which light of intensity I_0 impinges on a sample (a solution of absorbing molecules at a concentration C *moles liter*$^{-1}$) and travels a distance l cm within the sample. Let I be the intensity of the light that is not absorbed by the sample.

Consider now, a sample of molecules in a layer perpendicular to the direction of propagation of light and sufficiently thin (dl) so that the light intensity within this layer is

essentially constant. Then the fraction of light absorbed (*-dI / I*) is proportional to the number of absorbing molecules. The resulting equation is

$$-\frac{dI}{I} = C\varepsilon' dl \qquad 2.10$$

where ε' is a proportionality constant called the molar extinction coefficient, C is the concentration of absorbing molecules in moles liter^{-1} , and l is the path length the light travels in the sample. This equation when integrated for the entire sample is as follows

$$\ln(\frac{I_0}{I}) = C\varepsilon' l \qquad 2.11$$

Converting to log base 10, we have the common form of the Beer-Lambert's law:

$$A(\lambda) = \log(\frac{I_0}{I}) = \varepsilon(\lambda) Cl \qquad 2.12$$

$$\text{where } \varepsilon = \varepsilon' / 2.303 \qquad 2.13$$

The quantity A is called the absorbance or the optical density.

The molar extinction coefficient is related to the Einstein coefficient for stimulated absorption as follows

$$B_{ab} = (1000c / N_0 h)\int (\varepsilon' / \nu) d\nu \qquad 2.14$$

This integral is performed over frequency. Using this equation and equation (2.8), and converting ε' to ε we get the following relation

$$D_{ab} \equiv |< \psi_b \mid \underset{\sim}{\mu} \mid \psi_a >|^2 = 9.180 \times 10^{-3} \int (\varepsilon / \nu) d\nu \quad (debye)^2 \qquad 2.15$$

D_{ab} may be determined by integrating the area under an absorption band. Once D_{ab} is known, one can determine the length of the transition dipole $|\underset{\sim}{\mu}_{ba}| = |< \psi_b \mid \underset{\sim}{\mu} \mid \psi_a >|$.

Another useful measure is the oscillator strength, f_{ab}, which compares the intensity of absorption to that expected from a three-dimensional harmonic oscillator. This can be shown as

$$f_{ab} = (8\pi^2 mc/3h\nu)D_{ab} = 4.315\times10^{-9}\int \varepsilon(\nu)d\nu \quad \text{(dimensionless)} \qquad 2.16$$

here, m is the mass of the electron. For a strongly allowed transition, f_{ab} may have a value between 0.1 and 1.

Fluorescence

Fluorescence is the emission of light accompanying a transition from a singlet excited state to a singlet ground state. Emission of light can reveal properties of biological molecules quite different from the properties revealed by light absorption. The reason being that emission takes place at a much slower timescale (~nanosecond) as compared to absorption (~femtosecond), allowing a wider range of interactions and perturbations to influence the spectrum.

Consider a molecule with two energy levels, S_b and S_a. We have seen earlier that light of radiation density $I(\nu)$ induces transitions from state A to state B at a rate B_{ab} per molecule. The radiation induced emission process occurs at exactly the same rate; thus $B_{ab}=B_{ba}$. If the system originally contains n_a molecules in state S_a and n_b in state S_b, then the net rates of conversion are $n_aB_{ab}I(\nu)$ and $n_bB_{ba}I(\nu)$, respectively. At equilibrium, these rates are equal, hence, $n_aB_{ab}I(\nu) = n_bB_{ba}I(\nu)$,or $n_a=n_b$, independent of radiation density. However, without light, virtually all molecules will be in the ground state, S_a. At low light intensities there can be no major perturbation of the equilibrium values of n_a and n_b. Application of the Boltzmann distribution factor gives

$$n_a / n_b = e^{-(E_a-E_b)/kT} = e^{+h\nu/kT} \qquad 2.17$$

where h is Planck's constant.

In order to resolve this discrepancy, Einstein postulated the rate of spontaneous emission of a photon from a state S_b. The rate of this process is independent of $I(\nu)$. With the inclusion of spontaneous emission, when the rates of interconversion of S_a and S_b are set equal at equilibrium, the result is

$$n_a / n_b = [B_{ba} I(\nu) + A_{ba}] / B_{ab} I(\nu) = 1 + A_{ba} / B_{ab} I(\nu) \qquad 2.18$$

By equating 2.17 and 2.18 and by substituting for I(ν) the radiation density expected for a black body at a temperature T,

$$I(\nu) = 8\pi h\nu^3 / c^3 (e^{h\nu/kT} - 1) \qquad 2.19$$

we end up with an expression for A_{ba}

$$A_{ba} = 8\pi h\nu^3 c^{-3} B_{ab} \qquad 2.20$$

Because the dipole strength (D_{ab}) and the frequency (ν) usually can be measured from the absorption spectrum, the rate of spontaneous emission can be determined without performing an emission measurement at all. In the absence of radiation or any other perturbations or interactions, the rate of deexcitation of molecules initially in state S_b will be

$$-dn_b/dt = -(A_{ba} n_b) \qquad 2.21$$

The solution of the above differential equation is $n_b(t) = n_b(0)\exp(-A_{ba}t)$, where $n_b(0)$ is the concentration of excited states at zero time. Hence we can define the radiative lifetime of state S_b as

$$\tau_R = 1 / A_{ba} \qquad 2.22$$

In reality the actual observed lifetime of an excited singlet state is rarely as long as the theoretically predicted value because the excited state can lose its energy through many other competing processes besides direct emission of light.

The intrinsic fluorescence rate constant (k_F) may be expressed in terms of the molar extinction coefficient and oscillator strength as follows

$$k_F = 3\times10^{-9}\bar{\nu}_0^2\int \varepsilon\, d\bar{\nu} \cong \bar{\nu}_0^2 f \qquad 2.23$$

where $\bar{\nu}_0$ is the frequency in wavenumbers corresponding to the maximum wavelength of absorption

The radiative rate constant is related to the radiative lifetime also called the intrinsic lifetime as follows

$$k_F = 1/\tau_R \qquad 2.24$$

The above relation is valid as long as stimulated emission is negligible. The nonradiative processes (and their associated rate constants) that compete with fluorescence include internal-conversion (k_{ic}), intersystem crossing (k_{is}), and quenching of various types [$k_q(Q)$]. All of these processes compete directly to depopulate the excited singlet state.

Therefore the fraction of excited singlets that become deexcited through fluorescence, also called the fluorescence quantum yield, ϕ_F, is written as

$$\phi_F = \frac{k_F}{k_F + k_{ic} + k_{is} + k_q(Q)} \qquad 2.25$$

The fluorescence quantum yield (ϕ_F) is equal to the ratio of photons emitted to photons absorbed by the system.

Factors governing fluorescence intensity

A brief description of the factors that affect fluorescence

1. Internal conversion: In this process, excitation energy is lost by collision with solvent or by dissipation through internal vibrational modes. In general k_{ic} has been observed to increase with increasing temperature. Therefore the observed

fluorescence will decrease with increasing temperature. This intrinsic temperature dependence complicates attempts to monitor thermally induced macromolecular conformation changes.

2. Quenching: Deexcitation results from collisions or complexes with solute molecules (Q) capable of depopulating the excited state. Quenching can be a bimolecular process if collisions are involved.

$$S_b + Q \text{ --}k_q\text{--- } S_a + Q \qquad 2.26$$

Since Q is usually in vast molar excess over S_b, the actual observed rate is actually pseudo first order. The value of k_q maybe measured by varying the concentration of quencher [Q]. Aromatic fluorophores usually have radiative lifetimes in the range of $1\times10^{-9} to 100\times10^{-9}$ sec. The common quenchers are O_2 and I^- ion. The rates of collisions are limited only by diffusion.

3. Intersystem crossing: In this process the supposedly forbidden spin exchange converts an excited singlet into an excited triplet state. That state can, in turn, convert to the ground singlet state (S_a) either by phosphorescence or by internal conversion. The triplet state is generally lower in energy as compared to the excited singlet state and occurs at longer wavelengths. The intensity for direct singlet to triplet absorption is very weak; therefore triplet states can be seen by only emission spectroscopy.

Because of all the non-radiative processes occurring, the observed fluorescence lifetime is given by

$$\tau_F = (k_F + k_{ic} + k_{is} + k_q[Q])^{-1} \qquad 2.27$$

k_F, k_{ic}, k_{is} and k_q stand for the rate of decay by fluorescence, intersystem crossing, internal conversion and fluorescence quenching respectively and [Q] represents molar concentration of quencher. So, the quantum yield, ϕ_F may be written as

$$\phi_F = \frac{\tau_F}{\tau_R} \qquad 2.28$$

Since τ_R can be determined theoretically from the absorption spectrum, a measurement of the fluorescence decay rate (τ_F) is equivalent to a measurement of the quantum yield (ϕ_F).

Fluorescence measurements may be carried out in both the steady state and time-resolved modes. A brief description of the two forms of fluorescence detection is provided.

STEADY-STATE FLUORESCENCE

The sample is irradiated with light such that an equilibrium is established between the population of fluorophores undergoing excitation and those undergoing emission i.e., between fluorophores in the ground and excited states. One can thus measure the intensity of emission as a function of wavelength. This method is used to determine the quantum yields of fluorophores. The fluorescence intensity that is measured using steady-state fluorescence gives an average picture of the molecules in the excited state. A few of the properties that can be studied using the steady-state method are steady-state anisotropy, quenching, resonance energy transfer etc. However, steady-state studies are dominated by emissive states that emit more light thereby obscuring the true picture of decay processes involved. The exact time-evolution of these processes can be monitored using time-resolved methods.

TIME-RESOLVED FLUORESCENCE

Time-resolved fluorescence enables the fluorescence intensity decay to be analysed in terms of its individual decay rate components. The time-resolved method comprises the time-domain or the frequency domain method. With this method one can follow the time-evolution of fluorescence after excitation with a short pulse of light as in time-domain methods or by intensity modulated light as in the frequency domain. The time-domain method is described here.

The technique involves exciting the sample with a pulsed light source (the pulse width being as short as possible, typically in the range of nanosecond to picosecond) and

measuring the resulting fluorescence intensity decay as a function of time using the time-correlated single photon counting method.

$$I(t) = I_0 \exp(-t/\tau) \qquad 2.29$$

is a typical intensity decay equation for a sample having a single lifetime.

Here I (t) is intensity at any time t

And I_0 is the initial intensity

τ is the fluorescence lifetime

The main aim of the time-resolved method is to determine the lifetimes of fluorophores. The lifetime is the average amount of time a fluorophore spends in the excited state prior to emission.

For a single exponential decay the lifetime may be obtained by averaging t over the intensity decay of the sample

$$< t > = \frac{\int_0^\infty tI(t)dt}{\int_0^\infty I(t)dt} = \frac{\int_0^\infty t\exp(-t/\tau)dt}{\int_0^\infty \exp(-t/\tau)dt} \qquad 2.30$$

On integrating the above equation and taking the ratio the average value of time spent in the excited state is observed to be equal to τ.

$$<t>=\tau \qquad 2.31$$

A schematic of the time-resolved set up is given below.

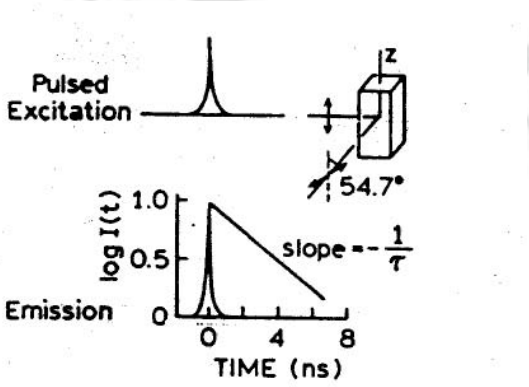

Figure2.1: Time-domain lifetime measurements (J. R. Lakowicz, Principles of Fluorescence Spectroscopy, Second Edition, 1999)

For a fluorophore undergoing multi-exponential decay the time-dependent intensity is given by

$$I(t) = \sum_i \alpha_i \exp(-t/\tau_i) \qquad 2.32$$

here, the variables α_i and τ_i denote the ith fractional amplitude and the ith lifetime respectively of the decay components. Also, $\sum_i \alpha_i = 1$.

The mean lifetime may be calculated using the equation

$$\tau_m = \sum_{i=1}^{n} \alpha_i \tau_i \qquad 2.33$$

In the above equation τ_m denotes the mean lifetime, τ_i. The summation is over n lifetime components. The mean lifetime is proportional to the area under the intensity decay curve.

A simple relation exists between the steady state fluorescence intensity and time-resolved decay parameters. The steady-state observation is actually an integrated time average over the time-resolved phenomena. Consider a fluorophore with a single decay time (τ) and a single rotational correlation time (θ)

$$I(t) = I_0 e^{-t/\tau}$$
$$r(t) = r_0 e^{-t/\theta} \qquad 2.34$$

The steady state intensity is given by the relationship

$$I_{ss} = \int_0^\infty I_0 e^{-t/\tau} dt = I_0 \tau \qquad 2.35$$

The time-resolved method has several advantages over the steady-state method viz., it is independent of the concentration of the sample and the presence of multiple kinetic components may be discerned from the lifetimes obtained. Time-resolved measurements can also reveal the type of quenching that is taking place in a system, viz., static or dynamic. A detailed picture of excited state photophysics requires the use of time-resolved techniques.

Instrumentation Involved in Time-Resolved Fluorescence Measurements

In time-resolved fluorescence measured in the time-domain, photons are detected using time-correlated single-photon counting method (TCSPC) (Goodsell, 1991; Shiraki, 2002; Demas, 1983; Birch and Imhof, 1991; Ware, 1971). The fluorescence photons are time-correlated to the excitation pulses. The measurement relies on the concept that the probability distribution of the emission of a single photon after an excitation yields the actual intensity against time distribution of all the photons emitted as a result of the excitation. By recording the single photon emission after a large number of excitation events, the experiment reconstructs this probability distribution.

A TCSPC schematic is given below (fig 2.2)

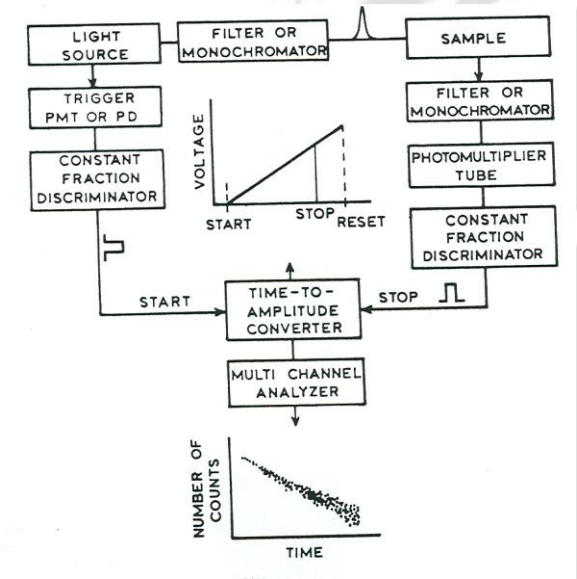

Figure 2.2 Setup for time-correlated single photon counting. The figure has been adapted from Principles in Fluorescence Spectroscopy by J. R. Lakowicz, second edition, 1999.

TCSPC is a digital technique, counting photons that are time-correlated to the excitation pulse. An essential component of the set up is a time-to amplitude converter (TAC) which is analogous to a fast stopwatch.

The experiment begins with the lamp or laser pulse, which excites the sample and starts the time measurement clock (TAC). The sample is repetitively excited using a pulsed light source, in our case with light from a nanoLED. Each pulse is optically monitored, by a high-speed photodiode or photomultiplier (PMT), to produce a start signal, which is used to trigger the voltage ramp of the TAC. The voltage ramp is stopped when the first

fluorescence photon from the sample is detected. The TAC provides an output pulse whose voltage is proportional to the time between start and stop signals. A multichannel analyzer (MCA) converts this voltage to the time channel using an analog to digital converter (ADC). Summing over many pulses, the MCA builds up a probability histogram of counts versus time channels. The experiment is continued until one has collected more than 10,000 counts in the peak channel. The constant fraction discriminators (CFD) are used to discriminate signal from noise.

A basic criterion of the TCSPC method is that only one fluorescence photon be detected per 100 excitation pulses. Under these conditions the histogram of the photon arrival times represents the true intensity decay of the sample. Non-adherence to this criterion will lead to pile up and subsequently erroneous lifetime decay.

A few of the phenomena encountered in fluorescence spectroscopy are described below, with emphasis on those involving the technique of time-resolved fluorescence.

COLLISIONAL OR DYNAMIC QUENCHING

Fluorescence quenching is a process that results in decrease of fluorescence intensity. Various types of molecular interactions can result in quenching, viz., fluorescence resonance energy transfer, excited state reactions, collisions with molecules of quencher and formation of ground state complexes. There are various atoms and molecules that serve as quenchers. Heavy atoms like iodide lead to quenching by the spin-orbit interaction. Molecular oxygen is also a very efficient quencher. Oxygen is a paramagnetic molecule and on collision with excited organic species promotes intersystem crossing.

Quenching may occur in two ways viz., by static and dynamic quenching. The topic of collisional/dynamic quenching is described here to a greater extent since we have employed it in the work presented here in this thesis.

In static quenching, the fluorophores form nonfluorescent complexes in the ground state thereby leading to a decrease in concentration of fluorophores undergoing excitation and lead to a decrease in fluorescence intensity.

Schematic showing static quenching

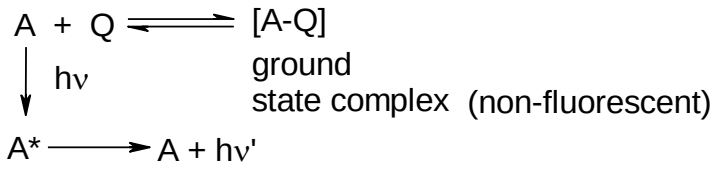

In the above schematic, A stands for the fluorophore, Q denotes the quencher and [AQ] denotes the ground-state complex that is formed on interaction between the fluorophore and the quencher in the ground state.

In dynamic or collisional quenching, collisions of the excited state fluorophores with quenchers lead to depopulation of the excited state due to dissipation of excited state energy as heat.

Schematic showing dynamic / collisional quenching

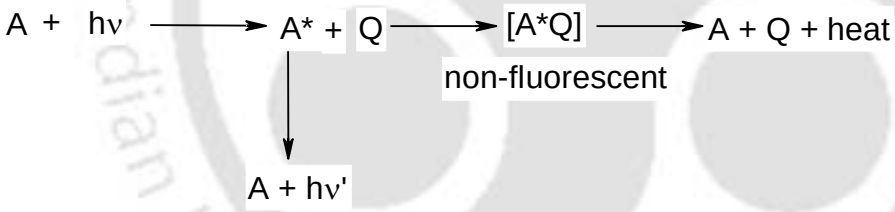

Like in the previous schematic, A denotes the fluorophore and Q the quencher. [A*Q] stands for the non-fluorescent complex formed in the excited state.

So while static quenching takes place in the ground state collisional quenching occurs in the excited state.

The best method to differentiate the two forms of quenching is by measuring the lifetime of the sample. If collisional quenching occurs, the excited state population decreases and leads to a decrease in the lifetime of the excited state. In the case of static quenching, however, the uncomplexed fluorophores are still excited and once excited their lifetime remains unaffected, hence $\tau_0/\tau = 1$ in cases of static quenching and greater than one in the case of dynamic quenching.

The equation used to describe collisional quenching is the Stern-Volmer equation

$$\frac{\tau_0}{\tau} = 1 + k_q \tau_0 [Q] = 1 + K_{SV}[Q] \qquad 2.36$$

here K_{SV} is called the Stern-Volmer constant or the dynamic quenching constant,

k_q is the bimolecular quenching constant

τ_0 is the unquenched lifetime of the fluorophore

τ is the lifetime of the fluorophore in the presence of quencher and

[Q] is the molar concentration of quencher.

The bimolecular quenching rate constant gives the efficiency of quenching. In case of diffusion controlled quenching, k_q has values close to $1x10^{10}M^{-1}s^{-1}$. It is related to the frequency of collisions between freely diffusing molecules.

The collisional frequency (Z) of a fluorophore with a quencher is given by

$Z=k_0[Q]$, here k_0 is the diffusion-controlled bimolecular rate constant. Using the Smoluchowski equation, the constant may be calculated as follows

$$k_0 = \frac{4\pi RDN}{1000} = \frac{4\pi N}{1000}(R_f + R_q)(D_f + D_q) \qquad 2.37$$

where R is the collision radius, which is assumed to be the sum of the molecular radii of the fluorophore (R_f) and quencher (R_q). D is the sum of the diffusion coefficients of the fluorophore (D_f) and quencher (D_q) and N is Avogadro's number.

The collision frequency is related to the bimolecular quenching constant by the following relation $k_q=f_Qk_0$, f_Q is the efficiency of quenching. Quenchers like oxygen, acrylamide and I^- have their efficiencies near about unity.

The efficiency of quenching can be calculated provided the molecular radii and diffusion coefficients are known. The diffusion coefficients may be determined by using the Stokes-Einstein equation $D=kT/6\pi\eta R$, where k is Boltzmann's constant, η is the viscosity of the solution, T is the absolute temperature and R is the molecular radius.

Fluorescence Anisotropy

Fluorescence anisotropy gives the extent of polarization of the emission from a fluorophore following its excitation by vertically polarized light. This phenomenon arises because of the existence of transition moments for absorption. In homogeneous solutions the ground state fluorophores are all randomly oriented. When exposed to polarized light, those fluorophores which have their absorption transition moments oriented along the

electric vector of incident light are preferentially excited. Hence a polarized excited state is obtained. This is also called photoselection. In the excited state, the fluorophores exist for ~10^{-9} s. In this period, rotational Brownian motion sets in and tends to depolarize the emission. The extent of depolarization depends on the rate of rotational diffusion.

Fluorophores whose rotational rates are comparable to their fluorescence lifetimes display non-zero anisotropy. Molecules which tumble too fast have their emission dipoles randomly oriented and show anisotropy values close to zero.

Anisotropy is given by the following equation:

$$r = \frac{I_{\parallel} - GI_{\perp}}{I_{\parallel} + 2GI_{\perp}} \qquad 2.38$$

Here $I_{\parallel}$ denotes the intensity of fluorescence emission when both the excitation and emission polarizers are oriented vertically and $I_{\perp}$ denotes cross orientation of the polarisers i.e., the polarizer at the excitation end is vertically oriented while that at the emission end has a horizontal orientation.

Anisotropy is a dimensionless quantity because the difference is normalized by the total intensity given in the denominator in eq 2.38.

Fluorescence emission depolarization can be expressed by another term called polarization which one comes across sometimes and has the same connotation as anisotropy. Polarisation is given by

$$P = \frac{I_{\parallel} - I_{\perp}}{I_{\parallel} + I_{\perp}} \qquad 2.39$$

In this equation the terms $I_{\parallel}$ and $I_{\perp}$ have the same meanings as described before in the equation for anisotropy.

In fact anisotropy, r, and polarization, P, are related by the following equations:

$$P = \frac{3r}{2+r}; \qquad r = \frac{2P}{3-P} \qquad 2.40$$

Theoretical expressions are simpler when anisotropy is used instead of polarization. This is especially pronounced when a mixture of fluorophores is considered. The polarization of a mixture of fluorophores with polarization P_i may be written as

$$\left(\frac{1}{P}-\frac{1}{3}\right)^{-1}=\sum_i \frac{f_i}{\left(\frac{1}{P_i}-\frac{1}{3}\right)} \qquad 2.41$$

In contrast, the average anisotropy $(\bar{r})$ is given by

$$\bar{r}=\sum_i f_i r_i \qquad 2.42$$

where r_i is the anisotropy of each individual species and f_i its corresponding fractional amplitude and $\sum_i f_i = 1$.

The above example clearly indicates why anisotropy is preferred.

The anisotropy decay of a spherical molecule following pulsed excitation is given by

$$r(t)=r_0 \exp(-t/\theta) \qquad 2.43$$

Where r_0, also called initial anisotropy is the anisotropy at t=0, and θ is the rotational correlation time of the molecule. The initial anisotropy may also be given by

$$r_0=\frac{2}{5}\left(\frac{3\langle\cos^2\beta\rangle-1}{2}\right) \qquad 2.44$$

r_0 will have a value of 2/5 based on the principle of photo-selection if one assumes that the absorption and emission dipoles are collinear. In cases where the absorption and emission dipoles are displaced by an angle β relative to each other, the initial anisotropy is given by eq 2.44. r_0 is also called the fundamental anisotropy and is observed in the absence of other depolarizing forces such as rotational diffusion or energy transfer.

The anisotropy that is measured in the presence of rotational diffusion is given by

$$r=\frac{2}{5}\left(\frac{3\langle\cos^2\beta\rangle-1}{2}\right)\left(\frac{3<\cos^2\theta-1>}{2}\right) \qquad 2.45$$

where $<\cos^2\theta>$ is the average angular displacement of the fluorophores with respect to the axis of the incident light. This relationship between the different causes of

depolarization in eq 2.45 is also called Soleillet's rule (Soleillet, 1929; Kawski, 1986; 1993).

In systems where multiple populations exist, the anisotropy at a given time t will be given by

$$r(t) = r_0 \sum_i g_j \exp(-t/\theta_j) \qquad 2.46$$

where g_j are the fractional amplitudes which decay with the correlation time θ_j. $\sum g_j$ in the above equation = 1.0. In this case the time-zero anisotropy is equal to r_0. The presence of multiple correlation times is often observed for macromolecules. The different components reflect the presence of different rotational modes viz., localized and global diffusion. The localized diffusion could arise due to independent rotation of a domain of the macromolecule. It is also called segmental motion (figure 2.3). Global diffusion (figure 2.3) reflects the overall rotational diffusion of the entire macromolecule for example, the anisotropy decay of dansyl conjugated IgG on analysis revealed two correlation times of 7.7 ns and 123 ns with amplitudes 0.075 and 0.14 respectively. The smaller correlation time component can only rise from some form of internal motion while the larger component may be attributed to to the rotation of the entire γ-globulin molecule (Wahl, 1969; Steiner, 1991).

Multiple correlation times may also arise due to non-spherical symmetry of fluorophores. The anisotropy decays of non-spherical molecules are usually described in terms of prolate and oblate ellipsoids (fig 2.4).

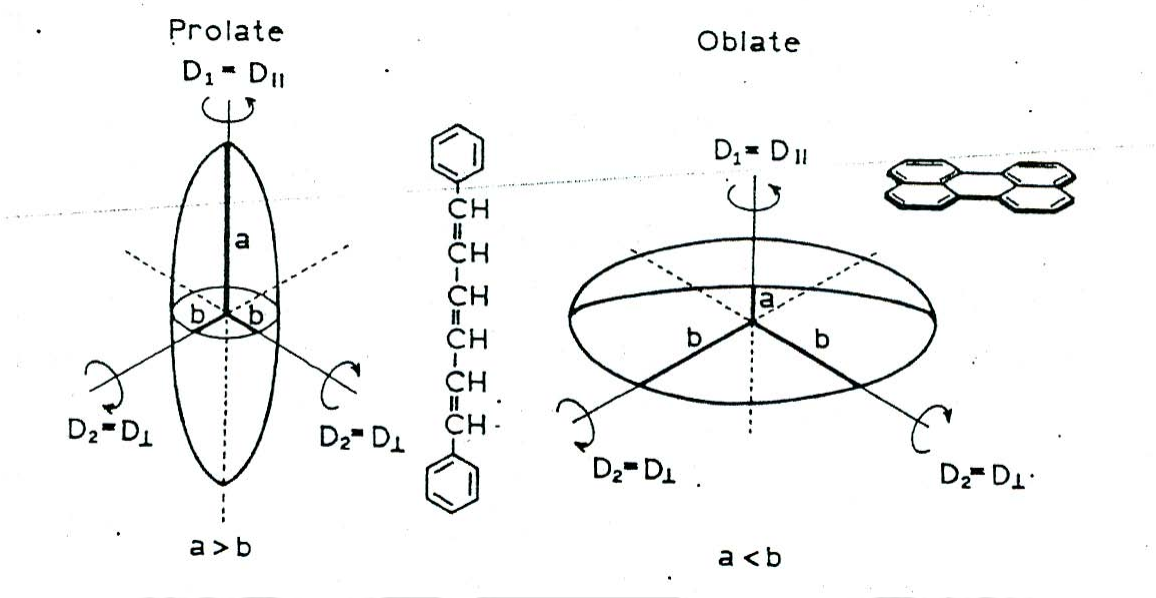

Figure 2.4 Prolate and oblate ellipsoids of revolution

The expected anisotropy decays of ellipsoids have been described in several review articles (Steiner, 1991; Brand et al., 1985; Barkley, 1981). They are actually modifications of the theory for rotational diffusion of ellipsoids and their measurements by fluorescence polarization reported by F. Perrin (Perrin, 1929a; 1929b; 1936a; 1936b). For a rigid ellipsoid with three unequal axes the anisotropy decays with five correlation times according to theory (Belford et al., 1972), however, in practice, only three rotational correlation times are expected for a non-spherical molecule since two pairs of correlation times will be very close in magnitude (Small and Isenberg, 1977).

Steady-state anisotropy is the average of the anisotropy decay (measured in the time-domain) over the intensity decay of the fluorophore.

$$r_{ss} = \frac{\int_0^\infty r(t)I(t)dt}{\int_0^\infty I(t)dt} \qquad 2.47$$

where r(t) is given by eq. 2.46 and I(t) is given by eq 2.32

For a single-exponent intensity decay, the steady-state anisotropy may also be written in the form of a Perrin equation

$$r_{SS} = \frac{r_0}{1+\frac{\tau}{\theta}} \qquad 2.48$$

In the time-domain, the polarized intensity decays $I_{\parallel}(t)$ and $I_{\perp}(t)$ are acquired in order to measure the rotational correlation time

$$r(t) = \frac{I_{\parallel}(t) - GI_{\perp}(t)}{I_{\parallel}(t) + 2GI_{\perp}(t)} \qquad 2.49$$

G in the above equation is called the G-factor which is the ratio of the sensitivity of the detection system for vertically and horizontally polarized light.

The rotational correlation time θ is the time taken by the anisotropy comes down to 1/e of its initial value. θ is sensitive to temperature (T), bulk viscosity (η) and hydrodynamic volume of a fluorophore and according to the Stokes-Einstein equation may be written as follows

$$\theta = \frac{\eta V}{RT} \qquad 2.50$$

Steady-state anisotropy and time-resolved anisotropies are both useful indicators of the rotational diffusion of a fluorophore, however, much more information is obtained from anisotropy decays –the anisotropy decay of a macromolecule contains information about its shape and flexibility. The steady-state anisotropy yields a single value irrespective of the form of r(t). The figure below shows typical anisotropy decay profiles of the protein chicken egg white lysozyme. In curve (a) the anisotropy decays to almost zero whereas in curve (b) there is a significant anisotropy at t=40 ns. The anisotropy at the end of an anisotropy decay profile is also called residual anisotropy, denoted by r_{∞}. Residual anisotropy is an indication of hindered rotation of the fluorophore under study. The origin of hindered rotation in this case (figure 2.5) is the formation of aggregates of the protein lysozyme in pH 12.2 buffer (details are available in chapter 6)

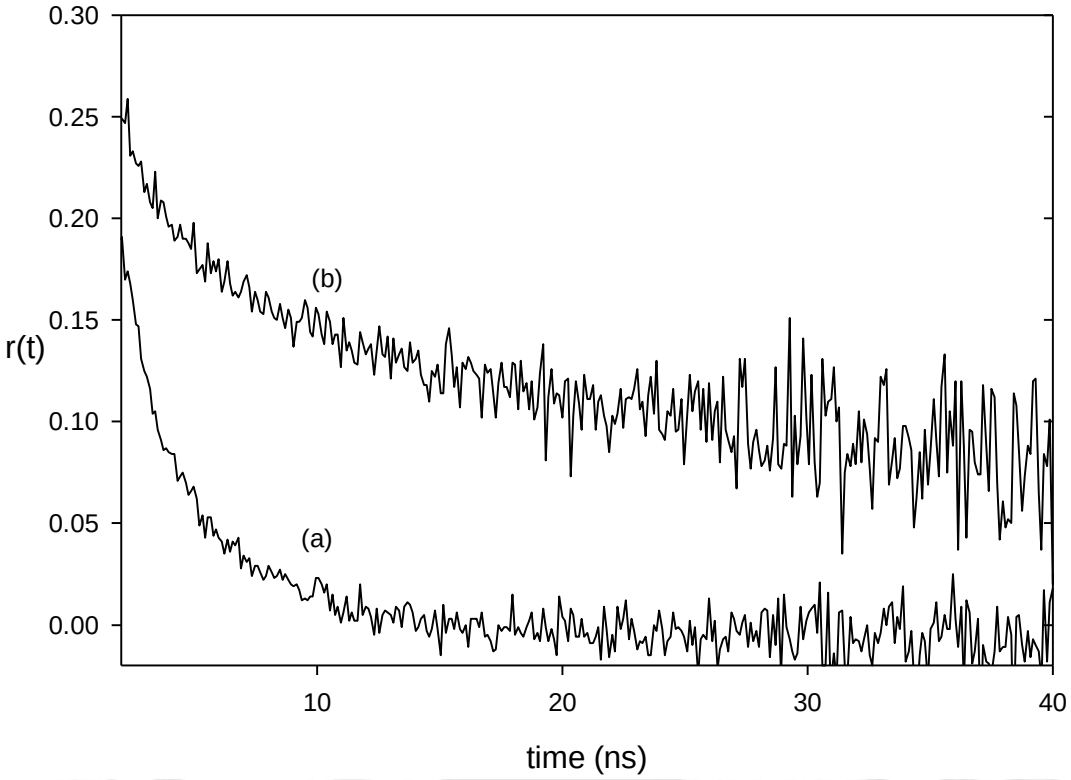

Figure 2.5 Anisotropy decay of chicken egg white lysozyme in (a) pH 7 buffer and (b) pH 12 buffer after ~ 6hours.

Time-Resolved Fluorescence Decay Analysis

Time-resolved intensity decay analysis

Time – resolved fluorescence data were collected using the technique of time-correlated single photon counting (TCSPC) described earlier in the thesis. In theTCSPC method, the intensity decay profile N (t_k) that is measured, is a convolution of the instrument-response function L (t_k) with the actual intensity decay of the sample, I (t_k). These functions are in terms of discrete times (t_k), because the counted photons are collected in channels, each with a known time (t_k) and width (Δt). The procedure involved in convolution is depicted below (fig. 2.6)

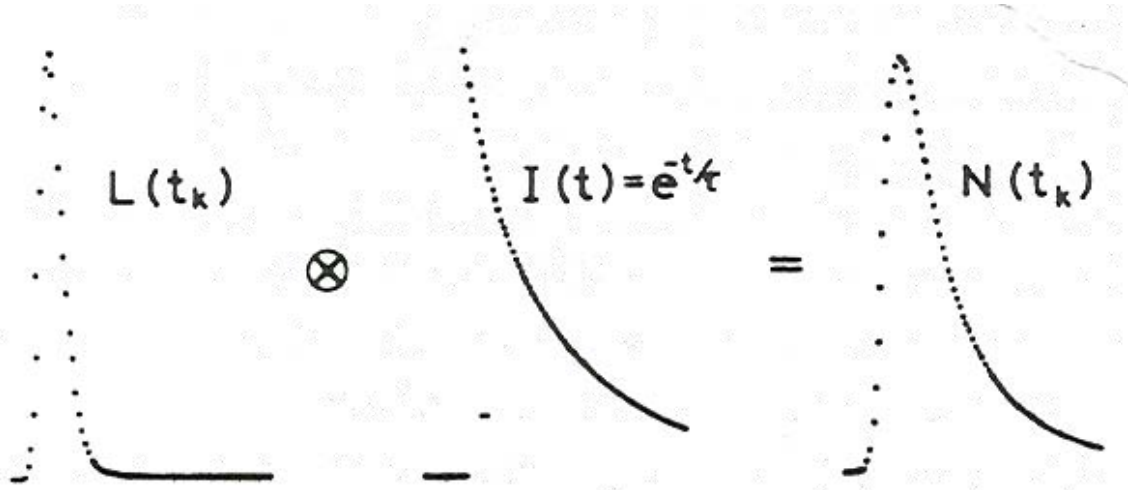

Figure 2.6 The figure shows the convolution of an impulse response function I(t) with a lamp profile $L(t_k)$ to yield the measured decay $N(t_k)$ The intensity decay shown in the above figure corresponds to that of a mono-exponential decay.

In general the intensity decay may be written as

$$I(t) = \sum_{i}^{n} \alpha_i \exp(-t/\tau_i) \qquad 2.51$$

$\Sigma\alpha_i$ is normalized to unity. The α_i values are called the preexponential factors and τ_i values denote decay times and n is the number of decay times.

The instrument response function also called the lamp function is the response of the instrument to a zero lifetime sample. This curve is collected using a dilute scattering solution. In our case we used a diluted solution of $Mg(OH)_2$. This decay represents the shortest time that can be measured by the instrument. The instrument response function is usually quite narrow, in our case the fwhm was ~1.3 ns.

The measured data $N(t_k)$ is the intensity decay of the sample as measured by the instrument. This has to be analyzed in order to determine the lifetime of the sample.

The data are analyzed using the method of non-linear least squares and iterative reconvolution.

In the non-linear least squares analysis one starts with a model which is assumed to describe the data, in this case an intensity decay law

A monoexponential decay $I(t)=I_0\exp(-t/\tau)$ is assumed with estimated values of the parameters I_0 and τ. This is then convoluted with the instrument response function to provide the calculated decay $N_c(t_k)$. This calculated decay is then compared with the experimentally determined decay $N(t_k)$. The goodness of fit parameter χ^2 is calculated to acertain the goodness of the fit.

$$\chi^2 = \sum_{k=1}^{n} \frac{1}{\sigma_k^2}[N(t_k) - N_c(t_k)]^2 = \sum_{k=1}^{n} \frac{[N(t_k) - N_c(t_k)]^2}{N(t_k)} \qquad 2.52$$

As the value of χ^2 in terms of data points is not always convenient to interpret, another parameter called the reduced χ^2 is used, denoted by χ_R^2,

$$\text{The value of } \chi_R^2 = \frac{\chi^2}{n-p} = \frac{\chi^2}{\upsilon} \qquad 2.53$$

where n is the number of data points, p is the number of floating parameters, and $\nu=n-p$ is the number of degrees of freedom.

If there is agreement between the calculated and experimentally determined data, χ_R^2 has a value close to unity. If the value of χ_R^2 is greater than 1, a new set of parameters are chosen by modifying the older parameters and the processes of convolution and matching are repeated iteratively till a χ_R^2 minimum is obtained. This process is also called iterative reconvolution. If after successive iterations there is no improvement in the value of χ^2_R then the analysis will terminate.

Another parameter used for inspecting the quality of fit is the distribution of weighted residuals or deviation plots. The difference between the measured and calculated intensities yields the deviations (D_k). These deviations when weighted by their standard deviations at each data point are plotted against time we get the deviation plots.

$$D_k = \frac{I(t_k) - I_c(t_k)}{\sqrt{I(t_k)}} \qquad 2.54$$

A good fit is indicated by the randomness of the residual distribution. Any distinct pattern in the residual distribution indicates an improper fit or perhaps a wrong decay model.

CONVOLUTION INTEGRAL

The impulse response mentioned in the previous paragraph is the intensity decay that would be observed if the instrument response function were a δ-function. However, in our case the FWHM of the instrument response is 1.3 ns and since the lifetime of the sample being measured is also in nanoseconds the measured decay will have a significant contribution from the IRF. The process of extracting the intensity decay data from the measured data is called iterative-reconvolution described earlier. Mathematically, the concept of convolution is expressed as follows (Birch and Imhof, 1991).

Each δ-function excitation is assumed to excite an impulse response function at t_k,

$$I_k(t) = L(t_k)I(t - t_k)\Delta t \qquad (t > t_k) \tag{2.55}$$

The term $(t-t_k)$ appears because the impulse response is started at $t=t_k$ and it is assumed that there is no emission before excitation (at $t<t_k$).

The measured decay N (t_k) is the sum of the impulse responses created by all the individual δ-function excitation pulses occurring until t_k

$$N(t_k) = \sum_{t=0}^{t=t_k} L(t_k)I(t - t_k)\Delta t \tag{2.56}$$

For small values of Δt, this equation can be expressed as an integral;

$$N(t_k) = \int_0^t L(t')I(t - t')dt' \tag{2.57}$$

According to this expression the experimentally measured intensity at time t is given by the sum of the intensities expected for all the δ-function excitation pulses which occur until time t. New intensity decays are created in the sample as long as there is nonzero intensity in L (t_k).

Time-resolved Anisotropy decay analysis

The time-resolved anisotropy decay data were analyzed based on the equations

$$I_{\parallel}(t) = \frac{1}{3}I(t)[1 + 2r(t)] \tag{2.58}$$

$$I_{\perp}(t) = \frac{1}{3} I(t)[1 - r(t)] \qquad 2.59$$

$$r(t) = r_0 \sum_i g_i \exp(-t/\theta_i) \quad \text{i=1 or 2} \qquad 2.60$$

Where r_0 is the initial anisotropy, g_i is the amplitude of the ith rotational correlation time θ_i such that $\Sigma_i g_i = 1$. $I_{\parallel}(t)$ and $I\perp(t)$ correspond to the intensity decay collected with the polarisers in the parallel and crossed orientations respectively. Typical intensity decay profiles involved in the measurement of anisotropy decay are shown in figures 6.8-6.15 towards the end of chapter 6.

In the case of a conjugated protein where the decay is biexponential, θ_1 corresponds to segmental motion of the covalently attached dansyl probe and θ_2 corresponds to the overall tumbling motion of the protein, respectively.

The method of non-linear least squares based on the Marquardt algorithm (Bevington and Robinson, was employed to extract the amplitude parameters α_i, g_j corresponding to the lifetimes τ_i, and correlation times θ_j respectively. $I_{\parallel}$ and $I\perp$ were analyzed using the measured instrument response function (IRF).

The values obtained from the above analysis were employed to calculate the steady-state anisotropy r_{ss} (Swaminathan et al., 1994a).

$$r_{ss} = \frac{r_0 \sum_i \sum_j \alpha_i g_j \left(\frac{1}{\tau_i} + \frac{1}{\theta_j} \right)^{-1}}{\sum_i \alpha_i \tau_i} \qquad 2.61$$

The calculated values of steady-state anisotropy were then compared with the values obtained from steady-state measurements.

Enzyme Kinetics

Enzymes are proteins that act as catalysts viz., they accelerate the rate of a reaction without altering the overall standard Gibbs-energy change in the reaction. Enzyme kinetics is concerned with measuring the rates of enzymatic reactions, and with factors that affect these rates. A few of the important factors that affect enzymatic reactions are

the concentrations of enzyme and substrate, pH, temperature and the presence of cofactors and metal ions.

A simplifying approach in kinetics experiments is to measure the initial rate, designated v_0 when substrate concentration, [S] is much greater than that of the enzyme [E]. If only the beginning of the reaction is monitored (the first 60 seconds or less), changes in [S] can be limited to a few percent and may be assumed constant. v_0 can the be measured as a function of initial substrate concentration. Plots of v_0 against [S] when [E] is held constant yield a hyperbola (figure 2.7). At low concentrations of substrate, v_0 increases almost linearly with increase in [S]. At higher substrate concentration, v_0 increases by smaller and smaller amounts with increasing [S], finally a point is reached when v_0 changes by vanishingly small increments with increasing [S]. In this plateau like region, v_0 is close to the maximum velocity or maximum initial rate, V_{max} of the reaction.

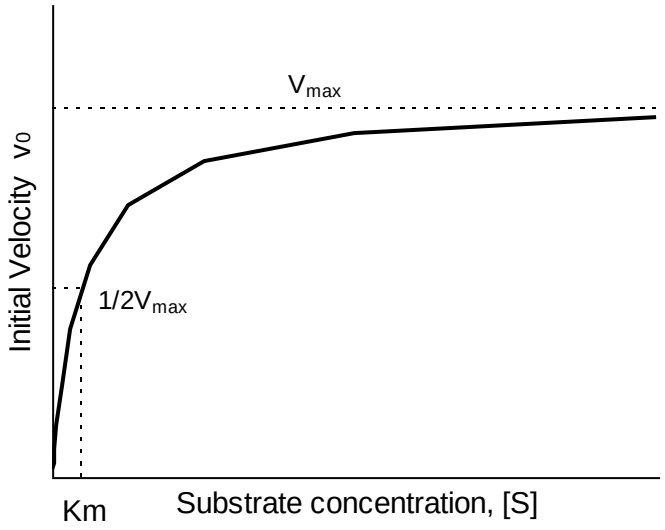

Figure 2.7 Plot of initial rate of reaction against initial substrate concentration for a reaction obeying Michaelis-Menten kinetics

A typical enzyme catalyzed reaction involving a single substrate may be written as

$$E + S \underset{k_{-1}}{\overset{k_1}{\rightleftharpoons}} [ES] \xrightarrow{k_2} E + P \qquad 2.62$$

In the above reaction given by equation 2.62, E, S, P and [ES] stand for the enzyme, substrate, product and the intermediate enzyme-substrate complex respectively. k_1, k_{-1} and k_2 are rate constants.

This reaction scheme was postulated by Michaelis and Menten in 1913. The [ES] complex is the key to understanding the kinetics of enzyme catalyzed reactions.

In the initial stages of the reaction when the enzyme is first mixed with substrate, the concentration of [ES] increases from zero, and the condition is called the pre-steady-state. This period is usually very short and lasts just a fraction of a second. The reaction quickly achieves a steady-state where [ES] remains almost constant over time.

The following equation is obeyed

$$\frac{d[ES]}{dt} = k_1[E][S] - k_{-1}[ES] - k_2[ES] = 0 \qquad 2.63$$

The v_0 that we measure actually reflects the steady-state and is limited to the early part of the reaction, and analysis of these initial rates is referred to as steady-state kinetics.

The equation relating the initial rate v_0 to $[S]_0$ may be written as

$$v_0 = \frac{V_{max}[S]_0}{K_m + [S]_0} \qquad 2.64$$

The above equation was derived by Michaelis and Menten from the basic hypothesis that the rate limiting step in enzymatic reactions is the breakdown of the ES complex to product and free enzyme. K_m is called the Michaelis-Menten coefficient and may be written as

$$K_m = \frac{k_{-1} + k_2}{k_1} \qquad 2.65$$

K_m has the units of concentration and as shown in the above figure corresponds to substrate concentration at (1/2) V_{max}.

The maximum velocity $V_{max} = k_2 [E]_0$, where $[E]_0$ denotes the total enzyme concentration and k_2 is rate limiting. This approximation is valid only at the initial stages of the reaction, since the concentration of substrate at this stage is almost equal to the initial concentration.

At very low substrate concentrations, the rate of the reaction is given by

$v = \frac{k_2}{K_m}[E]_0[S]$, i.e, the rate is bimolecular and k_2/K_m is a second-order rate constant.

Conversely, at very high substrate concentrations, the rate is given by

$v = k_2[E]_0$ and may be denoted by V_{max}, the maximum velocity of the reaction.

k_2 is the apparent first-order rate constant and may be denoted by k_{cat}. k_{cat} is also called the turnover number. It may be defined as the number of substrate molecules converted to product in unit time per molecule of enzyme when the enzyme is saturated with substrate.

The Michaelis-Menten equation, equation 2.63 may be algebraically transformed to equations that are more helpful in plotting experimental data. A common transformation is taking the reciprocal on both sides of the Michaelis-Menten equation:

$$\frac{1}{v_0} = \frac{K_m}{V_{max}} \frac{1}{[S]_0} + \frac{1}{V_{max}} \qquad 2.66$$

This equation is also called the Lineweaver-Burke equation.

Another form of the Michaelis Menten equation also called the Eadie-Hofstee equation may be written as follows

$$v_0 = -K_m \frac{v_0}{[S]_0} + V_{max} \qquad 2.67$$

The kinetics discussed above corresponds to the simple case of a one-substrate enzyme catalyzed hydrolysis. There are instances where more than one substrate may be present, in which case the equations will be more complex. The presence of inhibitors also affects the kinetics of the reaction depending on the nature of the inhibition viz., whether the inhibition is reversible or irreversible. Reversible inhibition may be further classified into the following three types viz., competitive, uncompetitive or mixed. A competitive inhibitor competes with the susbtrate to bind at the active site. In such cases, there is an increase in the apparent K_m of the reaction as compared to the K_m in the absence of the inhibitor. In uncompetitive inhibition, the inhibitor binds at a site that is distinct from the active site and such reactions are marked by decrease in apparent V_{max} and is also accompanied by a lowering of K_m. A mixed inhibitor binds at a site distinct from the active site and may bind either to the enzyme or to the enzyme-substrate complex. A special case of mixed inhibition is non-competitive inhibition in which only V_{max} is affected but not the K_m.

Irreversible inhibitors bind covalently to the enzyme or destroy a functional group on an enzyme that is important for its catalytic activity. They may also have stable non-covalent interactions with the enzyme.

Finally enzyme activity depends on pH. Every enzyme has a pH at which it has its optimal activity. This is because amino acid residues at the active site may act as weak acids and bases and the catalytic activity of the enzyme depends on their states of ionization for example alkaline phosphatase which is a phosphomonoesterase has its optimum activity in alkaline pH regions, pepsin which hydrolyses peptide bonds of proteins during digestion in the stomach has a pH optimum of 1.6.

Indian Institute of Technology Guwahati

CHAPTER 3
MATERIAL AND METHODS

This chapter contains a list of the materials used and a detailed description of the procedures and experimental methods followed. It has been split into different sections.

SECTION 1

Here we discuss the chemicals used and the procedures followed in the experiments that are described in the 4th chapter of the thesis.

1.1 Chemicals used

Alkaline phosphatase (P-7640) isolated from bovine intestinal mucosa was purchased from Sigma-Aldrich chemicals Pvt. Ltd. p-nitrophenyl phosphate di sodium salt was purchased from Sisco Research Laboratories. Ficoll 70, Ficoll 400 and glycine were all purchased from Sigma-Aldrich chemicals Pvt. Ltd. Dextrans of molecular weights 15, 40, 70, 200 and 500 kDa from *leuconostoc mesenteroides* were purchased from Fluka. The polydispersity of the dextrans were typically less than 2.0 as reported by the manufacturer. NaOH, KI and sucrose were purchased from E. Merck and Sodium-salt of fluorescein was purchased from Sigma-Aldrich chemicals Pvt. Ltd.

Other materials used include a pair of 1 cm path length quartz cuvettes (HELLMA precision cells) for uv-visible absorbance measurements.

1.2 Solutions prepared

1.2.1 Enzyme Hydrolysis

The activity of alkaline phosphatase was tested at different pH and was observed to be optimal at the alkaline pH of 9.5. We used a 50 mM pH 9.5 glycine buffer to monitor the hydrolysis reactions.

The pH 9.5 glycine buffer was prepared by dissolving 50 mM glycine in de-ionised water and adjusting the pH of the solution to 9.5 using 10 N NaOH with the help of a pH meter. Once the buffer is made all the solutions are prepared in it. The solutions that were prepared are described below. The concentrations mentioned below correspond to the final concentrations of the reactants in the cuvette.

- 1 mM para nitrophenyl phosphate solution
- 0.3 mg/ml (or 5.1 units/ml) alkaline phosphatase
- 15-200 kDa dextrans of concentrations 0, 5, 10, 20, 25 and 30% w/w respectively.
- 500kDa dextran of concentrations 0, 5, 10, 15, 20and 25% w/w respectively
- 70 and 400 kDa ficoll solutions from 0 to 30% w/w

1.2.2 Dynamic Fluorescence Quenching

For the dynamic or collisional quenching experiments, a 50 mM pH 9.5 glycine buffer was again used since the fluorescence of fluorescein is optimal in the alkaline pH region. Thus, in this case too, all solutions were prepared in pH 9.5 buffer. The solutions prepared were

- 0.5 μM fluorescein
- 0-300 mM KI (quencher)
- 0-25 % w/w solutions of 15, 70, 200 and 500 kDa dextrans and
- 0-25% w/w 70 kDa Ficoll

The concentrations mentioned above correspond to the final concentrations of reactants in the cuvette.

The concentration of fluorescein was determined by measuring its absorbance and by using the calculated value of its molar extinction coefficient, 83,000 $M^{-1}cm^{-1}$ at 492 nm (Haugland, 2002). For fluorescence measurements the concentration of fluorescein in the cuvette was maintained at ~0.5 μM

The KI solutions used for the quenching experiment were prepared by diluting a stock solution of 1 M KI prepared in the buffer.

1.3 Enzyme Hydrolysis

1.3.1 *Hydrolysis of p-nitrophenyl phosphate by alkaline phosphatase***:**

For the enzyme hydrolysis experiment a double-beam UV-visible spectrophotometer (Hitachi U-2001) was used. The hydrolysis reaction was monitored by following the absorbance of the product p-nitro phenol at 450 nm as a function of time.

A typical reaction mixture contained 2 μM alkaline phosphatase (which is equivelent to 5 units/ml) and 1mM para nitrophenyl phosphate (PNPP). The substrate concentration was

well above the measured K_m (~0.4 mM) under the reaction conditions employed. A high substrate to enzyme concentration was maintained analogous to similar ratios observed inside living cells (Albe et al., 1990). The concentrations of ficolls and dextrans were varied as mentioned above and the total weight of the reaction medium was kept constant at 0.5 g.

The dextran concentrations were expressed in fractional volume occupancies which were calculated by multiplying the concentration of dextran in g/ml (by converting the concentration in % w/w using the measured values of solution density) with the specific exclusion volume of dextran 0.75 ml/g reported earlier by Minton and his coworkers (Hatters et al., 2002; Rivas et al., 1999).

The values of fractional volume occupancies were found to be:

Concentration in %w/w of dextran	Fractional volume occupancy
0	0
5	0.038
10	0.078
15	0.119
20	0.161
25	0.207
30	0.253

The reaction was initiated by forcefully mixing the enzyme (in buffered aqueous medium inside a cuvette) with an aqueous buffered mixture containing PNPP and crowding agent, using a syringe to ensure complete mixing. The progress of the reaction was monitored using a spectrophotometer. The initial rate V was obtained by linear regression of the first 10 points of the absorbance vs. time data. This way, inhibition from appreciable build up of product, inorganic phosphate is avoided. The rate observed under identical conditions in the absence of crowding species yielded V_0.

The normalized rate was calculated as:

$$V_{norm} = (V/V_0) * 100 \qquad 3.1.1$$

The value of 100 was chosen to avoid negative numbers in the log scale. The points depicted in the figures are averages of at least four independent experiments done on different days. Experiments were carried out at 25^{o}C.

1.3.2 *Fitting enzyme kinetics data*

When the rate at which enzyme and substrate encounter each other in solution is rate limiting, the dependence of the observed rate V on the fractional volume occupancy may be written as follows (Minton, 1981):

$$V = V_0 \exp(-g\phi) \qquad 3.1.2$$

Here V_0 is the rate observed in the absence of the crowding agent.

This can be expressed in terms of V_{norm} as follows:

$$V_{norm}(\phi) = A \exp(-g\phi) \qquad 3.1.3$$

Here V_{norm}, the normalized rate is a function of ϕ, while, A is a constant and 'g' is another constant which is a function of the relative sizes and shapes of the enzyme, substrate and crowding macromolecule. The dependence of V_{norm} on ϕ for dextrans of different sizes was fitted to equation 3.1.3.

1.4 Dynamic or Collisional Quenching

The effects of dextrans, ficolls and sucrose on the bimolecular quenching constant were determined using this method. Fluorescence lifetimes were measured by nano-second time-domain fluorimetry, using the 'Fluorocube' supplied by IBH, Glasgow, UK. The samples of fluorescein were excited by pulses of light from a pulsed light source, in our case a nanoLED.

The fwhm of the pulse used was ~1.32 ns and the repetition rate of the pulses was 1 MHz. The fluorescence intensity (in counts) was measured with the emission polariser in the magic angle orientation (54.7^{o}). An OG 550 long pass filter was used at the emission end. The fluorescence intensity was detected using a cooled Model TBX-04 photon detector module (IBH, Glassgow) operating in the time-correlated single photon counting mode [O'Connor and Phillips, 1984]. The output from the detector was fed to a multichannel analyzer card interfaced to a personal computer. The fluorescence peak counts were measured upto a value of 10000 counts and the time interval between

successive points in the raw intensity/time data was 0.11295 ns. The data were fitted to a single exponential using the method of non-linear least squares with iterative reconvolution of the measured lamp profile. The goodness of fit was evaluated from the randomness of the residuals and the reduced χ^2. The fluorescence lifetime of fluorescein (0.5 uM) was measured (in a medium buffered at a pH of 9.5) in the presence of a series of concentrations of iodide from 0 to 200 mM. The medium also contained 0.1 mM $Na_2S_2O_3$ to prevent the formation of I_3^-. The bimolecular quenching constant, k_q was calculated from the Stern-Volmer equation given below (Lakowicz, 1999)

$$\tau_0/\tau=1+k_q\tau_0\,[Q] \qquad 3.1.4$$

Here, τ_0 is the fluorescence lifetime in the absence of the quencher, while τ is the lifetime in the presence of the quencher. Q refers to the molar concentration of the quencher in the medium. Our experiments on the dynamic quenching of fluorescein by iodide in aqueous buffer yielded a k_q of ~ $2.7x10^9$ $M^{-1}s^{-1}$ at 298 K. The above experiment was repeated in the presence of 20% w/w of each of the following dextrans, namely, 15kDa, 200kDa and 500 kDa dextran. The fluorescence lifetime of fluorescein in the absence of dextran (~ 4 ns) was unaffected by the added presence of dextrans mentioned above. Also the Stern-Volmer plots were linear in the added presence of dextrans indicating a single uniform environment for fluorescein in solution in the midst of dextrans.

SECTION 2

In this section, the experimental details corresponding to chapter 5 are presented.

2.1 **Chemicals used**

L-lysine Monohydrochloride (SRL and Sigma-Aldrich), Glycine (Sigma-Aldrich), NaH_2PO_4 (E. Merck), NaOH (E. Merck), L-arginine (SRL), L-serine (SRL), L-glutamate (SRL), L-isoleucine (SRL), pyrene (Sigma), CH_3OH (E.Merck, H.P.L.C. grade)

Human serum albumin (99% purity, fatty acid and globulin free, product #A3782), chicken-egg white lysozyme, subtilisin Carlsberg, calf thymus histone, guanidine hydrochloride (GdnCl), poly-L-lysine hydrobromide (mol.wt. 1000-4000) were purchased from Sigma-Aldrich foreign holding company, New Delhi. A W38FW44F mutant of barstar was also used. It was isolated from a bacterial over-expression system

(Swaminathan et al., 1996).Wild type barstar was not employed because it has 3 trp residues, which can under favorable conditions lead to unwanted interference from trp-trp $\pi-\pi$ interactions.

The absorption ratio A_{300}/A_{340}, for Human Serum Albumin was 3.11, in good agreement with the value (~3.0) obtained from the spectrum reported in literature (Hagag et al., 1983).

2.2 Solutions prepared:

Solutions of the amino acids and proteins mentioned above were mostly prepared in pH 7 buffer. The procedure followed in preparing the solutions are described below.

(a) The pH 7 buffer

The buffer was prepared at two different concentrations of 50 and 100 mM NaH_2PO_4. The amino acids were all dissolved in 100mM buffer while the proteins were dissolved in the 50mM buffer.

pH 7 buffer was prepared by dissolving NaH_2PO_4 in deionised water followed by adjustment of pH to 7 using 10 N NaOH.

(b) Solutions of L-lysine hydrochloride, glycine, L-glutamate, L-serine, L-isoleucine were prepared by dissolving the respective amino acids in pH7 buffer of strength 100 mM at room temperature. Multiple concentrations of lysine solution were prepared ranging from 0.05 to 1 M. These solutions were prepared by diluting a 2 M stock solution. The other amino acids used were prepared at a single concentration of 0.5 M.

© Solutions of proteins and poly-L-lysine hydrobromide were prepared likewise by dissolving them in 50mM pH 7 buffer respectively, at room temperature.

(d) Pyrene stock solution was prepared by dissolving 495 uM pyrene in methanol (1 mg pyrene in 10 ml methanol). This was then diluted to 25 μM in 0, 0.5 and 1 M lysine solutions prepared in pH 7 buffer.

(e) Guanidinium chloride (GdnCl) solutions were prepared by dissolving 6 M GdnCl.HCl in 0.05 M NaH_2PO_4 solution, following which the pH of the solution was adjusted to 7. Solutions of urea were also prepared by dissolving 8 M urea in 0.05M NaH_2PO_4 followed by adjustment of the pH to 7 using a pH meter and 10N NaOH. Experiments with guanidinium chloride were carried out after overnight incubation of protein at room temperature in the presence of the denaturant.

The experiments were all carried out at 25^{o}C.

2.3 Distance measurements between lysine residues in a protein

3-D structures of proteins were obtained from PDB and the distances between adjacent lysine residues were calculated using the software Rasmol (Version 2.6). The protein crystals are well hydrated and so the crystal structures are assumed to be not very different from their structures in solution (Cantor and Schimmel, 1980).

2.4 UV-Visible Absorbance measurements:

Absorbance measurements were carried out in a double beam Hitachi U-2001 spectrophotometer. The amino acid and protein solutions were taken in quartz cuvettes and the absorbance measurements were repeated multiple times so that the absorbance profiles displayed in the figures are all averages of at least 10 scans.

The concentrations of proteins were ascertained by measuring absorbance of their dilute solutions in pH 7 buffer at 280 nm. The measured absorbance values were related to molar extinction coefficients of the proteins to determine their actual concentrations. The absorbance of a 1cm path length in a 1 mg/ml protein solution at 280 nm is given by

$(5700 \times n_{trp} + 1300 \times n_{tyr})/ M$,

where M is the molecular weight of the protein (Cantor and Schimmel, 1980).

Here, n_{trp} denotes the number of tryptophan residues in the protein, the molar extinction coefficient of tryptophan at 280 nm is taken to be 5700 $M^{-1}cm^{-1}$, n_{tyr} indicates the number of tyrosine residues and 1300 $M^{-1}cm^{-1}$ gives the molar extinction coefficient of tyrosine

2.5 Steady-state fluorescence measurements

Steady-state fluorescence measurements of solutions of L-lysine were performed in a Shimadzu steady-state spectrofluorophotometer (model RF-5301 PC) with a 150 W Xenon lamp as the excitation source and a PMT for light detection. The excitation and emission slit widths used were both 5 nm respectively. The emission profiles shown in the figures were obtained after subtracting out contributions from their respective blanks at the appropriate excitation wavelengths.

2.6 pH determinations

pH measurements were carried out in a pH 510 pH/mV/^{o}C meter supplied by Eutech instruments.

SECTION 3

In this section the experimental procedure followed in the 6th chapter is presented. In this chapter we studied the growth of aggregates of lysozyme in alkaline pH following covalent labeling of chicken egg white lysozyme with an amine reactive probe.

The materials used are described below.

3.1 Materials used

Chicken Egg White lysozyme used for our studies was procured from Sigma (Cat. No. L-6876). Dansyl chloride (2-dimethyl amino naphthalene-6-sulfonyl chloride) (D-23) was obtained from molecular probes (Eugene, Oregon, USA). PD-10 desalting columns containing sephadex G-25 for separating groups with M_r > 5000 Da from those with M_r< 1000 were procured from Amersham Biosciences, 1 cm path length quartz fluorescence cuvettes (HELLMA precision cells)

Some other chemicals that were used were

$NaH_2PO_4.2H_2O$ (MERCK), $NaHCO_3$ (Merck), NaOH (MERCK), HCl (MERCK), glycine (SIGMA), CABS (cyclohexylaminobutane sulphonic acid) (SIGMA), Guanidinium hydrochloride (MERCK), Tris Buffer GR (MERCK), Dimethyl Formamide (DMF) HPLC grade (MERCK), tri-sodium citrate (MERCK) and Na-acetate (MERCK), L-arginine hydrochloride (SIGMA).

3.2 Buffers used

50 mM pH 7 phosphate buffer (for the native protein), 100 mM pH 7 phosphate buffer (for testing reversibility of aggregation), 50 mM pH 12 phosphate buffer(pH dependence studies), 100 mM pH 9 bicarbonate buffer (for labeling lysozyme with Dansyl chloride), 50 mM pH 4 glycine buffer(pH dependence studies), 50 mM pH 5 acetate buffer (pH dependence studies), 50 mM pH 6 citrate buffer (pH dependence studies), 50 mM pH 9.5 glycine buffer(pH dependence studies), 50 mM pH 10.8 CABS buffer (pH dependence studies). These buffers were prepared by dissolving the respective salts in water and adjusting the pH to the required value by adding 10 N NaOH or 10 N HCl as required with the help of a pH meter.

3.3 Procedure for labeling lysozyme with Dansyl probe:

The following procedure is recommended by molecular probes for labeling using dansyl chloride (Haugland, 2002).

3.5 mM solution of chicken egg white lysozyme in 1 ml 0.1 M pH 9 bicarbonate buffer was initially prepared. 75 mM dansyl chloride (an amine reactive fluorescent probe) solution was prepared by dissolving the probe in DMF. To the 1 ml lysozyme solution, 50 μl of the 75 mM dansyl chloride in DMF was added (final concentration of dansyl chloride was 3.6 mM).

The protein lysozyme has 6 lysine residues to which the dansyl chloride may attach itself covalently (figure 3.3.1)

A reaction schematic is given below for a typical reaction between dansyl chloride and an amine.

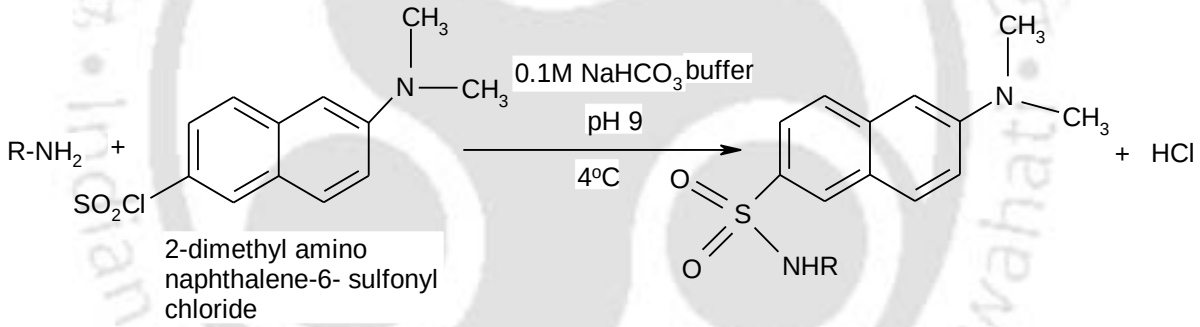

The concentrations of the protein and dye were taken such that in the final mixture we have an approximately 1:1 ratio of the two components. The reaction mixture was kept at 4^{o}C with constant stirring for three hours. After this period 1.5 ml pH 9.5 $NaHCO_3$ buffer was added to the reaction mixture. The mixture containing both labeled and unlabeled fluorophores was then passed through a PD-10 desalting column previously eluted with 50 mM pH 7 phosphate buffer to separate out the unlabeled fluorophores. Protein concentrations were determined by measuring the absorbance at 280 nm and the dye concentration was measured from the absorbance at 339 nm. The molar extinction coefficient of the dye at this wavelength for the labeled probe = 3370 $M^{-1}cm^{-1}$ (Levi and

recha, 2003; Chen, 1968). The ratio of the molar concentration of the protein to dye was calculated to be 1:1.

3.4 The Aggregation Reaction:

For triggering the formation of aggregates, 50 μl of the labeled lysozyme solution in 50 mM pH 7 phosphate buffer at a higher concentration was diluted to 1 ml in 50 mM pH 12.2 phosphate buffer. The anisotropy measurements of these solutions were then carried out.

3.5 pH dependence measurements

For the pH dependence studies, 50 μl of the labeled chicken egg white lysozyme were diluted to 1ml in pH 4, pH 5, pH 6, pH 8.3, pH 9.5, pH 10.8 and pH 12.2 buffers respectively.

3.6 Reversibility of aggregation

A 40 μM lysozyme solution in pH 12.2 buffer was prepared. Subsequently, 100 μl of this solution was transferred to 900 μl of 100 mM pH 7 buffer at regular intervals (5 mins, 30 mins, 60 mins, 120 mins, 180 mins, 240mins, 300 mins). Steady-state anisotropy measurements were carried immediately after the transfer as well as after leaving the solutions overnight at room temperature.

3.7 Experiment with guanidinium chloride

100 μl of day old aggregates obtained after overnight incubation of 40 μM dansyl labeled lysozyme in pH 12 buffer, were transferred to 900 μl of 6 M guanidinium chloride buffered at pH 7 and allowed to stand overnight in the denaturant at room temperature.

3.8 Steady-state fluorescence measurements

Steady-state fluorescence measurements were carried out in a Jobin-Yvon Fluoromax-3 spectrofluorometer equipped with motorized Glan-Thompson polarisers and a PMT operating at a voltage of 950V in photon counting mode. The emission spectrum of the labeled protein was measured and it was observed to have its emission maximum at 443 nm. To remain in step with the experiments done using the time-resolved set up the samples were excited at 370 nm.

Steady-state anisotropy measurements were done keeping the excitation and emission wavelengths fixed at 370 nm and 443 nm respectively. The excitation slit width was fixed

at 1nm and the emission slit width was varied from 5 to 10 nm. The concentrations of the labeled protein solutions were varied from 4 to 200 μM. The fluorescent measurements were carried out in quartz cuvettes. The background intensity from Raman scatter was observed to be negligible (less than 5%) compared to sample emission intensity under identical conditions as observed with blank samples. All the steady-state anisotropy data are G-factor corrected.

3.9 Time-resolved fluorescence measurements

Time-resolved fluorescence intensity decay and anisotropy decay measurements were carried out in an IBH fluorocube using the time-correlated single photon counting method. The system was provided with motorized Glan-Thompson polarisers and an IBH TBX04 photon-detection module. For excitation an IBH 370 nm nanoLED with a FWHM of 1.3 ns and a repetitive-rate of 1 MHz was used. Because of the absence of monochromators, the emission from the sample was detected via a Schott 420nm long pass filter fitted at the emission end. A neutral density filter OD=3 was fitted at the excitation end to attenuate the light falling on the sample. A Schott UG-1 filter was also used at the excitation end to cut out the long wavelength glow from the 370 nm light source. The fluorescence lifetime measurements were carried out with the emission polarizer at the magic angle position of 54.7^{o}.

The time-resolved anisotropy measurements were carried out with the emission polarizer parallel ($I_{\parallel}$) and perpendicular ($I_{\perp}$) to the orientation of the excitation polarizer.

Fluorescence intensity decay were collected in 1024 channels with a time-resolution of 0.113 ns/channel. Peak counts collected were between 10000-15000 counts.

3.10 Viscosity measurement

The viscosity of aqueous solution of 0.9 M L-Arginine.HCl was measured using an Ostwald's Viscometer with water as the reference.

Apparatus used: Ostwald's viscometer

Flow time of water=t_1

Flow time of 0.9 M L-Arginine. HCl= t_2

Density of water= ρ_1

Density of 0.9 M L- Arginine HCl= ρ_2

Viscosity of water =η_1

Viscosity of 0.9 M Arginine . HCl= η_2 (to be determined)

Equation used

$$\eta_2 = \frac{\eta_1 \rho_2 t_2}{\rho_1 t_1}$$

Liquids	Flow time (i) (seconds)	Flow time (ii) (seconds)	Flow time (iii) (seconds)	Mean flow time (seconds)	Density (ρ) $1x10^3 kg/m^3$	Viscosity (η) ($1x10^3$ kg $m^{-1}s^{-1}$)
Water	77.72	78.84	78.69	78.42	0.99473	0.7523
0.9 M L-Arg.HCl	115.31	115.56	114.72	115.20	1.05564	1.1728

Viscosity of 0.9 M L-Arginine.HCl=1.1728 $x10^3$kg $m^{-1}s^{-1}$

Therefore, viscosity of 0.9 M arginine relative to that of water at 33 ^oC = 1.56

CHAPTER 4

Influence of Macromolecular Crowding on the Initial Rate of Alkaline Phosphatase Catalyzed Hydrolysis

The aqueous phase of the cytoplasm is crowded with macromolecules such as soluble proteins, nucleic acids, membranes that often approach total concentration in the range of 300-400 mg/ml (Zimmerman and Trach, 1991; Fulton, 1982). This corresponds to occupation of a substantial volume fraction of the cell interior. Enzyme catalyzed reactions, in living systems, take place within such crowded environments.

Our aim was to investigate, *in vitro*, the effect of crowding on the initial rate of enzyme catalyzed reactions occurring in cellular media, especially those reactions which are catalyzed by non-allosteric enzymes. Alkaline phosphatase is just such a non-allosteric enzyme. The progress of the hydrolysis of alkaline phosphatase catalyzed hydrolysis of p-nitro phenyl phosphate monitored by UV-vis spectroscopy displays a hyperbolic profile typical of non-allosteric enzymes. To artificially mimic cellular crowding, we introduced inert polymers such as, dextrans of molecular masses ranging from 15 to 500 kDa and ficolls 70 and 400 kDa, respectively in the reaction medium. The concentrations of the above synthetic polysaccharides were typically varied from 0 to 30% w/w.

A few of the reasons for choosing the alkaline phosphatase reaction as a model to investigate the influence of macromolecular crowding on biochemical reactions were as follows:

1) The reaction is accompanied by minimal change in the excluded volume. In fact the substrate, PNPP (M_w~ 220 Da) and product p-nitrophenol (M_w~ 140 Da) are tiny compared to surrounding macromolecules (M_w~ 15,000 or more), such that excluded volume effects can be safely neglected
2) The progress of the reaction can be monitored conveniently by uv-vis spectroscopy using the absorbance of the yellow product, p-nitrophenol
3) Alkaline phosphatase, which is a homodimeric enzyme (M_w~ 105,000), diffuses relatively less compared to the substrate (M_w~ 220 Da). The substrate is initially 500 fold in excess as compared to the enzyme. Thus, effectively it is the diffusion

of the substrate in the midst of the relatively immobile enzyme and obstacles that is relevant for enzyme-substrate encounter.

Our initial effort was directed towards determining the nature of the enzyme catalyzed reaction in the absence of crowding agents. The second-order rate constant k_{cat}/K_m was therefore measured and the value obtained, 1.38×10^4 $M^{-1}s^{-1}$, indicated that the reaction is only partially diffusion controlled under the conditions employed by us. A fully diffusion controlled reaction is expected to have a second-order rate constant of the order of 10^9-10^{10} $M^{-1}s^{-1}$.

The initial rate of formation of p-nitro phenol was measured in 0-30% w/w solutions of dextran 15-200 kDa, in 0-25% w/w solutions of 500 kDa and in Ficoll solutions of concentrations 0-30 % w/w. The figures 4.1 A-4.1 E show the profiles of the hydrolysis reaction in the presence of increasing concentrations (expressed in fractional volume occupancies) of dextrans (15-500 kDa). Figures 4.1F and 4.1 G show the hydrolysis profiles in the presence of 70 kDa and 400kDa Ficoll respectively.

Indian Institute of Technology Guwahati

Figure 4.1 A

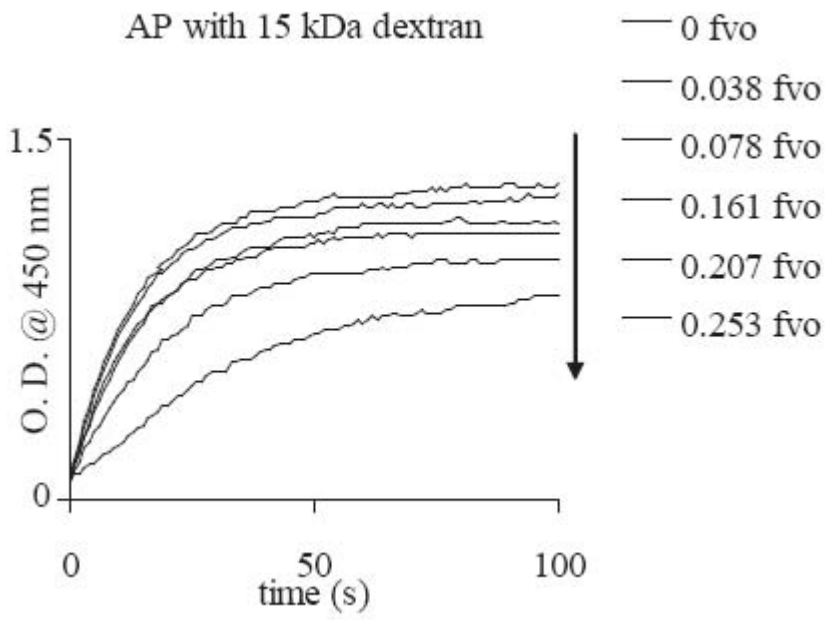

Figure 4.1 B

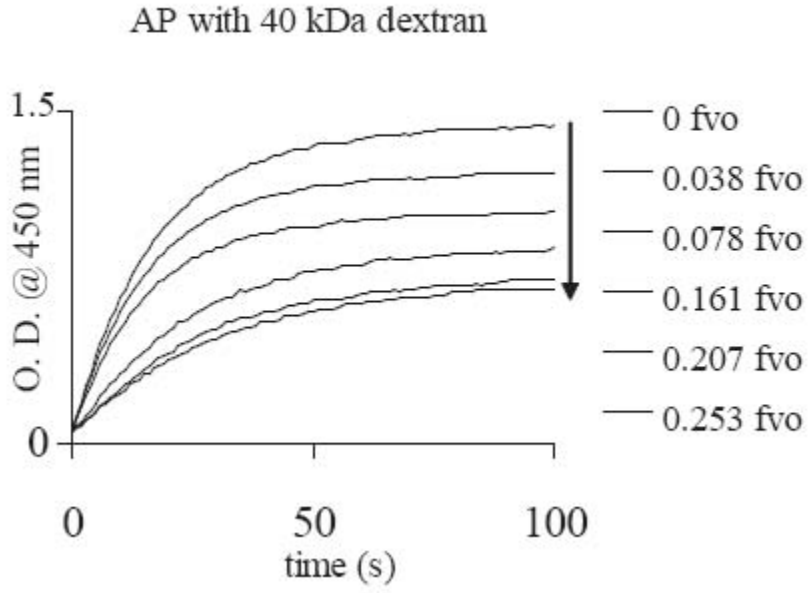

Figure 4.1 C

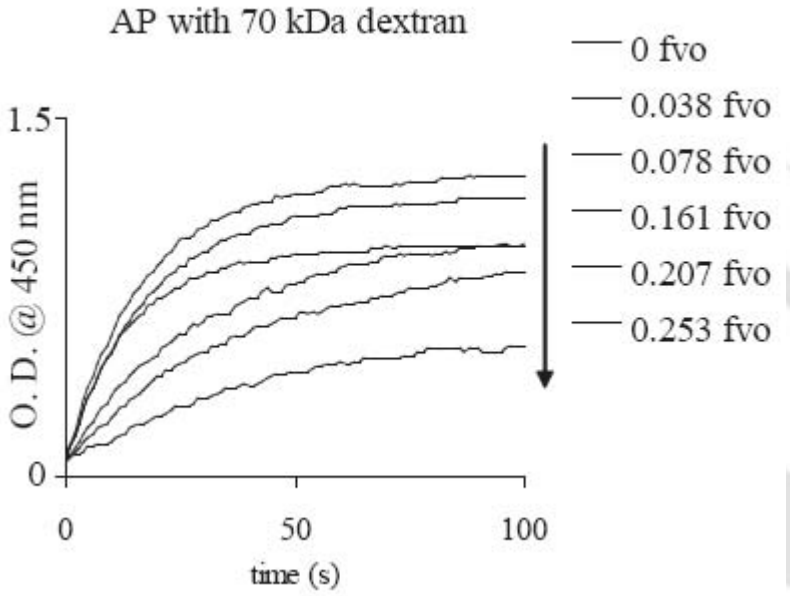

Figure 4.1 D

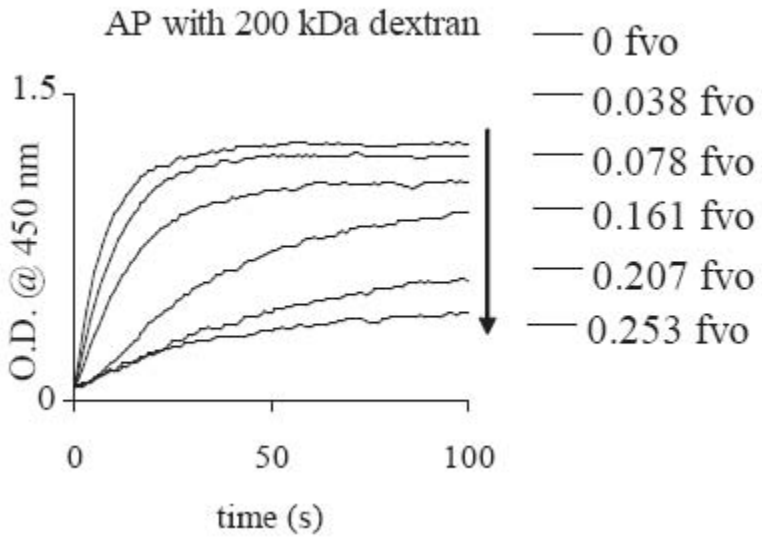

Figure 4.1 E

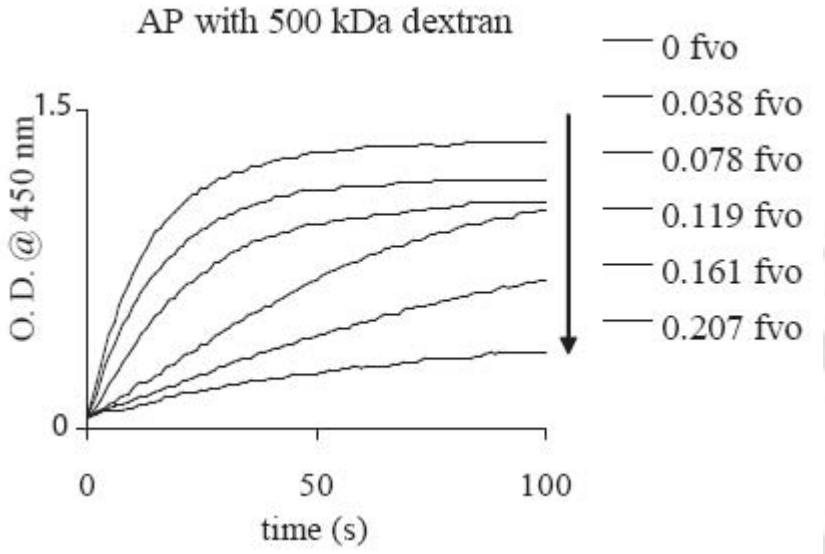

Figure 4.1 F

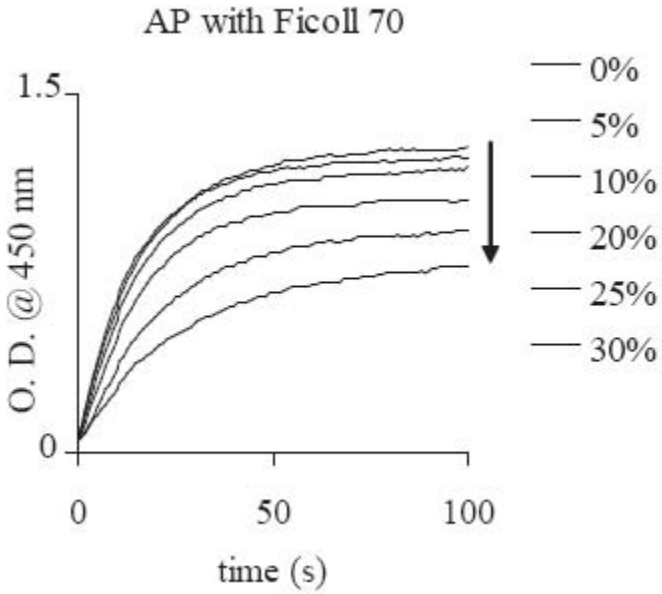

Figure 4.1 G

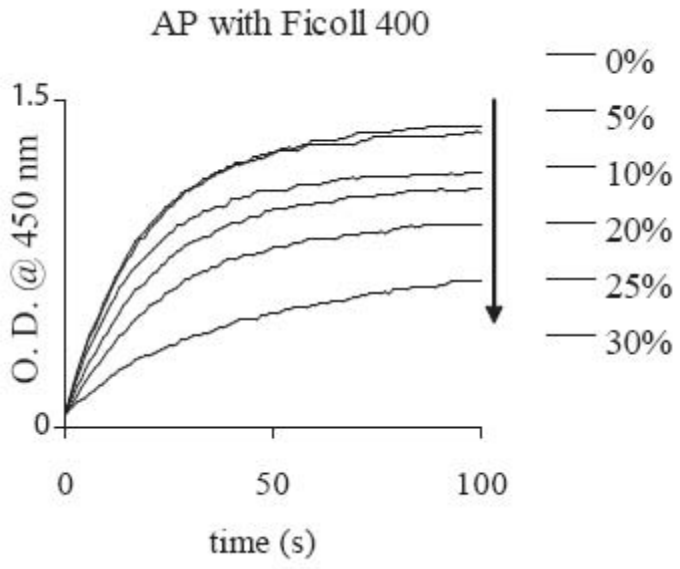

Figure 4.1: The figures 4.1 A - 4.1E show representative hydrolysis profiles obtained in 15-500 kDa dextran with increasing fractional volume occupancies. The figures 4.1 F and 4.1 G show the profiles obtained in 0-30% w/w 70 and 400 kDa Ficolls. The Ficolls were not expressed in fractional volume occupancies because we were unable to find out the specific exclusion volume of Ficoll.

The figures 4.1 A-4.1 E show that 15-70 kDa dextran slow down the rates only marginally, whereas a much greater drop is perceptible with dextrans with masses greater than 200 kDa and 500 kDa. From figures 4.1D and 4.1 E we can make out that, at an fvo = 0.207 which is equivalent to 25 % w/w, the reaction slows down appreciably.

The figures 4.1F and 4.1G show the reaction profiles in the presence of ficolls 70 and 400 kDa. Only a marginal drop in rates is observed with increasing concentration of Ficolls, especially Ficoll 70.

The initial velocity of the reaction was selected as the experimental parameter to measure in this study. This approach is simple and unambiguous because i) the substrate to enzyme density ratio is sufficiently large during this interval (10s) and ii) inhibition of the enzyme by the product (P_i) can be neglected. Other kinetic parameters like V_{max}, K_m and k_{cat} were avoided for reasons that are described later in this chapter.

The effect of different concentrations of 15 kDa, 40 kDa, 70kDa, 200kDa and 500 kDa Dextran, taken individually, on the normalized reaction rate is depicted in figure 4.2.

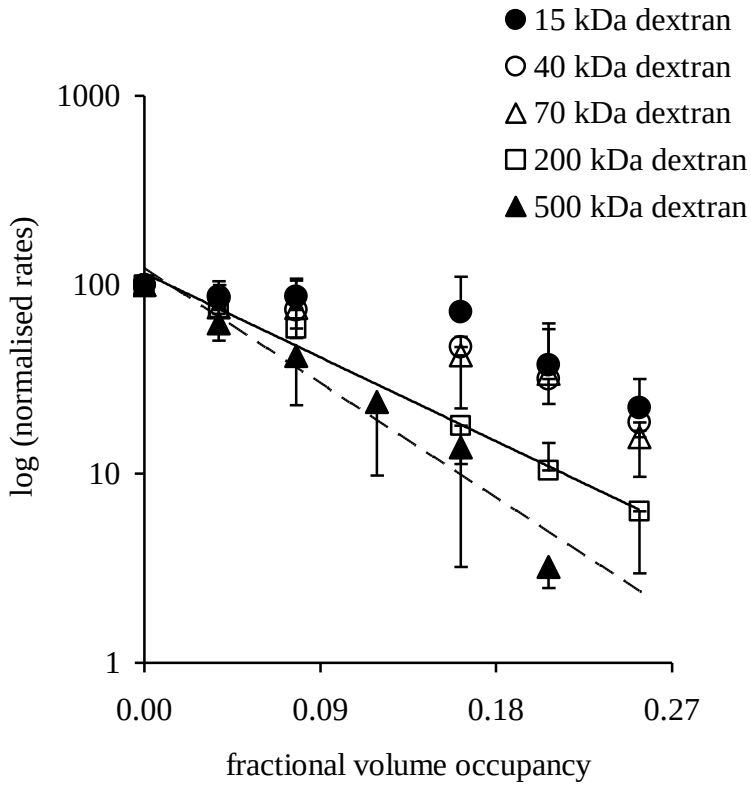

Figure 4.2 Dependence of enzymatic rate on size and concentrationof dextrans is shown. The normalized rate, V_{norm}, is plotted on a logarithmic scale against the fractional volume occupancy for different sizes of dextran employed in the study. Here [PNPP] = 1mM for all cases. The dextran sizes are represented by symbols as follows: filled circles 15kDa; open circles 40 kDa; open triangle 70 kDa; open square 200 kDa and filled triangle 500 kDa. The 200 and 500 kDa dextran data could be fitted to equation 3.1.3 for evaluating g as shown by straight lines: the value of g as determined from the fit are as follows: 11.4 in 200 kDa and 14.5 in 500 kDa. The value for A was in the range of 115-121.

It is observed that dextrans in size range 15-70 kDa show a similar influence in retarding the reaction. They also indicate a trend that is expected to be observed for a reaction that is neither fully transition state-limited nor fully diffusion limited (the point where curves a and b meet in figure 4.3).

A monotonic decrease in the normalized rate (plotted in a logarithmic scale) was observed with increasing fractional volume occupancy of dextran for 200 and 500 kDa dextran. This behaviour is predicted when the encounter between substrate and enzyme is rate limiting (Ellis, 2001a; Minton, 1981). In the case of transition state limited reactions, one would see an increase in the rate at low obstacle density due to increase in thermodynamic activity of the transition state complex, followed by a gradual decrease due to decrease in encounter rate owing to reduced diffusion as the obstacle density becomes higher (Ellis, 2001a) (figure 4.3).

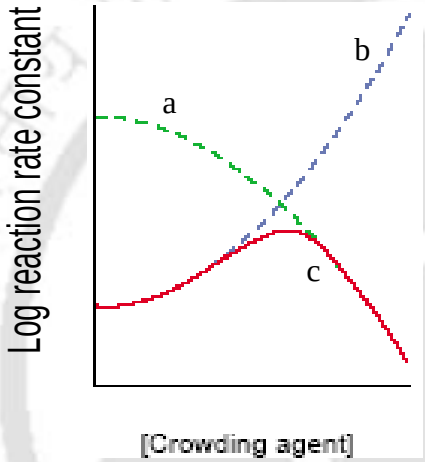

Figure 4.3 Dependence of reaction rate on concentration of crowding agent, in cases in which the reaction is either diffusion-limited (a) or transition state limited (b), reaction rate is transition state limited at low concentrations of crowding agents and diffusion limited at high concentrations (c).

R. J. Ellis, Curr. Opin. Struct. Biol.,2001, 11:114-119

It appears therefore that, with small obstacle sizes (15-70 kDa) the reaction behaves as a part transition state limited reaction and part diffusion limited one, while with larger obstacles it shows a trend similar to that of one that is substrate, enzyme encounter limited. This implies that the size of crowding agent plays a significant role in the kinetics of the reaction.

Another noticeable feature is that the drop in the normalized rate is more pronounced for larger dextrans (200 and 500 kDa) at a constant fractional volume occupancy, especially

at higher concentrations (fvo >0.16)(see fig 4.2). Clearly, the larger dextrans hinder the movement of the substrate to a large extent. A feature that deserves mention is that dextrans in the size-range 15-70 kDa possess an almost similar influence in reaction. This is interesting. We know that proteins constitute the majority of soluble macromolecules that crowd the cytoplasm (Zimmerman and Trach, 1991; Albe et al., 1990) and it is widely believed that the average molecular mass of proteins present in the cytosol (typically at concentrations ~0.15 fvo) is around ~ 40kDa (Goodsell, 1991). Thus it appears that crowding by dextrans of sizes comparable to those of proteins present in the cytosol, slows the reaction by only ~2 fold.

In the above discussions we have observed that there is a pronounced drop in rate of alkaline phosphatase catalysed hydrolysis of p-nitrophenyl phosphate in 200-500 kDa dextrans. We had also stated earlier that the sizes of the substrate molecules being much smaller than that of enzyme and dextrans, effectively the diffusion of the substrate molecules towards the fairly inert enzyme brings about the reaction. In order to know the viscosity sensed by the substrate molecule (PNPP) in solutions of crowding agents, we measured the bimolecular quenching constant (k_q) of the fluorescence quenching reaction in which fluorescein (which has a size similar to PNPP) serves as the fluorophore and KI the quenching agent. The molecular weight of fluorescein is 376 and it is comparable to that of PNPP whose molecular weight is 371. For this purpose we made use of the technique of time-resolved fluorescence measurements. The bimolecular quenching constants were determined in the presence of 15, 70, 200 and 500 kDa dextrans in the concentration range 0-25 %w/w. The experimental details are given in chapter 3 – section1. Dynamic fluorescence quenching requires that the fluorophore in the excited state and the quencher collide with each other for fluorescence quenching to occur. This demands diffusion of the fluorophore and the quencher for the encounter. The bimolecular quenching constant, k_q for this reaction in purely aqueous medium is generally diffusion limited with a rate constant > $10^9 M^{-1}s^{-1}$. Hence, comparison of k_q in dextran solutions with that in aqueous buffer will give us information on the role played by viscosity in slowing the translational diffusion of small molecules in the dextran medium. It is assumed that the quenching efficiency of iodide is unlikely to be affected

by an inert macromolecule like dextran. As the root-mean-square distance ($=(6D\tau)^{1/2}$, where D is diffusion coefficient of the quencher ($\sim 2x10^{-5} cm^2/s$ for iodide at 298 K (Atkins, 1998))) and τ is the lifetime of the fluorophore (~ 4 ns for fluorescein) that is getting quenched), over which iodide ion can diffuse during the lifetime of fluorescein is ~69 Å, it is unlikely that any other parameter apart from viscosity will have a role to play in the translational diffusion.

Figure 4.4 shows the intensity decay profiles obtained with increasing concentrations of iodide from 0-200 mM in the presence of 20% w/w 15 kDa dextran. The figure 4.4 is just an example of the intensity decay profiles obtained with increasing concentrations of KI.

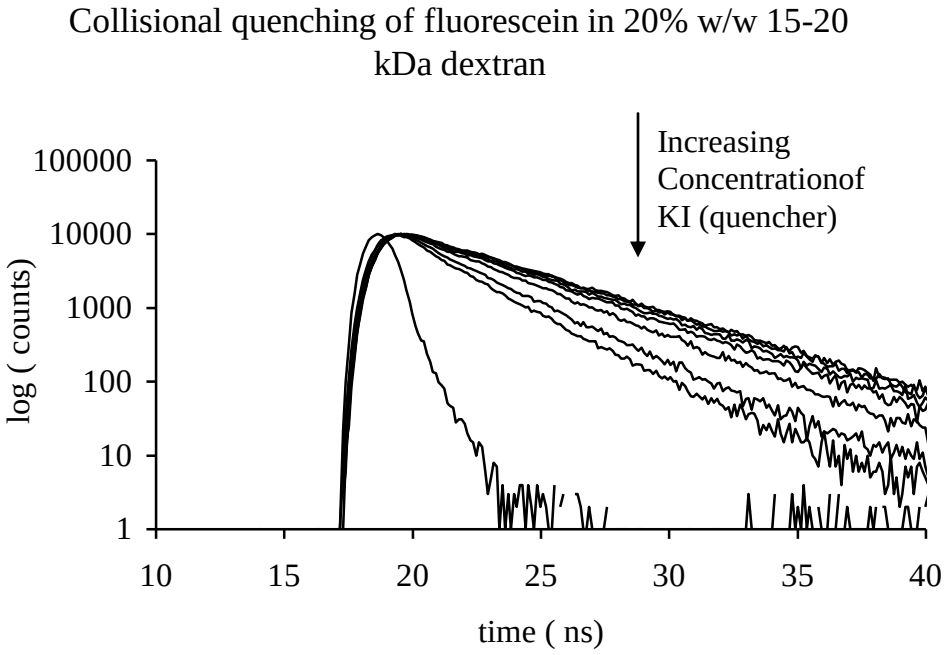

Figure 4.4 Intensity decay profiles of fluorescein with increasing concentrations of KI from 0 to 0.2 M. From top to bottom the concentrations of KI are 0, 10, 25, 50, 100, 200 and 300 mM.

The Stern-Volmer plots obtained in the presence of 15 kDa and 200 kDa dextrans in the concentration range 0 to 25%w/w are given below (Figures 4.5A and 4.5B).

Figure 4.5 A

Stern- Volmer Plot:quenching of fluorescein fluorescence by KI in 0 to 25 % w/w 15 kDa dextran

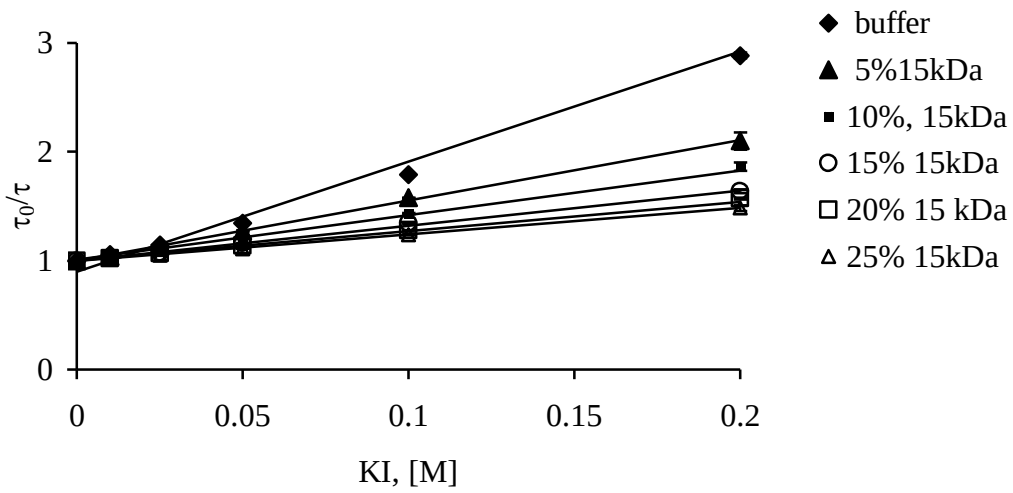

Figure 4.5 B

Stern-Volmer Plot: quenching of fluorescein fluorescence by KI in 0-25% w/w in 200 kDa dextran

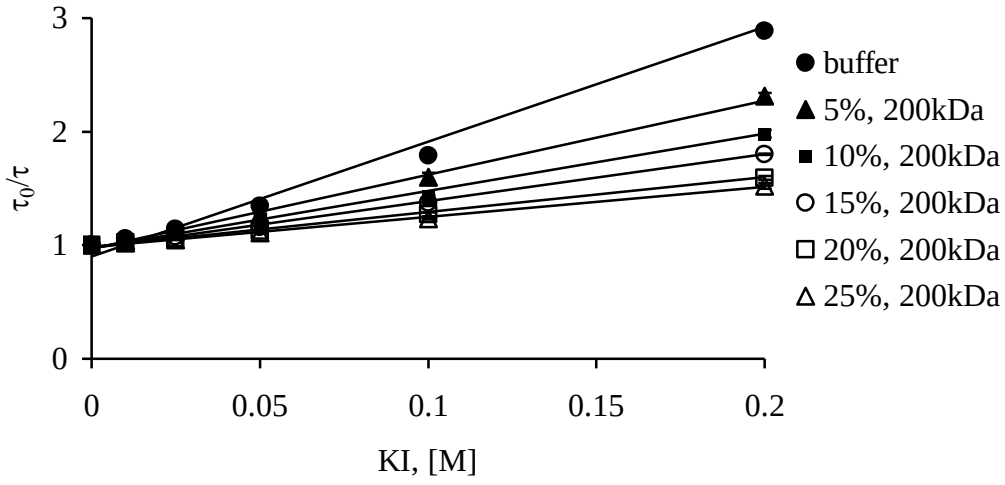

From the slopes of the Stern-Volmer plots, the Stern-Volmer constants, K_{SV}, may be determined which ultimately give us the values of the bimolecular quenching constants, k_q. The bimolecular quenching constants obtained in the presence of 0-25% w/w 15 and 200 kDa dextrans are given in Table IA and IB respectively. The τ_0 values indicate the lifetime of the fluorophores determined in the absence of quencher (KI).From the data in the tables it appears that the bimolecular quenching constants are not affected significantly by increasing concentrations of 15 and 200 kDa dextran.

Table IA: bimolecular quenching constants in 0 to 25% w/w of 15 kDa dextran

15 kDa dextran (%w/w)	K_{SV} M^{-1}	τ_0 ns	k_q $M^{-1}s^{-1}$
0	10.1	4	2.5×10^9
5	5.57	4	1.4×10^9
10	4.10	4	1.0×10^9
15	3.22	4	8.1×10^8
20	2.67	4	6.7×10^8
25	2.44	4	6.1×10^8

Table IB: Bimolecular quenching constants in 0 to 25 % w/w 200 kDa dextran

200 kDa dextran (% w/w)	K_{SV} M^{-1}	τ_0 ns	k_q $M^{-1}s^{-1}$
0	10.1	4	2.5×10^9
5	6.53	4	1.6×10^9
10	5.04	4	1.3×10^9
15	4.13	4	1.0×10^9
20	3.08	4	7.7×10^8
25	2.64	4	6.6×10^8

In the figure 4.6 below, the mean fold drop in rates observed in the alkaline phosphatase catalysed hydrolysis for two different substrate concentrations 1 and 20 mM and the mean fold drop of bimolecular quenching constants observed in 20% w/w concentrations of sucrose, 15-500 kDa dextrans and 70 and 400 kDa Ficolls are plotted.

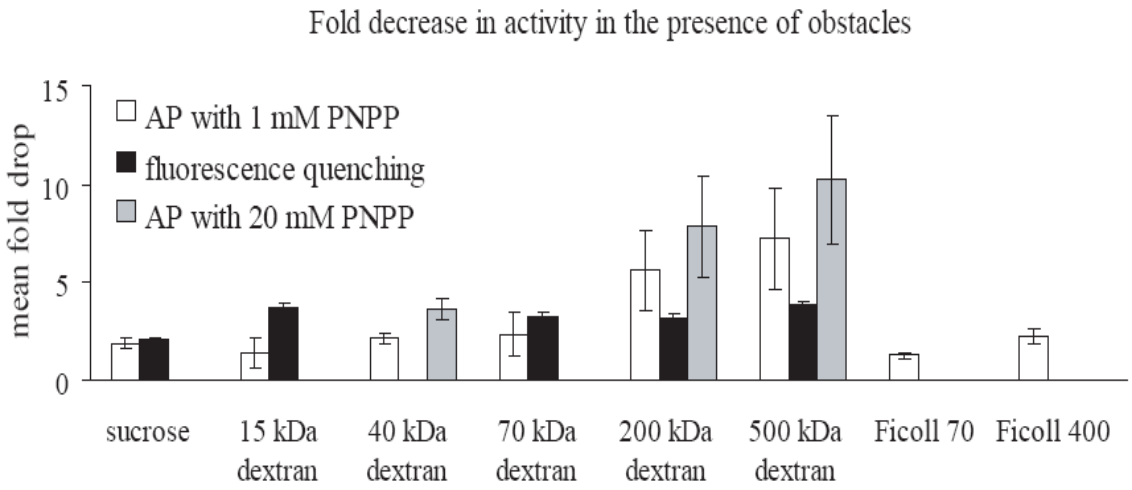

Figure 4.6 Decrease in bimolecular encounter rates owing to crowding. The unfilled bars indicate the mean fold drop in rate (V_0/V), as observed from alkaline phosphatase catalysed hydrolysis of p-nitrophenyl phosphate (here [PNPP]= 1mM) in the presence of sucrose/dextrans/ficolls as indicated in the X-axis.The grey filled bars show the mean fold drop in rate when [PNPP= 20mM].The black bars highlight the mean fold drop in the bimolecular quenching constant, (k_{q0}/k_q) observed by dynamic fluorescence quenching of fluorescein by KI in the presence of sucrose/dextrans/ficolls as indicated in the X-axis. The reduced χ^2 obtained during the non-linear least squares fitting for determining fluorescence lifetime during quenching were between 1.0 and 1.3 in all cases. For all cases above, the concentration of the background molecules (sucrose/dextran/ficoll) were kept constant at 20% w/w to facilitate comparison

The unfilled bars show the effect of the different macromolecules that were used in this piece of work, on the fold decrease in the rate of alkaline phosphatase catalysed hydrolysis of PNPP. To enable comparison the concentration of the crowding agent was maintained constant at 20% w/w (equivalent to fractional volume occupancy of 0.16 for dextrans), a value that comes close enough to the concentration of soluble macromolecules in the cytoplasm. As observed earlier, dextrans in the range 15-70 kDa slow the reaction by 1.4-2.4 fold only. A similar influence is also exerted by sucrose. The effect of sucrose on the reaction rate may be explained by the proportional increase in the solution viscosity. The presence of 200 kDa dextran slows the reaction by ~ 5.6 fold while the same in the presence of 500 kDa dextran is slowed by ~ 7.2 fold. In contrast,

solutions containing Ficoll 70 and Ficoll 400 slow the reaction by ~1.3 and ~2.3 fold respectively. The influence of ficolls is discussed later. The grey filled bars show the fold decrease observed when PNPP concentration is raised by 20 fold. A marginal increase is observed in the degree of slowing compared to 1mM data (unfilled bars). This experiment was done to see if the drop in rates observed with 1 mM substrate had any contribution from non-specific binding interaction between substrate and the crowding macromolecule. However, as the trend observed with 20 mM substrate is almost similar to that with 1mM substrate, it seems unlikely that the decrease in enzymatic rate is because PNPP gets stuck inside the dextran leading to a decrease in its effective concentration and consequently the rate of hydrolysis.

In figure 4.6, the black bars show the influence crowding agents have on bimolecular quenching constant, k_q for the dynamic fluorescence quenching of fluorescein by iodide. In aqueous buffer we observed a k_q of ~ 2.6×10^9 M^{-1} s^{-1} at 298 K during dynamic quenching of fluorescein fluorescence by iodide. Sucrose reduced k_q by ~2 fold consistent with the two fold increase in solution viscosity for 20%(w/w) sucrose-water mixture at room temperature (Lide, 1995). In presence of 15 kDa, 70 kDa, 200 kDa or 500 kDa dextran the mean fold decrease in k_q is confined to a narrow range between 3.2-3.8 fold only. This implies that the viscosity as sensed by a small molecule like iodide or fluorescein during translational diffusion in crowded dextran solutions, for a constant dextran concentration (20% w/w), is independent of the size of dextran macromolecule. The above result is consistent with previous observations based on fluorescence photobleaching recovery of BCECF (2, 7-bis-(2-carboxyethyl)-5-(and-6-)-carboxyfluorescein) in dextran solutions, where it was shown that the D_0/D dependence on dextran concentration was independent of dextran size in the range 10-2000 kDa (Kao et al., 1993). Kao and coworkers observed a ~4 fold decrease in diffusion of BCECF (a fluorescein derivative) compared to aqueous medium in the presence of 20% w/w dextran (Figure 6B, Kao et al., 1993) which is consistent with our results (3.2 - 3.8 fold) from dynamic fluorescence quenching on the diffusion of iodide and fluorescein. It is also in agreement with previous reports in literature on the diffusion of small solutes in solutions containing macromolecules (Blum et al., 1986; Furukawa, 1991). It is thus likely that the

diffusion coefficient of PNPP is independent of the size of dextran crowding the solution at any given dextran concentration.

Based on the facts above, the ~ 2 fold decrease in the enzyme catalysed rate of PNPP in dextran solutions of size range 15-70 kDa actually implies a small increase in the activity of the enzyme owing to crowding. A roughly ~ 3.5 fold decrease in rate was to be expected here owing to the effect of viscosity on PNPP diffusion. One possible explanation for the increase in activity in the presence of crowding is likely to be the homodimeric nature of alkaline phosphatase. It has been shown recently that the dimeric alkaline phosphatase is 10,000 times more active than the monomer (Boulanger and Kantrowitz, 2003). It is well known that due to volume exclusion, macromolecular crowding can favour the dimeric enzyme more strongly in a monomer-dimer equilibrium, especially when the monomeric enzyme is comparable in size to the crowding agent (Minton, 2001). Indeed, crowding agents have been shown to have an effect on the state of association of an enzyme, which may be linked to changes in specific activity of the enzyme (Minton and Wilf, 1981).

The question we ask ourselves now is why the larger dextrans have a major influence on the reaction rate? We know now that a) their observed decrease is slightly less than the real decrease owing to an offsetting increase in the enzyme activity and b) viscosity accounts for, only a minor part in this effect. From earlier data (Fig 4.2) it seems likely that rate of encounter between [S] and [E] is affected in the presence of larger dextrans. Therefore it is possible that the substrate has to encounter a tortuous path to meet the enzyme active site in the presence of larger dextrans.

We now discuss the influence of ficolls on the reaction rate. Ficolls 70 and 400 are seen to have a minor influence on the reaction rate in comparison with dextrans of similar size Figure 4.6). Figure 4.7 reveals the variation in the normalized reaction rate with the concentrations (in wt %) of 70 and 400 kDa Ficoll. The data obtained in the presence of 40 kDa and 500 kDa dextran are also plotted in the same figure to facilitate comparison. These were plotted employing a concentration scale of %w/w as the specific excluded volume was not available for ficolls. Clearly, the ficolls show a reduced overall influence

on the rate relative to dextrans of similar size. In fact, the trend observed with 400 kDa ficoll is close to that observed with 40 kDa dextran as shown in figure 4.7.

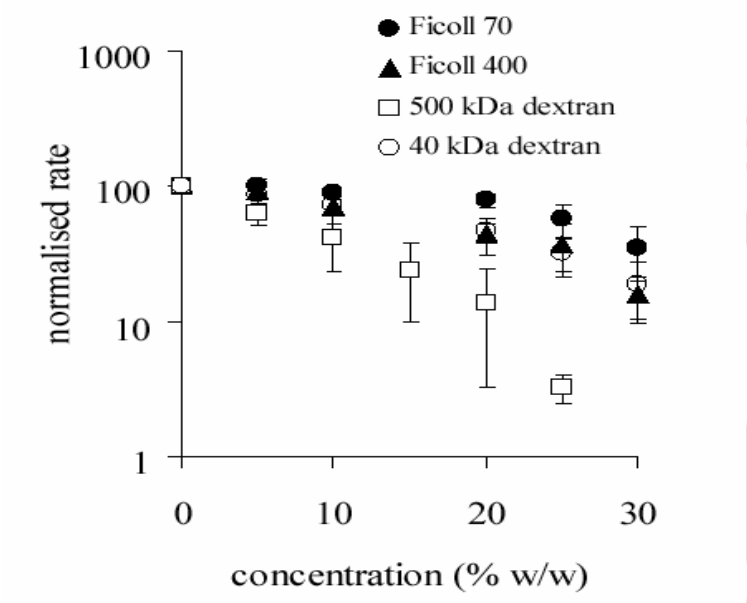

Figure 4.7 The normalized rate, V_{norm} is plotted on a logarithmic scale against the concentration of the crowding macromolecule for different sizes of dextran and ficoll employed in the study. Here [PNPP]=1mM for all cases. The sizes are represented by symbols as follows: filled circles ficoll 70; filled triangle ficoll 400; open square dextran 500 kDa and open circle dextran 40 kDa.

The disparity of results between Ficoll and dextran of similar size maybe explained by the fact that in comparison to dextran, ficoll is more compact, highly branched and less flexible on a molecular weight basis (Luby-Phelps et al., 1987). Dextran, being a linear polysaccharide, is a flexible, ribbon like, quasi-random coil molecule with few and short branches (Luby-Phelps et al., 1987; Dumitriu, 1998). Ficoll approximates a sphere much more closely than dextran. It has also been observed that at higher concentrations (>100 g/l) of ficoll 70, interpenetration and/or compression occurs (Wenner and Bloomfield, 1999). It is thus likely that the trajectory of the substrate is a more tortuous one if dextran is placed as the barrier in comparison to ficoll. Thus from this discussion one can

conclude that the shape of the barrier too, has a major part to play in influencing the reaction rate.

We will now explain why parameters like K_m, V_{max} and k_{cat} were not considered in this study. Figure 4.8 shows the initial rate of the reaction as a function of the substrate concentration in the presence (20% w/w) and absence of different crowding agents, namely, 40, 200 and 500 kDa dextrans.

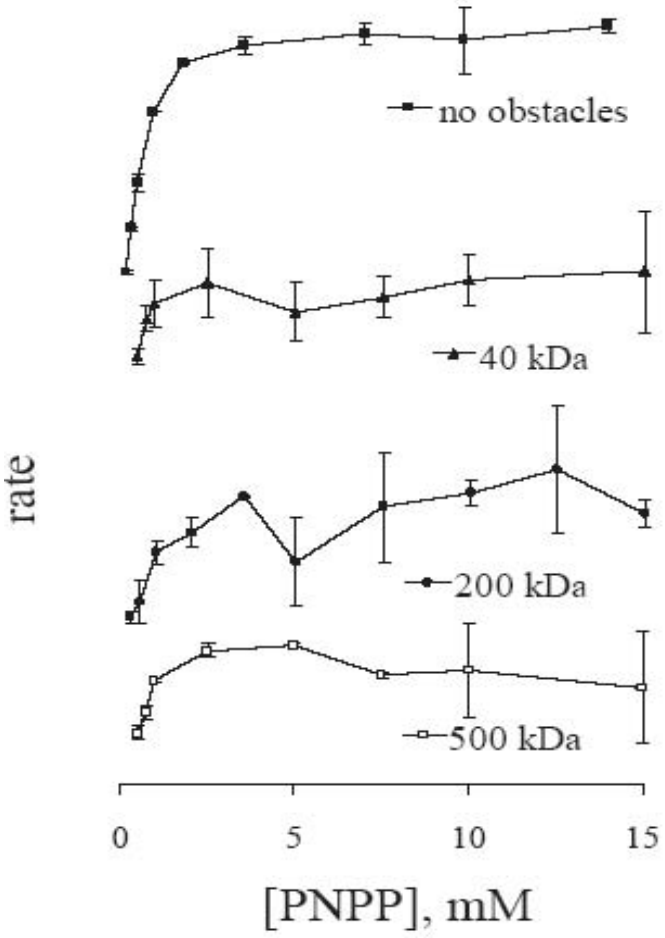

Figure 4.8 Rate vs substrate concentration profile for the alkaline phosphatase catalysed hydrolysis of PNPP observed in the presence and absence of different dextrans is shown. The symbols stand as follows: Filled square, no obstacles; filled triangle, 40 kDa dextran; filled circle, 200 kDa dextran; open square, 500 kDa dextran. The concentration of dextran was kept constant at 20% w/w in all three cases. The highest rate in each

individual plot is normalized to a constant value in order to facilitate comparison.

In the absence of crowding agent, the rate vs [S] curve displays the expected profile for Michaelis-Menten kinetics. In the presence of a significant fraction of macromolecules (20% w/w) this is clearly not the case. The curves that are displayed in figure 4.8 represent the mean of multiple measurements repeated several times. From the profiles it appears that in the presence of crowding agents, Michaelis-Menten behaviour may not be applicable. Indeed, it has been argued previously (Berry, 2002) that in disordered media (as encountered in the crowded ambience here), the conventional equations of enzyme kinetics may no longer be valid as the assumptions on which their derivation is based are no longer true. The equations need to be modified to account for fractal kinetics and anomalous diffusion during the formation of the ES complex, especially in the regime of high obstacle densities.

A factor that can have an influence on the results above is the non-specific binding of substrate (PNPP) to the crowding macromolecule. However, there are several reasons why such a possibility is unlikely. 1) We have observed the kinetics of the PNPP hydrolysis reaction in the presence of obstacles at 200s or later. The absorbances at these times, in almost all cases are greater than 90% of the value obtained in the absence of obstacles at same time. This clearly implies that less than 10% of the substrate, if any, is likely to remain bound to macromolecules. 2) It has been shown in an earlier report that carbohydrate additives like sucrose, fructose, lactose etc. exert no non-specific solute effects either on PNPP or alkaline phosphatase (Zimmerman and Minton, 1993; Terefe et al., 2004). 3) Figure 4.7 shows the fold decrease in the enzymatic rate at 1mM and 20 mM PNPP concentrations. Significant binding of PNPP to obstacles would have resulted in a much larger disparity in the fold decrease between 1 mM and 20 mM substrate concentrations.

Binding of enzyme without loss of activity is not of concern here because the enzyme is relatively immobile compared to PNPP in the reaction. Loss in activity of enzyme is unlikely as explained earlier. The ~ 2 fold decrease in ficoll is too less to be explained in terms of decreased enzyme activity. It has been shown that carbohydrates

like fructose, sucrose, and cellulose do not cause any denaturation or loss in activity of AP (Terefe et al., 2004). Thus, on the whole, the obstacles employed in the study are likely to be inert with relation to the enzyme.

This is the first time that influence of size of the crowder in an enzyme catalysed reaction has been investigated. Quantitative interpretation of the results described here is at present not possible. This requires a theoretical model and framework for the system employed, which is presently unavailable.

CONCLUSIONS:

1. Our results indicated that at 20% w/w concentrations, smaller dextrans (15 - 70 kDa) exert a moderate influence (1.4-2.4 fold slowing) on the initial rate of alkaline phosphatase catalysed reaction, while larger dextrans (> 200 kDa) retard the reaction considerably (> 5 fold). Ficolls (70 & 400 kDa) reduced the enzymatic rate moderately (1.3-2.3 fold). A minor offsetting increase in enzyme activity was also observed owing to crowding. The reduced influence of Ficolls was accounted by their compact shape in comparison to dextrans.
2. Large dextrans (< 200 kDa) most likely retard the reaction by influencing the rate of enzyme substrate encounter.
3. Classical Michaelis-Menten kinetics may not be valid when studying enzyme reactions in crowded media.

CHAPTER 5

Novel spectroscopic features arising from the amino acid L-lysine

A sequential treatment of the absorbance and luminescence features of L-lysine is presented here. In section 5.1 the discovery of near-ultraviolet and visible absorption and luminescence features of L-lysine HCl is discussed. Section 5.2 covers the application of the lysine features to studies of folding and unfolding as well as aggregation of lysine rich proteins

5.1 Novel Absorbance and Fluorescence characteristics of L-Lysine.HCl

Several peptides and many proteins are known to form aggregates in the solution phase (Fink, 1998; De Yound et al., 1993; Jayakumar et al., 1994; Swaminathan et al., 1994a). The presence of protein aggregates (amyloid) is known to be associated with diseases like Alzheimer's (Pitschke et al., 1998). Consequently investigations of these complexes have acquired importance in recent years. Among the amino acids, lysine was identified as a key residue causing protein aggregation (Anderluh et al., 2000). Several reports on crystalline aggregates involving lysine residues have also been made (Pratap et al., 2000; Venkatraman et al., 1997). However, there have been no other reports of amino acid lysine forming aggregates in the fluid phase.

In this work we report our observations on L-lysine using absorption and steady state fluorescence techniques, which indicate that lysine is likely to be aggregated in the aqueous phase.

Absorbance spectra of lysine from 0.1 to 1 M concentration at pH7 are shown in figure 5.1.1. Similar results were obtained in deionised water and 0.1 M acetate buffer, pH 4.6.

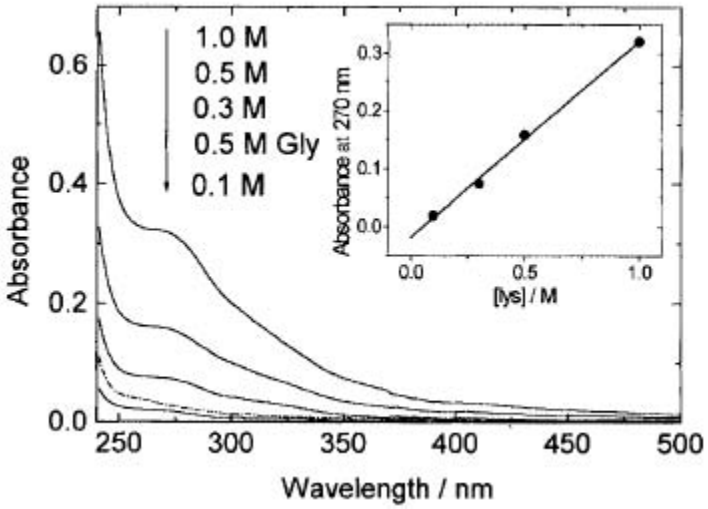

Figure 5.1.1 Absorbance spectra of L-lysine monohydrochloride (——) from 0.1 to 1 M in 0.1 M NaH_2PO_4 at room temperature. Same is also shown for 0.5 M glycine (- - - - -). INSET: The absorbance at 270 nm is plotted against lysine concentration.

The absorbance is observed to increase with increasing concentrations of lysine. The spectra show a distinct shoulder beginning at 270 nm. Figure 5.1.1 also contains the absorption spectrum of 0.5 M glycine under similar conditions. The 5-fold higher absorbance of 0.5 M lysine as compared to that of 0.5 M glycine led us to believe that the side chain of L-lysine is responsible for its absorbance and that the α–amino and α–carboxyl groups are much less involved.

On plotting absorbance against concentration of lysine a straight line was obtained (Inset in figure 5.1.1) showing that absorbance increased proportionately with concentration of lysine. From the slope, the molar extinction coefficient was calculated to be 0.34 $M^{-1}cm^{-1}$ at 270 nm.

Fluorescence emission spectra of lysine were measured in aqueous solutions at pH 7 (figure 5.1.2).

On excitation at 290 nm tiny fluorescence peaks were observed with low concentrations of lysine (~0.01 M) at ~ 321 nm and ~334 nm respectively. Negligible emission was bserved around ~420 nm. With gradual increase in concentration upto 1 M, a rise in fluorescence intensity at ~420 nm was observed. The excitation was chosen at 290 nm to highlight the observation that emission peaks at 321 and 334 nm remain unaffected by

concentration changes. There was a slight decrease in intensity at 420 nm at concentrations higher than 0.3 M due to inner filter effect.

The fluorescence spectrum was observed to be broad and devoid of vibrational features. This emission was not observed under identical conditions in glycine, L-arginine, L-serine, L-glutamate and L-isoleucine. These amino acids were chosen randomly. The observed fluorescence appears to be unique to lysine and is difficult to account since it lacks a conjugated system or an aromatic moiety (Turro, 1991).

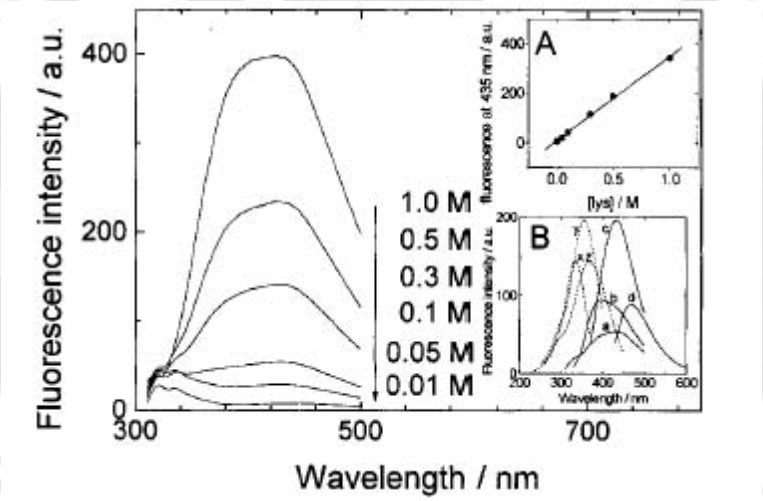

Figure 5.1.2 Emission spectra of L-lysine monohydrochloride from 0.01 to 1 M (λ_{exc}= 290 nm). Excitation slit width = 5nm; emission slit width =10 nm. INSET A: Emission intensity at 435 nm is plotted against lysine concentration, here λ_{exc}= 355 nm. B: Emission spectra (_____), the excitation wavelengths are: (a) = 290 nm, (b) = 310 nm, (c) = 355 nm and (d) = 410 nm. Excitation spectra (--------), the emission wavelengths are: (x) = 393 nm, (y) = 435 nm and (z) = 471 nm. For all spectra above, excitation and emission slit widths = 5 nm and [lysine] =0.5 M.

Figure 5.1.2.A shows the variation of fluorescence intensity at 435 nm with lysine concentration on excitation at 355 nm. A linear dependence of fluorescence intensity on concentration was observed. Based on the observation of the dependence on concentration, and the absence of vibrational features from the emission spectrum, the presence of molecular aggregates or complexes of lysine in the solutions studied were

assumed to be responsible for these features. A heterogeneous population of these aggregates appears to be responsible for these features as indicated by the figure 5.1.2.B where excitation at different wavelengths results in separate emission bands.

On excitation at 290 nm (curve a), emission was only faintly visible. However, a four fold increase in intensity was observed on exciting at 355 nm (curve c). The blue fluorescence (λ_{max}= 435 nm) was clearly visible to the naked eye.

The excitation spectra for curves b, c and d are shown in curves x, y and z.

The presence of multiple excitation and emission bands indicates that multiple states/species are involved.

At this point we attributed the formation of lysine aggregates to the presence of the four methylene groups in the lysine side-chain. These groups, we surmised, could result in the formation of a hydrophobic core. To ascertain this, we carried out an experiment with pyrene which has been used extensively in the past as a probe for measuring solvent polarity (Kalyanasundaram and Thomas, 1977; Dong and Winnik, 1982; Kalyanasundaram, 1987). Pyrene at high concentrations shows excimer bands and at low concentrations displays the monomer peaks. These peaks correspond to the vibronic bands of pyrene and show a strong dependence on solvent polarity. In the presence of polar solvents there is an enhancement in the intensity of the forbidden 0-0 band at the expense of other bands. The ratio of the 3rd peak to the 1st peak is used to detect changes in solvent polarity. The 3rd peak is chosen since it displays minimum change in intensity with changes in solvent polarity. Figure 5.1.3 shows pyrene fluorescence in the presence of 0, 0.5 and 1.0 M lysine respectively.

A marked decrease in pyrene excimer fluorescence was observed (~467 nm) coupled with an increase in monomer intensity (peaks at 373 and 392 nm) in 0.5 M lysine. Further increase in lysine concentration to 1 M resulted in a similar trend. Pyrene being strongly hydrophobic has a low solubility in water (2-3 μM) and probably interacts more with lysine molecules or aggregates compared to pyrene monomers, when both pyrene and lysine are present. This was indicated by a decrease in the peak intensity ratio of vibronic bands I/III in pyrene emission from 1.87 in aqueous buffer to 1.65 in 0.5 M lysine. The value of 1.65 shows that pyrene molecules are bound to small clusters of lysine molecules in a mildly non-polar environment.

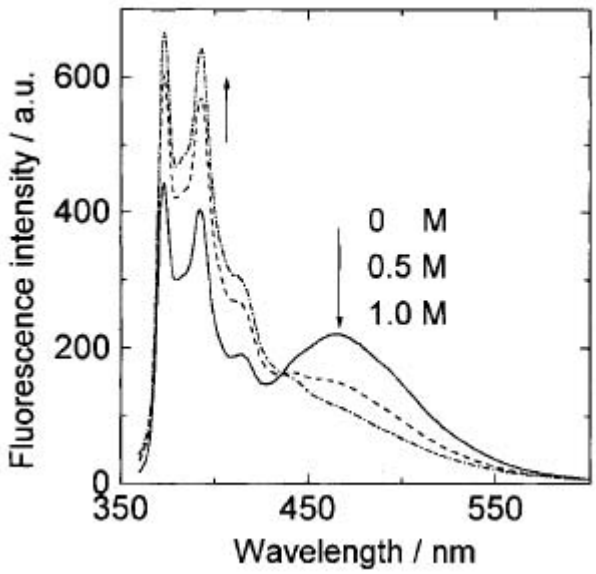

Figure 5.1.3 Fluorescence emission spectrum of pyrene in the presence of 0 (solid line), 0.5 (dashed line) and 1.0 M (dots and dashes) L-lysine monohydrochloride. λ_{exc}= 340 nm. [pyrene] = 2.5 x 10^{-5} M for all curves. Excitation slit width = 3 nm and emission slit width = 5 nm.

In order to rule out any contribution from impurities, we carried out experiments with lysine from various sources. Extracts with ether from lysine failed to yield any extraneous component that could account for the observations. Also, the spectra are broad and structureless similar to those observed in molecular complexes.

The above observations indicate likelihood for the presence of aggregates in concentrated solutions of lysine. These molecular complexes are likely to have a heterogeneous population as indicated by the fluorescence data.

The results obtained above prompted us to explore similar interactions among proximal lysine residues in proteins. The outcomes of the experiments are described in the next section.

CONCLUSIONS:

1. A new lysine absorption peak was detected at 270 nm (ε=0.34 $M^{-1}cm^{-1}$)
2. Blue fluorescence with emission maximum at ~ 435 nm was observed on excitation at 355 nm.
3. The exact nature of the chromophore responsible for the absorbance features could not be determined. The lysine molecule has no chromophoric group

attached to it and so we concluded that the observed spectroscopic features actually arise due to *intermolecular* interactions between lysine molecules in solution.

4. Experiments with pyrene indicated the formation of lysine clusters in solution. However, detailed theoretical calculations are required to determine the nature of the interactions giving rise to the spectroscopic features.

5.2 Near Ultra-Violet Absorption Arising From Lysine Residues in Close Proximity: A Probe to Monitor Protein Unfolding and Aggregation in Lysine Rich Proteins

Here we discuss applications of the novel absorption features of lysine described before. Though there are a lot of probes available for studying absorption and fluorescence characteristics of proteins, there is a dearth of probes for studying phenomena like protein aggregation. Normally, the absorbance and luminescence properties of amino acids like tyrosine and tryptophan are used in studying protein structure (Beechem and Brand, 1985; Eftink, 2001). Of these, tryptophan is normally used for studying proteins. Tryptophan is highly sensitive to its local environment and therefore can be used to study protein conformational transitions, subunit association, substrate binding and denaturation (Lakowicz, 1999; Swaminathan et al., 1994b). However, tryptophan has been of limited use in monitoring protein aggregation owing to its short fluorescence lifetime (~3 ns). It is worthwhile therefore to have another probe that can be utilized to monitor protein folding and aggregation. One such attempt is presented in this work employing interactions between spatially proximal lysine residues. Earlier work by us had shown that L-lysine displays new-near ultraviolet (~270 nm) absorption at high concentrations (~0.5 M) in aqueous medium at pH 7 (Homchaudhuri and Swaminathan, 2001). The new spectra were deduced to arise from *intermolecular* interactions between adjacent lysine side chains in the aggregates. In this section, similar observations arising from *intramolecular* interactions between two or more lysine residues present in close spatial vicinity in human serum albumin (HA), poly-L-lysine and calf thymus histone are presented. Consistent with the *intramolecular* nature of the interactions, these

spectroscopic features were observed at dilute concentrations (~100 μM for HA). Also, as predicted from the earlier study, the lysine side chain and not the terminal amino or carboxyl groups, play a major role in the above interaction. Importantly, the present investigation showed that the above spectral features are dependent on the proximity of the lysine side-chains in the protein. This property was subsequently exploited to observe the unfolding and aggregation of calf thymus histone from the absorption spectra.

Figure 5.2.1 contains the absorption spectrum of human serum albumin (a), referred to henceforth as HA.

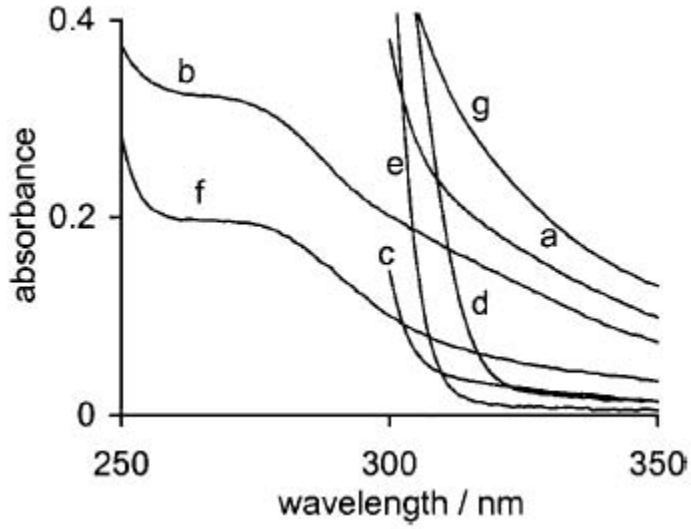

Figure 5.2.1 : Absorption: The absorption spectrum of (a) human serum albumin [1.08x10^{-4}M]; (b) L-lysine [1.0 M]; (c) subtilisin Carlsberg [1.5 x10^{-4} M]; (d) mutant barstar [1.5 x10^{-4} M]; (e)lysozyme [1.5 x10^{-4}M]; (f) poly-L-lysine hydrobromide [10 mg/ml]; and (g) calf-thymus histone [11 mg/ml]. All proteins were dissolved in 0.05 M NaH_2PO_4 adjusted to pH 7.

Absorbance was examined beyond 315 nm because contribution from lysine within 270-310 nm would be masked by the more prominent tryptophan and tyrosine absorbances in proteins. A broad tail of absorbance was observed to exist for HA beyond 315 nm. A similar tail was reported earlier for HA and the molar extinction coefficient measured was 1546 M^{-1}cm^{-1} at 325 nm (Hagag et al., 1983). Lysozyme (curve e) showed a sharp drop in absorbance beginning at 304 nm with very little absorbance at 315 nm. Contributions from trp, tyr, phe, cysteine and cystine to the absorbance of HA were

neglected because they have very small extinction coefficients beyond 315 nm at neutral pH (Fasman, 1992). Besides the amino acids mentioned above, no other amino acid is known to have significant electronic absorption at wavelengths 315 nm and beyond (Fasman, 1992). Thus the broad tail of absorbance of HA cannot be attributed to either of the amino acids mentioned above.

Experiments were then carried out with poly-L-lysine to account for the absorbance observed beyond 315 nm. Poly-L-lys (f) shows a similar absorption spectrum as lys (b), but at a concentration 250 fold less than that of the lysine amino acid since the interactions are intramolecular in this case.

The absorptions of the different proteins were compared by measuring the ratio of their absorbances at 350 and at 325 nm respectively, (A_{350}/A_{325}). This enabled comparison of protein absorbance in a concentration independent manner. The wavelengths 325 nm and 350 nm were chosen to avoid trp absorption. The ratios for lysine, HA and the protein histone were observed to be similar (0.6) [See table I]. This indicates a similar shape in their absorption spectra between 325 and 350 nm. Poly-L-lysine shows a ratio 0.66 which is not very different. This ratio can serve as a spectroscopic ruler for identifying lysine rich proteins from a mixture of unknown proteins

Table I: Absorbance Ratio (350 nm/ 325 nm)

Sample	A_{350}/A_{325}
L-lysine	0.57
HA	0.59
Histone	0.59
Poly-L-lysine	0.66

The absorbance ratio for lysozyme, mutant barstar and subtilisin Carlsberg are not shown as their absorbance at 350 nm are too less to be meaningfully interpreted.

Thus the spectra for the above proteins appear fairly similar in shape to that of lysine, hinting at a common origin.

Figure 5.2.2 depicts normalized spectra of the absorption spectra of lysine, HA, poly-L-lysine and histone. The spectra appear nearly superimposable on each other above 325

nm. This could be attributed to their common origin. Also shown in the figure is a Rayleigh scatter plot obtained with $Mg(OH)_2$ as scatterer and a simulated scatter plot assuming λ^{-4} dependence. There is a clear difference between the spectra of the protein and polylysine from that due to scatter. Hence, the possibility of the absorbance features occurring due to scattering may be ruled out.

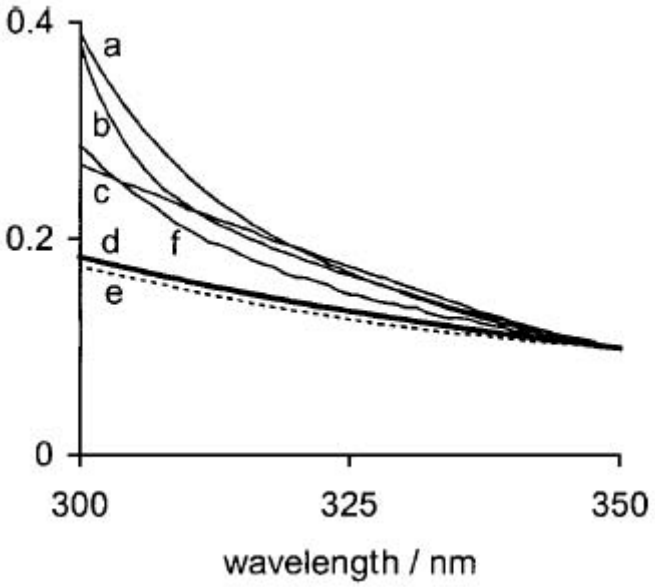

Figure 5.2.2 Can it be due to Rayleigh scattering?: The absorption spectra are as follows: (a) calf thymus histone; (b) human serum albumin; (c) L-lysine; (d) simulated scatter (thick line); (e) a dilute scattering solution of $Mg(OH)_2$ (dashed line); and (f) poly-L-lysine. For the sake of comparison, all absorption spectra except human serum albumin were normalized to have identical absorption at 350 nm.

From figure 5.2.1 it is also apparent that the absorbance of HA is much greater than that of barstar, subtilisin Carlsberg or lysozyme. We will now try to explain these features based on the 3-D structure of the proteins in their native state (as obtained from PDB).

The spatial distributions of lysine residues in the proteins studied are given in table II. The values clearly show that barstar and Subtilisin Carlsberg have no lysine pairs separated by less than 7.2 A, whereas lysozyme has only one pair of proximal lysine residues. This could account for the low absorption values of lysozyme, barstar and subtilisin Carlsberg and for the comparatively higher absorbance of human serum albumin and histone. If intermolecular interactions among the proximal lysine residues

are responsible for the observed structures, then, just such distance dependence should be observed.

Table II: Spatial distribution of Lysine residues in the proteins studied

Protein	PDB code	Number of lysines in the protein sequence	Number of lysine pairs separated by less than 7.2 Å
Lysozyme	1E8L	6	1
Barstar	1BTA	6	0
Subtilisin Carlsberg	1SCA	9	0
Human Serum Albumin	1AO6	59	7

Figure 5.2.3 shows the proximal lysine pairs in HA (separated by less than 7.2A). The distances calculated from the 3-D structures are only average indicators of the true picture in solution at any given time. Yet, based on these correlations above, it appears plausible to link the observed absorption spectra with proximal lysine residues.

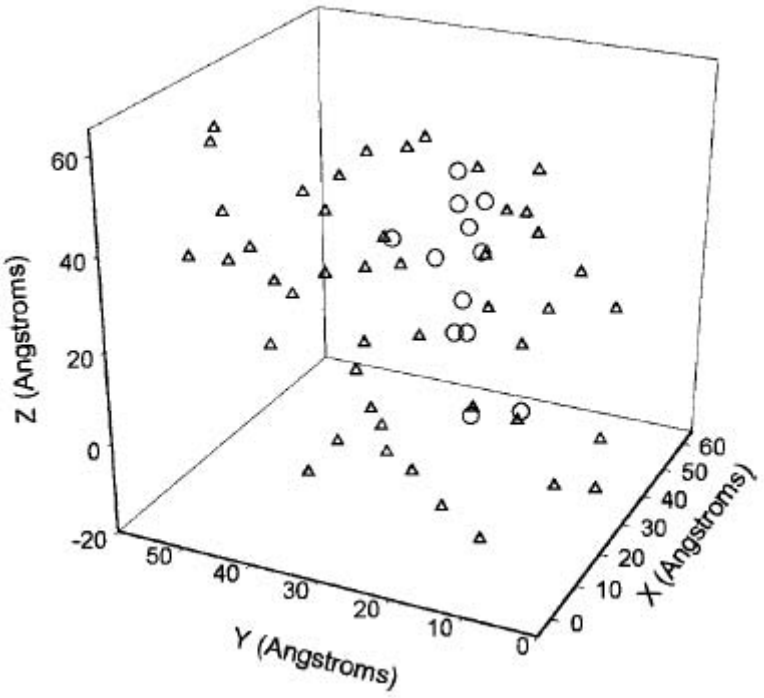

Figure 5.2.3 Lysine clusters in human serum albumin: The three-dimensional spatial distribution of ε-amino N atoms in HA are shown employing the crystal structure from PDB (1AO6, Chain A). The atoms that are closer to one another by less than 7.2 Å in space are indicated as open circles, while the rest are shown as open triangles.

The large value of ε_{325} in HA(~1546 $M^{-1}cm^{-1}$) can be attributed to the folded globular protein architecture which enables a multitude of possible interactions among the lysine residues. Poly-L-lysine on the other hand is known to have a random coil structure near neutral pH and 25^{o}C (Rosenheck and Doty, 1961).

To verify the above assumptions, two sets of experiments were carried out with histones. One in which absorbance was measured in the absence and presence of 6 M guanidinium chloride, denoted henceforth, as GdnCl (fig5.2.4). The addition of the 6 M GdnCl caused a sharp decrease (4-fold at 325 nm) in absorbance which can be attributed to a drop in the population of proximal lysine pairs.

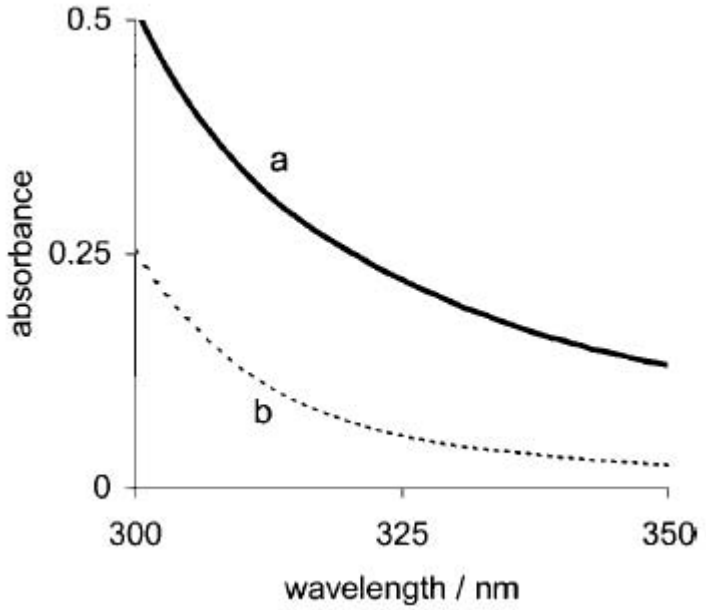

Figure 5.2.4 Monitoring protein unfolding: The absorption spectra of calf-thymus histone [11 mg/ml] is shown at pH 7 in the absence (curve "a") and presence (curve "b") of 6 M guanidine chloride (buffered at pH7). Other conditions are similar to figure 5.2.1

A similar drop in absorbance was observed with 8 M urea as shown in Figure 5.2.5

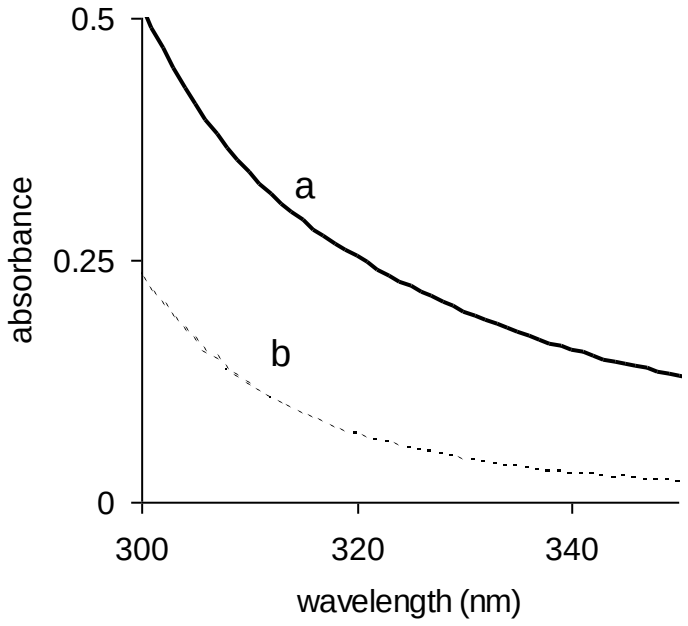

Figure 5.2.5 Unfolding of 11 mg/ml histone: at pH 7 in native state (curve a) and in unfolded state in 8 M urea (curve b) also buffered at pH 7. Conditions are similar to those used in figure 5.2.1.

In another experiment, the absorbance of histone was monitored with increasing concentration of histone from 0.7 mg/ml to 10 mg/ml. The absorbance was plotted against protein concentration at 325 nm as shown in fig 5.2.6. This wavelength was chosen to be away from trp absorption. A distinct break in linearity is observed at a concentration of 7.1 mg/ml. The biphasic transition clearly indicates the formation of histone aggregates. After aggregation the lys lys absorption shows a more rapid increase with concentration due to an increase in the population of lys lys pairs post aggregation.

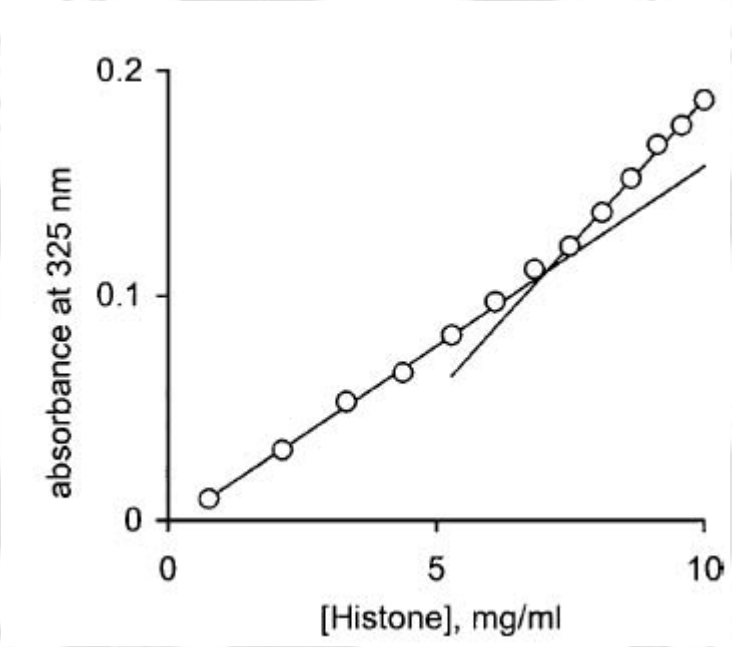

Figure 5.2.6 Monitoring protein aggregation: The absorbance of calf thymus histone at 325 nm is plotted against its concentration. Five consecutive points from both ends were joined to obtain the fitted straight lines. The lines intersect at a concentration of 7.1 mg/ml. Other conditions are similar to figure 5.2.1

The results in figures 5.2.4, 5.2.5 and 5.2.6 clearly argue against the role of impurities in producing the observed lysine spectra. Since it is not likely that GdnCl can affect absorbance of impurities or that impurities could have a non-linear dependence on concentration. The above experiments demonstrate a simple and economical method to monitor protein aggregation and unfolding of lysine rich proteins.

A brief discussion now, on the nature of the forces that can cause lys-lys interaction in proteins. One hypothesis is the bridging water molecule between each of the N-H groups of the Lys-Lys pair. The two lone pairs in the O atom of the bridging water molecule can each act as hydrogen bond acceptors for one H atom each from each of the two nitrogens. Such an arrangement is a) is not uncommon in proteins (Arteca and Luo, 2000); b) requires the distance between the two nitrogen atoms to be around ~7Å; c) is not affected if the ε– amino groupexists as $–NH_3^+$ since the N lone pair is not involved. In fact, our data with lysine amino acid indicate only a minor change in the absorption in the pH range from 2 to 11(unpublished results). More work is required to prove this interaction.

The major question that remains to be answered is the nature of the chromophore involved. Here, one should avoid speculation; it is imperative that we perform quantum chemical calculations a) to support possible structure and b) to determine the oscillator strength for the transition theoretically.

Neutron diffraction studies of crystals of L-lysine.HCl indicate the presence of infinite sheets of hydrogen bonds involving chloride ions and the terminal amine groups in crystals of L-lysine.HCl. The sequence N-H···O-H···Cl···H binds the infinite chains of lysine molecules in the structure together (Koetzle et.al, 1972). There are ten hydrogen bonds per asymmetric unit of the crystal structure. The packing scheme that is shown in the figure below consists of chains of lysine cations interconnected through the water molecules and chloride ions. An interesting feature of these structures especially in the light of our previous discussion of the nature of interactions taking place, in concentrated aqueous solutions of L-lysine.HCl is that there is no evidence for the formation of *intramolecular* hydrogen bonds. So, if indeed, hydrogen bonds are responsible for the absorbance features that we have seen, a theoretical investigation will be required to ascertain exactly how they can give rise to the observed spectroscopic features.

Koetzle et. al, Acta Cryst. (1972) B78, 3207
Neutron diffraction structure of L-lysine.HCl dihydrate.

Table 4. *Hydrogen bond distances* (Å) *and angles* (°)

A–H···B–C	A–H	A···B	H···B	∠A–H···B	∠H···B–C
$N–H^1\cdots O^{w2}$ (H^{w2}, H^{w22})	1·034 (4)	2·824 (4)	1·836 (6)	158·5 (4)	96·4 (4) 131·2 (6)
$N–H^2\cdots Cl^-$	1·028 (4)	3·217 (2)	2·196 (4)	172·0 (4)	
$N–H^3\cdots O^2–C$	1·059 (4)	2·795 (3)	1·740 (5)	173·4 (4)	110·9 (2)
$N^c–H^{c1}\cdots O–C$	1·016 (5)	2·887 (3)	2·083 (6)	134·4 (6)	135·4 (2)
$N^c–H^{c2}\cdots O^2–C$	1·024 (5)	2·788 (2)	1·865 (6)	148·3 (5)	131·2 (2)
$N^c–H^{c1}\cdots Cl^-$	1·026 (4)	3·173 (2)	2·150 (5)	174·8 (4)	
$O^{w1}–H^{w11}\cdots O^1–C$	0·960 (9)	2·805 (5)	1·857 (7)	169·2 (7)	113·5 (2)
$O^{w1}–H^{w12}\cdots Cl^-$	0·953 (11)	3·220 (5)	2·273 (8)	172·7 (6)	
$O^{w2}–H^{w21}\cdots O^{w1}$ (H^{w11}, H^{w12})	0·957 (11)	2·718 (6)	1·775 (9)	167·9 (6)	111·2 (6) 123·9 (6)
$O^{w2}–H^{w22}\cdots Cl^-$	0·936 (9)	3·254 (4)	2·329 (7)	169·7 (6)	

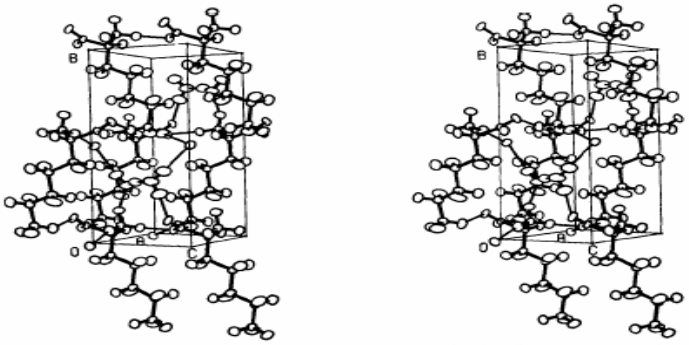

Fig. 2. Stereoscopic view of the packing around one unit cell with thermal ellipsoids drawn to enclose 30 % probability. Molecular bonds are drawn thick and hydrogen bonds thin.

CONCLUSIONS:

1. Absorbance features were observed beyond 315 nm in the proteins human serum albumin and histone which were similar in shape to the absorbance band of lysine. Similar features were not observed in case of barstar, lysozyme and subtilisin Carlsberg.
2. The ratios of absorbances A_{350}/A_{325} were measured. These ratios were used to compare the shapes of the different proteins, lysine and poly-L-lysine in a concentration independent manner. Comparison of the A_{350}/A_{325} ratios indicated that the absorbance features that were observed arise due to lysine-lysine interactions.
3. Comparison of the absorbance ratios obtained with the proteins HSA and histone with that of poly-L-lysine indicated that the interactions giving rise to the absorbance features are *intramolecular* in origin.
4. PDB crystal structures of the proteins HSA, lysozyme and barstar, indicated the presence of seven proximal lysine pairs in HSA which could account for its

higher absorbance as compared with those of lysozyme which has one pair and subtilisin Carlsberg and barstar which have none.

5. The absorbance feature of histone could be used to monitor unfolding and aggregation of histone.
6. The exact nature of the interactions that give rise to these features could not be ascertained. Crystal structures of lysine indicate the presence of infinite sheets of lysine molecules linked together by hydrogen bonds involving the hydrogen atoms of the α–ammonium groups and water molecules and chloride ions. However, to actually determine the nature of the chromophore involved, detailed quantum-mechanical calculations are required.

Indian Institute of Technology Guwahati

CHAPTER 6

Slow Aggregation of Lysozyme in Alkaline pH Monitored in Real Time Employing the Fluorescence Anisotropy of Covalently Labeled Dansyl Probe

The occurrence of protein aggregates has wide ranging repercussions in biology (Cleland et al., 1993; Chi et al., 2003). Insoluble protein aggregates like amyloid fibrils and inclusion bodies are associated with a large number of diseases that arise due to the degeneration of nerve cells (Thirumalai et al., 2003; Selkoe, 2001; Hardy and Selkoe, 2002; Prusiner, 1998). The importance of understanding the molecular basis of these aggregates cannot be overstated. Recent findings indicate that soluble oligomers of proteins which are precursors to these insoluble aggregates are actually the toxic species (Lambert, 1998; Hardy and Selkoe, 2002; Walsh et al., 1999). Reports by Walsh et al.(Walsh et al., 2002) indicate that soluble amyloid-beta peptide-levels in Alzheimer's disease brains have a stronger correlation with the severity of dementia (which is an outcome of Alzheimer's disease) as compared to the quantity of insoluble fibrillar deposits. Moreover, in experiments conducted with proteins not associated with diseases, but which formed fibrils in *in vitro* conditions, aggregates formed prior to the appearance of fibrils were found to be toxic to cells (Bucciantini et al., 2002). It has also been observed that in most cases where protein aggregation and disease associated phenotypes were separated in time, fibrous proteinacious inclusions were observed much after the onset of the behavioral or neuro-pathological symptoms (Caughey and Lansbury, 2003; Lansbury, 1999; Goldberg and Lansbury, 2000; Haass and Steiner; 2001).

There is thus an urgent need to identify the early stages involved in the aggregation process (Thirumalai et al., 2003; Bessen et al., 1995; Collinge et al., 1996; Safar et al., 1998). In most of the cases this poses a problem because of the rapid rate at which most proteins aggregate e. g., barstar a protein that inhibits barnase, aggregates as soon as it is transferred from a pH 7 to a pH 3 buffer. In such cases it becomes difficult to study the intermediates involved in the aggregation process. Identification of the intermediates

involved could lead to development of therapeutic procedures to arrest the further growth of these aggregates and perhaps also make the process reversible (Collinge et al., 1996).

We report in this chapter the observation of slow growth of aggregates of hen egg white lysozyme in pH 12.2 buffer. The growth of these aggregates was traced over a period of about 18 hours using fluorescence anisotropy of covalently labeled dansyl probe. There have not been too many reports tracking the growth of soluble oligomers in real time using anisotropy. Fluorescence anisotropy is an excellent technique to study the rotational motion of fluorophores in the excited state following their excitation using plane polarized light (Levi and Recha, 2003). Steady-state fluorescence anisotropy (r_{ss}) gives us a time integrated average value of the rotational motion of molecules in the excited state. This parameter is however dependent both on the fluorescence lifetime and rotational correlation time of the fluorescent probe. Time-resolved anisotropy decay observations can reveal the multiple rotational motions experienced by the fluorophore in the excited state in terms of their rotational correlation times, ϕ_i. As ϕ arising from whole protein tumbling, is directly related to the size (volume) of the fluorophore conjugated protein, using the Stokes-Einstein equation any event like protein aggregation can be directly monitored by measuring ϕ. The advantage of using anisotropy over other techniques is its sensitivity and selectivity (Allsop et al., 2001). In our work, HEWL was covalently tagged with the fluorescent probe, 2-dimethylamino naphthalene sulfonyl chloride (dansyl chloride) in order to specifically monitor the rotational motion of lysozyme in solution under two different conditions. A) pH 12.2 (aggregation prone condition) and (b) pH 7 (native state). There have been earlier reports of the formation of dimers of lysozyme at alkaline pH (Sophianopoulos and van Holde, 1961;1964) and also reports on the formation of fibrils by reduced hen egg white lysozyme(Arnaudov and Vries, 2005; Krebs et al., 2000).

For our experiments we have used commercially available chicken egg white lysozyme which we then labeled with the probe dansyl chloride. Refer to section 3 of chapter 3 for details regarding the labeling. We have used two conditions in our experiments viz., an alkaline pH condition using a 50mM pH 12.2 phosphate buffer and a pH 7 medium using a 50 mM phosphate buffer. The reasons for choosing the alkaline pH

of 12.2 for our studies are discussed in section 6.1.6. pH 7 buffer was used to have the protein in its native monomeric state.

6.1 Steady-State Fluorescence Measurements

Solutions of the dansyl labeled proteins in both pH 7 and pH 12 buffers had their emission maxima at 443 nm. The fluorescence measurements were carried out with 370 nm excitation, though the emission maximum of the dansyl probe is at ~339 nm. This particular wavelength was chosen for both steady-state and time-resolved measurements because this is the shortest wavelength available to us in our time-resolved setup. The light source being a 370 nm nanoLED.

6.2 Steady-State Anisotropy Experiments

Steady-state anisotropy measurements of dansyl labeled lysozyme in pH 7 and pH 12.2 were carried out at room temperature. The measurements were made over periods of 6 hours initially and then after overnight incubation of the respective solutions at room temperature. Figure 6.1 shows the variation of steady-state anisotropy (r_{ss}) of the dansyl labeled lysozyme with time and also as a function of pH and concentration of the labeled lysozyme.

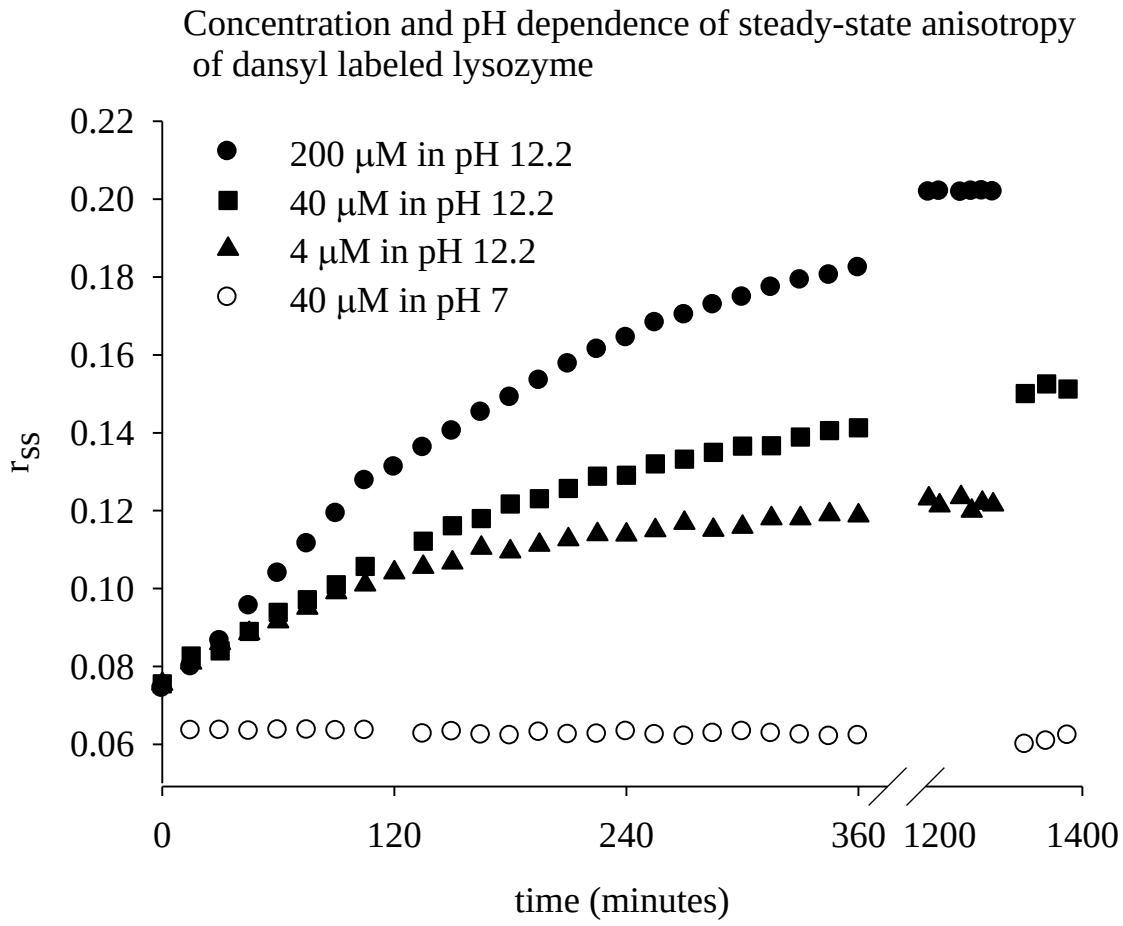

Figure 6.1 Change in steady-state anisotropy of dansyl labled lysozyme with time, pH 7, 40 μM, open circles; pH 12.2, 4 μM, filled triangles; pH 12.2, 40 μM, filled squares; pH 12.2, 200 μM, filled circles.

There is a clear difference between the four curves. The steady-state anisotropy, r_{ss}, was observed to have values of 0.06 at pH 7. This value remained unchanged even after overnight incubation. The r_{ss} of 0.06 was obtained with different concentrations of the labeled protein in pH 7 buffer (data not shown) and the values were observed to remain unchanged with time. However, immediately on transferring the labeled protein to the pH 12.2 buffer, the r_{ss} immediately increased to 0.08 and kept increasing gradually during the initial 360 minutes of measurement, eventually saturating after overnight incubation. Now, steady-state anisotropy is a function of both fluorescence lifetime (τ) and the rotational correlation time (θ) of the protein (eq. 2.48). So, this change in anisotropy could be due to a change in quantum yield of the probe that is used or could be due to an

increase in θ of the protein. In order to determine what is actually happening, time-resolved measurements were carried out. However, it is also apparent from figure 6.1, that the r_{ss} values show a marked dependence on concentration of the labeled protein. The concentrations were varied from 4 to 200 μM. The r_{ss} of 4 μM sample in pH 12.2 was observed to saturate at 0.13 after overnight incubation, that of 40 μM sample was observed to saturate at 0.15 and the r_{ss} of the 200 μM sample was observed to saturate at 0.20. This marked concentration dependence that is observed in the rise of r_{ss} could serve as an indicator of the onset of aggregation which would result in a change of θ. Indeed, whatever the nature of the kinetics involved, the growth rate of aggregates will ultimately depend on the concentration of the monomers in solution. The difference in the r_{ss} values reached at saturation with the different concentrations of labeled protein seems to indicate that the sizes of the aggregates formed are also dependent on the concentrations of the monomers used. Larger aggregates appear to form at higher concentrations. Another fact to be noted is that, the 200 μM sample used contained just 40μM labeled protein. This seems to rule out the role of the dansyl probe in promoting aggregation.

6.3 Time-Resolved Fluorescence Measurements

Analysis of time-resolved fluorescence intensity decays revealed the presence of three lifetimes. A larger component of 12 ns, a medium component of ~6 ns and a short component of ~1 ns was present. In both pH 7 and pH 12 buffers the three components could be observed. The occurrence of these three components may indicate the structural heterogeneity of lysozyme in solution (Wang et al. 2002; 2004). The figures 6.2A and 6.2B depict the intensity decay profiles of the labeled lysozyme in pH 7 and pH 12 buffer respectively. Tables 1 and 2 show the data obtained on analyzing the intensity decay profiles at pH 7 and pH 12 respectively.

Fluorescence intensity decay of 40 μM dansyl labeled lysozyme at pH 7

$\chi^2 = 1.4$

$\tau_1 = 5.03$ ns; $\alpha_1 = 0.059$

$\tau_2 = 12.14$ ns; $\alpha_2 = 0.92$

$\tau_3 = 0.963$ ns; $\alpha_3 = 0.02$

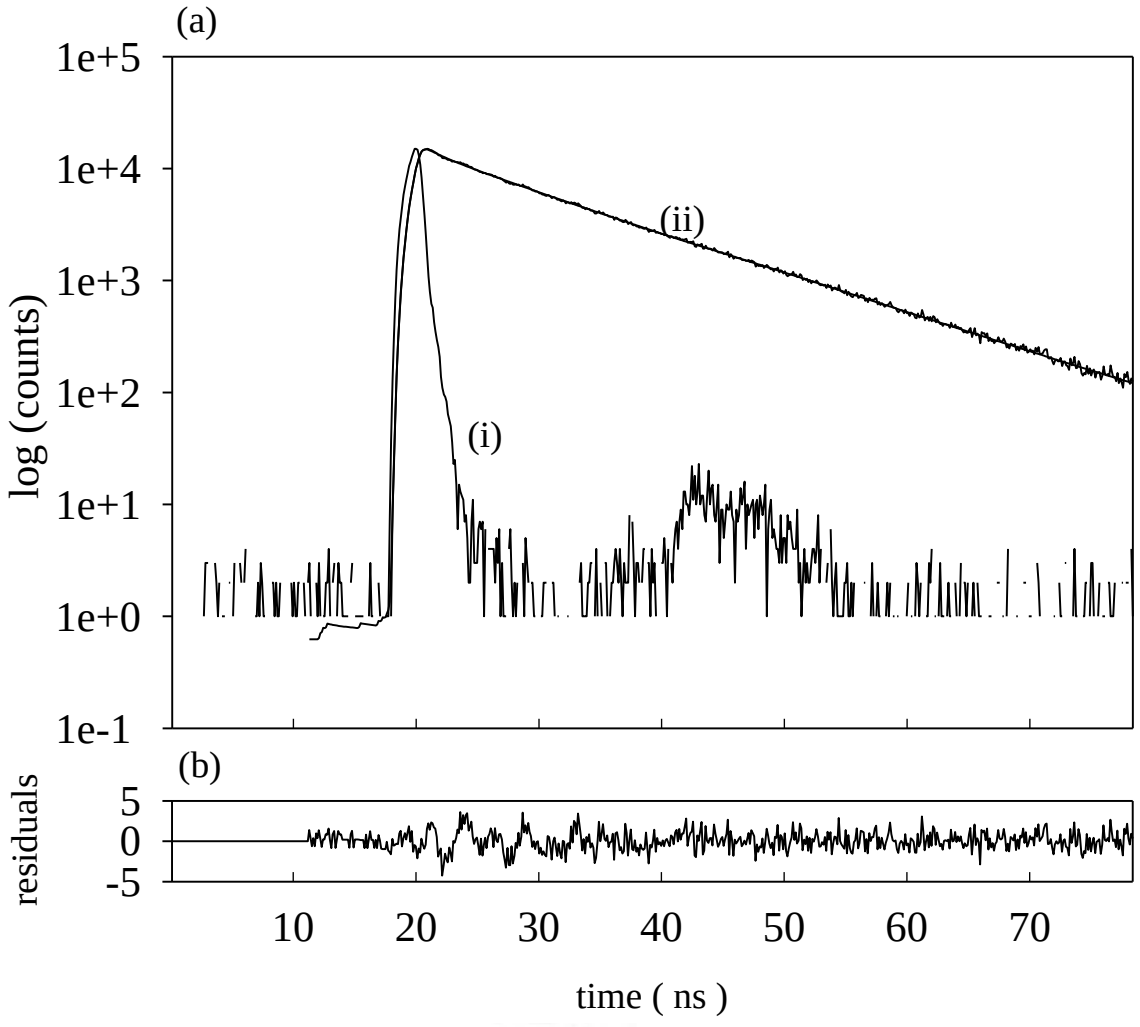

Figure 6.2A

The curves in (a) shown above correspond to (i) IRF; (ii)measured intensity decay with fit; and (b) corresponds to the residual plot.

Fluorescence intensity decay of 40 μM dansyl labeled lysozyme at pH 12.2

$\chi^2 = 1.4$

$\tau_1 = 5.14$ ns; $\alpha_1 = 0.12$
$\tau_2 = 12.44$ ns; $\alpha_2 = 0.86$
$\tau_3 = 0.73$ ns; $\alpha_3 = 0.02$

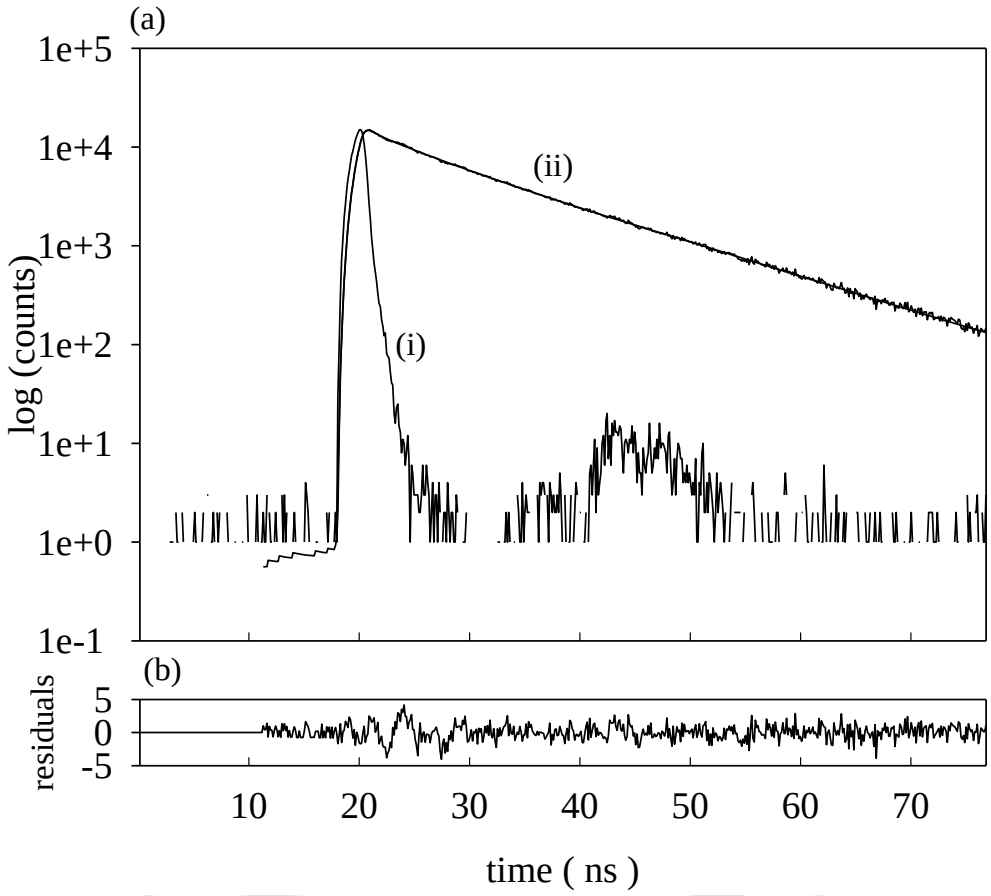

Figure 6.2B

The curves in (a) correspond to (i) IRF; (ii) measured intensity decay with fit; (b) corresponds to the plot of residuals

Table 1 Fluorescence lifetime of 40 μM dansyl labeled lysoszyme in pH 7 buffer

t mins	τ_1 (ns)	α_1	τ_2 (ns)	α_2	τ_3 (ns)	α_3	χ^2	Mean lifetime (τ_m) (ns)
15	5.6	0.07	12	0.9	0.88	0.03	1.8	11.22
57	5.4	0.07	12	0.9	0.75	0.02	1.4	11.31
87	5.8	0.08	12	0.9	0.94	0.02	1.4	11.28
116	5.8	0.07	12	0.9	1.1	0.02	1.3	11.23
144	5.9	0.09	12	0.9	1.1	0.02	1.4	11.35
172	5.9	0.08	12	0.9	1.0	0.02	1.2	11.29
200	5.9	0.09	12	0.9	1.0	0.02	1.2	11.35
229	5.9	0.07	12	0.9	1.2	0.02	1.4	11.24
262	5.8	0.08	12	0.9	0.98	0.02	1.5	11.28
289	5.8	0.07	12	0.9	1.1	0.02	1.4	11.23
317	5.8	0.09	12	0.9	0.74	0.02	1.3	11.34
349	5.7	0.07	12	0.9	1.1	0.02	1.7	11.22
393	5.7	0.07	12	0.9	1.2	0.02	1.7	11.22

Table 2 Fluorescence lifetime of 40 μM lysozyme in pH 12.2 buffer

t mins	τ_1 (ns)	α_1	τ_2 (ns)	α_2	τ_3 (ns)	α_3	χ^2	Mean lifetime (τ_m) (ns)
19	5.6	0.19	13	0.79	0.7	0.02	1.2	11.35
48	5.5	0.22	13	0.76	0.73	0.02	1.4	11.10
78	5.5	0.22	13	0.76	0.87	0.02	1.4	11.11
106	5.5	0.22	13	0.76	0.82	0.02	1.3	11.11
135	6.3	0.25	13	0.72	1.4	0.03	1.3	10.98
163	6.4	0.27	13	0.70	1.3	0.02	1.2	10.85
191	6.1	0.25	13	0.72	1.2	0.02	1.3	10.91
220	7.0	0.32	13	0.65	1.7	0.03	1.3	10.74
252	5.7	0.22	13	0.76	1.0	0.02	1.4	11.15
278	6.6	0.24	13	0.72	1.9	0.04	1.4	11.02
327	5.8	0.22	13	0.76	1.1	0.02	1.6	11.18
355	5.8	0.22	13	0.77	0.97	0.02	1.6	11.30

Mean lifetimes (τ_m) of the labeled protein were calculated in pH 7 and pH 12 buffers to enable comparison. The mean lifetimes were found to vary from 11.2-11.3 ns in pH 7 buffer and from 10.7-11.4 in pH 12.2 buffer over the period of 360 minutes. The almost unchanging value of mean lifetimes in pH 7 and pH 12.2 buffers respectively could be due to attachment of the dansyl probe to ε–amino groups of L-lysine residues in the protein which remain exposed to the polar solvent in both the monomeric and aggregated forms. Figure 6.3 shows a plot of mean fluorescence lifetime (ns) as a function of time (minutes). The concentration of the labeled protein solution used for the time-resolved measurements was 40μM.

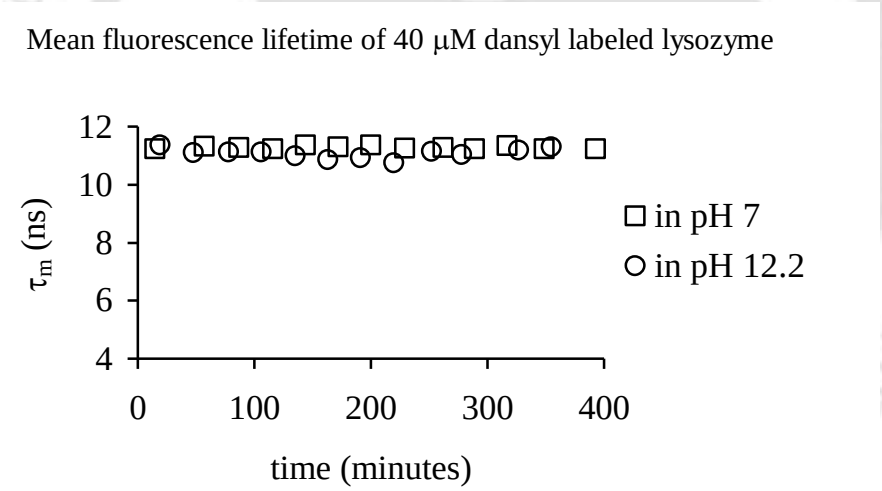

Figure 6.3 Mean fluorescence lifetime, τ_m, of 40 μM dansyl labeled chicken egg white lysozyme was calculated using the formula $\tau_m = \sum_{i=1}^{3} \alpha_i \tau_i$ where τ_i and α_i correspond to the ith lifetime component and its amplitude. The intensity decays shown in figure 1 could be fit to 3-exponential decay models; hence the 3 lifetime components. The intensity decays were monitored over a period of ~360 minutes. The mean fluorescence lifetimes (τ_m) were determined in pH 7 buffer (depicted by open squares) and in pH 12.2 buffer (shown as open circles). The values were observed to remain unchanged over the duration of the measurement (~360 minutes) and were also observed to not vary with pH.

From, the fluorescence lifetime measurements we may conclude that the rise in r_{ss} observed earlier may not be attributed to change in fluorescence lifetime of the protein. We then set out to determine the rotational correlation time of the labeled protein.

6.4 Time-Resolved Anisotropy Decay Measurements

Anisotropy decay measurements were done to determine the rotational correlation times of 40 μM labeled protein in both pH 7 and pH 12 buffers respectively. The correlation times were monitored over a period of ~ 18 hours (the correlation times were monitored initially over a period of ~ 360 minutes and then again after overnight incubation of the respective protein solutions at room temperature).

Figure 6.4 shows anisotropy decay profiles of 40 μM dansyl labeled lysozyme in pH 7 and pH 12 buffers respectively. The anisotropy decay profile at pH 7 shows a rapid decay whereas, the profile of the sample at pH 12.2 decays less rapidly even at the beginning of the measurement. The anisotropy r(t) is observed to decay less and less rapidly at pH 12.2 with increasing time (minutes) and there is a residual anisotropy at long times (30 ns) . The residual anisotropy is observed to increase with time till t=355 minutes, after which a small drop occurs after overnight incubation.

Analysis of the anisotropy decay profiles (details are provided in chapter 3-section3) revealed that at pH 7 the labeled protein undergoes a mono-exponential decay with a rotational correlation time of 3.6 ns. This value is in close agreement with values reported earlier for monomeric lysozyme at pH 7 (Vos et al., 1987). The r_0 value at pH 7 was observed to be 0.18 which is much less than the expected value of r_0 (0.27). This could arise due to ultrafast segmental motions that take place at sub-nano second time-scales beyond the resolution of the instrument used by us (FWHM of the 370 nm nanoLED ~ 1.3 ns. Table 3 contains the results of the anisotropy decay analysis.

Analysis of the anisotropy decay profile in pH 12.2 buffer at t=15 minutes revealed the presence of two correlation times, a long component of ~ 9.6 ns with an amplitude of 0.6 and a short component of 2.4 ns with an amplitude of 0.4. The long time component could arise due to formation of oligomers in solution, since even the r_{ss} values at pH 12.2 begin with values of 0.08 whereas r_{ss} values at pH 7 are in the range 0.06. The short component of 2.4 ns may be accounted for by fast segmental motions. As time

progresses, the long component increases from 9.6 to 45 ns. This is a clear indication of the formation of aggregates in solution since in no other way can a protein of the size of lysozyme (M_r~14,300 Da) in its monomeric form, however distorted, have such a long correlation time. After overnight incubation an insignificant drop in the long component was observed, from 45 ns at t=355 mins to ~43 ns at t=1188 minutes. The almost similar magnitude of the long component after overnight incubation shows that the aggregates that form are rather stable. The short component showed an increase in magnitude from 2.4 to 4.1 ns and after overnight incubation the value dropped slightly to 3.5 ns. This slight increase from the initial value could be due to hindered segmental motion of the aggregate. Now, in the figure 6.4, is also displayed the anisotropy decay profile at t= 60 minutes. This anisotropy decay profile had to be fitted to a 3-exponential decay model, since analysis with a 2-exponential model yielded a reduced χ^2 value of 3.12. The 3-exponential fit (with a reduced χ^2=1.4) revealed rotational correlation times, 1.4, 7.0 and 42 ns with amplitudes 0.19, 0.52, 0.29 respectively and a calculated r_{ss}= 0.118. The need of fitting the data to a 3-exponential decay model indicates the presence of a heterogeneous ground state population of oligomers owing to the presence of dimeric and multimeric aggregate species in the initial stages. Another interesting observation was made viz., that the aggregates appear to be fairly reversible during the first 60 minutes (see Table.5) after which time, they tend to be irreversible. This could, as stated before, indicate the presence of a significant population of smaller oligomers viz., dimers and maybe even monomers alongwith the higher oligomers at pH 12.2 in the first 60 minutes. Their populations obviously go down significantly with time as aggregation proceeds, which results in the formation of more of the higher oligomers. Curves obtained beyond 60 minutes e.g. at t=100 minutes, 215 minutes (see table 3) could be fitted to a 2-exponential decay model, possibly because the population at this stage comprises mostly the higher oligomers.

6.5 Effect of L-Arginine.HCl on aggregation

We have also studied the effect of arginine on the oligomerization of 40 μM labeled lysozyme in pH 12.2 buffer (figure 6.5a and b). There have been earlier reports of this

amino acid being the most effective among amino acids in suppressing the growth of aggregates in the reduced form of lysozyme after subjecting it to heat induced denaturation (Reddy et al., 2005; Shiraki et al., 2002). We observed that in the presence of high concentrations of arginine, 0.9 M, in pH 12.2 buffer, the anisotropy decays showed a much lower residual anisotropy at t=1140 minutes as compared to that obtained in the absence of arginine (Figure 6.5). The long correlation time component in the presence of arginine was 14 ns initially. The value increased to 20 ns at t=135 minutes; after overnight incubation the long component stabilized at 13 ns. The calculated steady-state anisotropy values were observed to come down from an initial value of 0.11 to 0.07 after overnight incubation. In the case of the pH 12.2 control however, the long correlation time component increased from 9 ns at t=20 minutes to 43 ns at t=1140 minutes with corresponding increase in steady-state anistropy values from 0.08 to 0.14 (table 3).

It is clear from the data in table 4 that 0.9 M Arginine is effective in arresting the growth of aggregates. The initial value of the long correlation time component of 14 ns in 0.9 M arginine at pH 12.2 as against 9 ns in the control at pH 12.2 may be explained by increase in viscosity by 1.56 fold of the protein solution on addition of 0.9 M Arginine.HCl. The value of 20 ns at t=135 minutes in the presence of 0.9 M arginine could actually indicate the formation of small oligomers initially which ultimately dissociate. Though the use of arginine as an inhibitor of aggregation is known, the mechanism of its action is still not known.

Table 3 Anisotropy decay data of 40 μM lysozyme

pH	t mins	r_0[a]	r_{ss}[b]	r_{ss}[m]	ϕ_1[c] (ns)	ϕ_2[c] (ns)	ϕ_3[c] (ns)	α_1[d]	α_2[d]	α_3[d]	χ^2[e]
7.0	--	0.18	0.043	0.06	3.6	--	--	1.0	--	--	1.6
12.2	15	0.24	0.08	0.082	2.4	9.6	--	0.40	0.60	--	1.4
12.2	60	0.26	0.118	0.094	1.4	7.0	42	0.19	0.52	0.29	1.4
12.2	100	0.24	0.127	0.11	5.3	39	--	0.53	0.47	--	1.4
12.2	215	0.24	0.14	0.13	3.7	39	--	0.36	0.64	--	1.4
12.2	355	0.25	0.15	0.15	4.1	45	--	0.36	0.64	--	1.5
12.2	1188	0.22	0.14	0.15	3.5	43		0.32	0.68		1.6

[a] initial anisotropy; [b]steady state anisotropy calculated from fit; [c]rotational correlation time(s);[d]fractional amplitudes associated with correlation time; [e]reduced chisquare value or the fit; [m] experimentally measured steady-state anisotropy.

Table 4 Anisotropy decay data of 40 μM lysozyme in pH 12.2 buffer with 0.9 M L-Arginine.HCl

pH	t (mins)	r_0	r_{ss}	ϕ_1[c] (ns)	ϕ_2[c] (ns)	α_1[d]	α_2[d]	χ^2[e]
12.2 Arg	22	0.25	0.11	2.9	14	0.33	0.67	1.4
-do-	135	0.23	0.11	3.3	20	0.37	0.63	1.4
-do-	1140	0.20	0.069	1.9	13	0.49	0.51	1.6
12.2 Control	20	0.24	0.08	2.7	9	0.43	0.57	1.4
-do-	1140	0.22	0.14	3.5	42	0.32	0.67	1.6

[a] initial anisotropy; [b]steady state anisotropy calculated from fit; [c]rotational correlation time(s);[d]fractional amplitudes associated with correlation time; [e]reduced chisquare value or the fit.

6.6 Reversibility:

The aggregates that formed with 40 μM dansyl labeled lysozyme at pH 12.2 were observed to be reversible in the first 60 minutes of the experiment, however, aggregates obtained after t=60 minutes were fairly irreversible. (Table 5) To study reversibility 100 μl aliquots of 40 μM sample at pH 12.2 were transferred to 900 μl of 100 mM phosphate buffer at pH 7 at different times. The final concentration of the protein was 4 μM.

Table 5 Reversibility data

time (mins)	r_{ss} of 40 μM protein solution in 50 mM pH 12.2 buffer	Initial r_{ss} of 4 μM in 100 mM pH 7 buffer after transferring	r_{ss} after overnight incubation (pH 7) at room temperature
5	0.073 ± 0.001	0.065 ± 0.004	0.063 ± 0.002
30	0.080 ± 0.001	0.070 ± 0.001	0.066 ± 0.001
60	0.082 ± 0.001	0.081 ± 0.001	0.075 ± 0.003
120	0.093 ± 0.001	0.097 ± 0.001	0.092 ± 0.001
180	0.10 ± 0.001	0.11 ± 0.001	0.12 ± 0.002
300	0.11 ± 0.001	0.14 ± 0.001	0.13± 0.004

6.7 pH dependence:

Steady-state anisotropy measurements of 40 μM lysozyme were done in buffers with pH ranging from 4 to 12.2. The pH dependence of the formation of aggregates was also studied with 40 μM dansyl labeled lysozyme as shown in figure 6.6. It is clear from the figure that, at the concentration we have used, aggregates do not form at pH values below 12.2. In earlier reports Sophianopoulos et al observed dimer formation in the pH range 5-9 (Sophianopoulos and van Holde, 1961; 1964). However, the concentration of lysozyme used by them was much higher ~1.5 mM whereas in our case the concentrations were 40 μM.

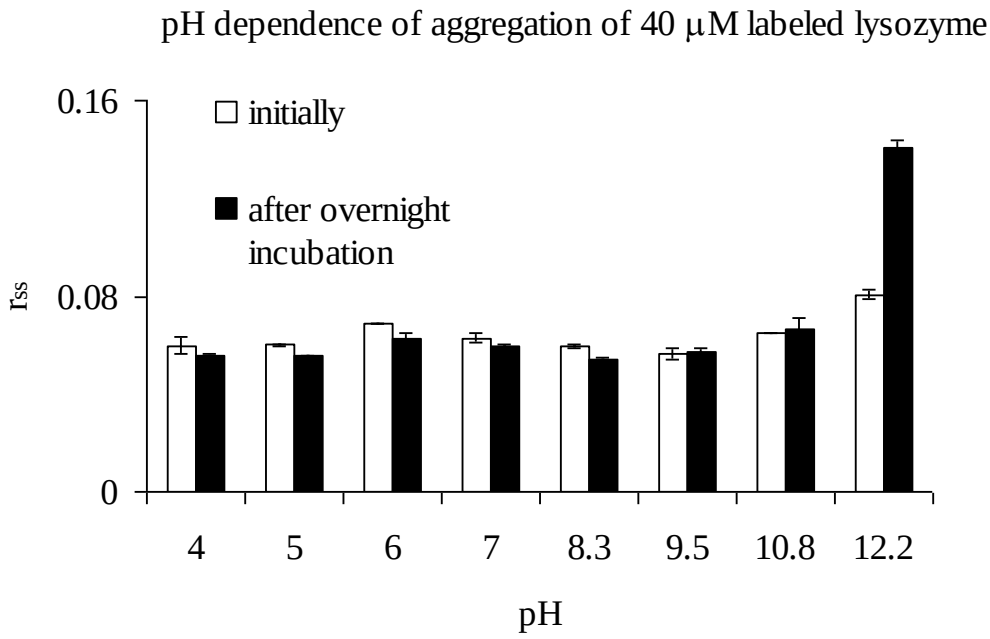

Figure 6.6 The above plot shows steady-state anisotropy values of 40 μM dansyl labeled chicken egg white lysozyme in different pH buffers. The buffers used were:
pH 4 buffer= glycine; pH 5= acetate; pH 6= citrate; pH 7= phosphate; pH 8.3=tris; pH 9.5= glycine; pH 10.8= CABS; pH 12.2= phosphate
In the above figure the white columns show the r_{ss} values of the protein solutions immediately after preparation and the black columns denote the r_{ss} values after overnight incubation of the protein solutions in the respective buffers at room temperature.

6.8 Experiments with Guanidinium Chloride:

We attempted to denature day old aggregates that were obtained by overnight incubation of 40 μM dansyl labeled lysozyme in pH 12.2 buffer with 6 M guanidinium chloride. For the purpose, 100 μl aliquot of the aggregate solution was added to 900 μl of 6M guanidinium chloride buffered at pH7. The steady-state anisotropy of the resulting solution was measured immediately after preparation and after allowing the solution to stand overnight at room temperature. No significant change in r_{ss} was observed indicating that even a strong denaturant like guanidinium hydrochloride was unsuccessful in breaking up the aggregates.(table 6)

Table 6: Effect of guanidinium chloride on day old aggregates

r_{ss} immediately after mixing	r_{ss} after overnight incubation
0.1284 ± 0.002	0.1167 ± 0.001

6.9 Experiments with KCl

Steady-state anisotropy measurements of the protein in 150 mM KCl at pH 12.2 showed no change as compared with the control of the same concentration at pH 12.2 in the absence of KCl (fig.6.7). This could indicate absence of electrostatic interactions.

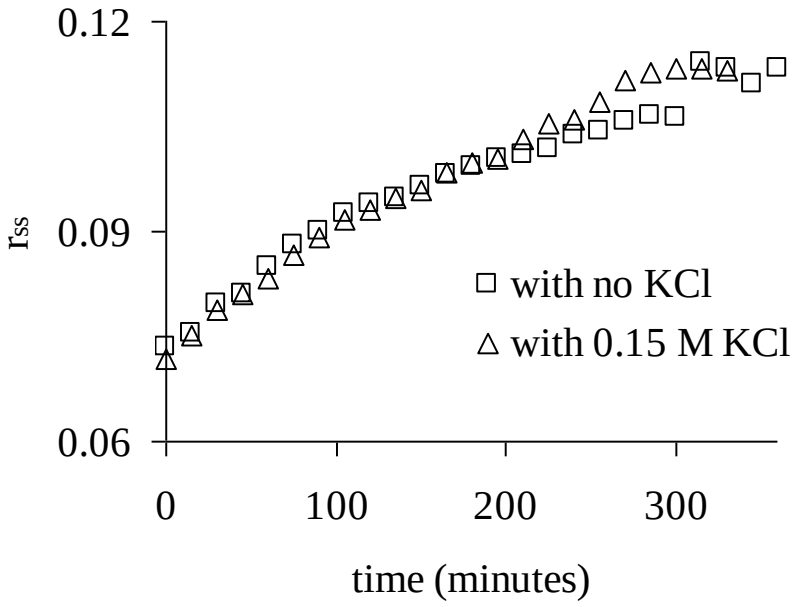

Figure 6.7 Steady-state anisotropy plots of 40 μM solutions of chicken egg white lysozyme in pH 12 buffer with 0.15 M KCl (open triangles) and without KCl (open squares). No change is observed in the presence of 0.15 M KCl.

The protein lysozyme that we have used for our studies is a well characterized system. There are numerous structures of it available in PDB. The slow aggregation of lysozyme that we have observed in pH 12.2 may be used to unravel the detailed molecular mechanisms involved in aggregation using techniques like nuclear magnetic resonance spectroscopy.

Conclusions:

1. Slow growth of soluble aggregates of lysozyme was tracked in real time using steady-state and time-resolved fluorescence anisotropy.
2. The rotational correlation time of 39-44 ns that was observed in pH 12.2 buffer implies the formation of a lysozyme aggregate ~10 monomeric units

3. L- Arginine HCl (0.9 M) was observed to prevent growth of aggregates
4. The aggregation was observed to be reversible in the initial 60 minutes after the protein is exposed to pH 12.2 buffer.
5. Day old aggregates of lysozyme in pH 12.2 buffer could not be broken up on addition of 6 M guanidium chloride, which is a known denaturant.
6. Lysozyme was observed to have a propensity to aggregate at the alkaline pH 12.2.
7. The sensitivity of fluorescence anisotropy enables detection of aggregates at the earliest stages of their formation.

TH-265_004703

Bibliography

1. Albe, K. R.; Butler, M. H.; Wright, B. E. Cellular concentrations of enzymes and their substrates. *J. Theor. Biol*. **1990**, 143, 163-195.
2. Al-Habori, M. Macromolecular crowding and its role as intracellular signaling of cell volume regulation *Int. J. Biochem. Cell Biol*. **2001**, 33, 844-864.
3. Allsop, D.; Swanson, L.; Moore, S.; Davies, Y.; York, A.; El-Agnaf, O. M. A.; Soutar, I., K. The effects of arginine on the refolding of aggregated proteins: Not facilitate refolding but suppress aggregation, *Biochem. Biophys. Res. Commun*. **2003,** 304, 148-152.
4. Argyrakis, P.; Kopelman, R. Nearest-neighbour distance distribution and self-ordering in diffusion-controlled reactions. *Phys. Rev. A* **1990**, 41, 2114-2126.
5. Arnaudov, L. N.; Vries, R. D. Thermally induced fibrillar aggregation of hen egg white lysozyme, Biophys. J. **2005**, 88, 515-526.
6. Arteca, G. R.; Luo, X. Structural complexity and population analysis ofhydrogen-bonded networks in proteins *J. Mol. Struct. THEOCHEM*. **2000**, 479, 501-502.
7. Asaad, N.; Engberts, J. B. F. N. Cytosol-Mimetic Chemistry: Kinetics of the trypsin catalyzed hydrolysis of p-nitrophenyl acetate upon addition of polyethylene glycol and N-tert-Butyl Acetoacetamide *J. Am. Chem. Soc*. **2003**,125, 6874-6875.
8. Atkins, P. W. (1998) Physical Chemistry. Oxford University Press, New Delhi
9. Badea, M. G.; Brand, L., Time-Resolved Fluorescence Measurements, *Methods in Enzymol.* **1971**, 61, 378-425.
10. Bam, N. B.; Randolph, T. W.; Cleland, J. L. Stability of protein formulations: investigation of surfactant effects by a novel EPR spectroscopic technique *Pharm. Res*. **1995,** 12, 2-11.
11. Barber, B. J.; Babbitt, R. A.; Parameswaran, S.; Dutta, S. Age-related changes in rat interstitial matrix hydration and serum proteins *J. Gerontolol. A. Biol.Sci.Med. Sci*.**1995**, 50, B282-B287.

12. Barkley, M. D., Kowalczyk, A.A., and Brand. L. Fluorescence decay studies of anisotropic rotations: Internal motions in DNA, in Bimolecular Stereodynamics, Vol.1, R. H. Sarma (ed.), Adenine Press, New York,1981, pp. 391-403.
13. Bates, G, Huntingtin aggregation and toxicity in Huntington's disease. *Lancet* **2003**, 361, 1642-1644.
14. Beechem, J. M.; Brand, L. Time-resolved fluorescence of proteins *Annu. Rev. Biochem.* **1985,** 54, 43-71.
15. Belford, G. G., Belford, R. L., and Weber, G. Dynamics of fluorescence polarization in macromolecules Proc. Natl. Acad. Sci. U. S. A.1972, 69, 1392-1393.
16. Berke, S. J.; Paulson, H. L. Protein aggregation and the ubiquitin proteasome pathway: gaining the UPPer hand on neurodegeneration. *Curr. Opin. Genet. Dev*. **2003**, 13, 253-261.
17. Berry, H. Monte Carlo simulations of enzyme reactions in two dimensions: fractal kinetics and spatial segregation *Biophys. J.* **2002**, 83, 1891-1901.
18. Bessen, R. A.; Raymond, D. A. G. J.; Nandan, S.; Lansbury, P. T.; Caughey, B. Non-genetic propagation of strain specific properties of scrapie prion protein *Nature 1995*, 375, 698-700.
19. Bevington, P. R.; Robinson, D. K. Data reduction and error analysis for the physical sciences Second edition, McGraw-Hill, Inc., 1992.
20. Birch, D. J. S.; Imhof, R. E. Time-domain fluorescence spectroscopy using time-correlated single photon couting, in Topics in Fluorescence Spectroscopy, Volume 1, Techniques, J. R. Lakowicz (ed.),Plenum Press, New York, **1991**, pp1-95.
21. Blum, F. D. et al. Solvent self diffusion in polymer solutions *J. Colloid Interface Sci.* **1986**, 113, 336-341.
22. Booth, D. R.; Sunde, M.; Bellotti, V.; Robinson, C. V. ; Hutchinson, W. L.; Fraser, P. E.; Hawkins, P. N.; Dobson, C. M.; Radford, S. E.; Blake, C. C. F.; Pepys, M. B. Instability, unfolding and aggregation of human lysozyme variants underlying amyloid fibrillogenesis *Nature* **1995**, 385, 787-793.

23. Boren K.; Andersson, P.; Larsson, M.; Carlsson, U. Characterization of a molten globule state of bovine carbonic anhydrase III: loss of asymmetrical environment of the aromatic residues has a profound effect on both the near- and far- UV CD Spectrum. *Biochim. Biophys. Acta* **1999**, 1430, 111-118.
24. Boulanger, Jr. R. R.; Kantrowitz, E. R. Characterization of a monomeric Escherichia Coli alkaline phosphatase formed upon a single amino acid substitution. *J. Biol. Chem*. **2003**, 278, 23497-23501.
25. Brand, L., Knutson, J. R., Davenport, L., Beechem, J. M., Dale, R.E., Walbridge, D. G., and Kowalczyk, A. A. Time-resolved fluorescence spectroscopy: Some applications of associative behaviour to studies of proteins and membranes, in Spectroscopy and the Dynamics of Molecular Biological Systems, P. Bayley and R. E. Dale (eds.), Academic Press, London, 1985, pp. 259-305.
26. Bronsted, J. N. Theory of chemical reaction velocity Z. Phys. Chem. **1922**, 102, 169-207.
27. Bucciantini, M.; Giannoni, E.; Chiti, F.; Baroni, F.; Formigli,L.; Zurdo, J.; Taddei, N.; Ramponi, G.; Dobson, C. M.; Stefani, M. Inherent toxicity of aggregates implies a common mechanism for misfolding diseases *Nature* **2002**, 416, 507-511.
28. Bullock, A. N.; Fersht, A. R. Rescuing the functions of mutant p53 *Nature Rev. Cancer* **2001**, 1 68-76.
29. Callahan, M. A.; Xiong, L.; Caughey, B. Reversibility of scrapie-associated prion protein aggregation, *J. Biol. Chem*. **2001**, 276, 28022-28028.
30. Cantor, C. R.; Schimmel, P. R."Biophysical chemistry, Part II: Techniques for the study of biological structure and function", W.H. Freeman and Company, New York 1980.
31. Caughey, B.; Lansbury, P. T. Jr. Protofibrils, pores, fibrils and neurodegeneration: Separating the responsible protein aggregates from the innocent bystanders *Annu. Rev. NeuroSci*. **2003**, 26, 267-298.
32. Cayley, S.; Lewis, B. A.; Guttman, H. J.; Record, M. T. Jr. Characterization of the cytoplasm of Escherichia coli K-12 as a function of external osmolarity.

Implications for protein-DNA interactions in vivo. *J. Mol. Biol*. **1991**, 222, 281-300.

33. Chen, R. F. Dansyl labeled proteins: determination of extinction coefficient and number of bound residues with radioactive dansyl chloride *Anal. Biochem*. **1968**, 25, 412-416.
34. Chi, E. Y.; Krishnan, S.; Randolph, T. W.; Carpenter, J. F. Physical stability of proteins in aqueous solutions: mechanism and driving forces in non-native protein aggregation *Pharm. Res.* **2003**, 20, 1325-1336.
35. Chothia, C.; Janin, J. Principles of protein-protein recognition *Nature* **1975**, 256, 705-708.
36. Clarke, G.; Collins, R. A.; Leavitt, B. R.; Andrews, D. F., Hayden, M. R.; Lumsden, C. J.; McInnes, R. R. A one-hit model of cell death in inherited neuronal degenerations *Nature* **2000**, 406, 195-199.
37. Cleland, J. L.; Powell, M. F.; Shire, S. J. The development of stable protein formulations- a close look at protein aggregation deamidation and oxidation *Crit. Rev. Ther. Drug Carrier Syst*. **1993**, 10, 307-377.
38. Cohen, A. S.; Calkins, E. Electron microscopic observation on a fibrous component in amyloid of diverse origins *Nature* **1959**, 183, 1202-1203.
39. Cohen, F. E.; Kelly, J. W. Therapeutic approaches to protein misfolding diseases, *Nature* **2003**, 426, 905-909.
40. Cohen, F. E.; Kelly, J. W. Therapeutic approaches to protein-misfolding diseases *Nature* **2003**, 426, 905-909.
41. Collinge, J.; Sidle, K. C.; Meads, J.; Ironside, J.; Hill, A. F. Molecular analysis of prion strain variation and the etiology of new variant CJD. *Nature* **1996**, 383, 685-690.
42. Cooper G. J. S.; Willis, A. C.; Clark, A.; Turner, R. C.; Sim, R. B.; Reid, K. B. M. Purification and characterization of a peptide from amyloid-rich pancreas of type 2 diabetic patients. *Proc. Natl. Acad. Sci. USA* **1987**, 84, 628-632.
43. De Young, L. R.; Fink, A. L.; Dill, K. A. Aggregation of globular proteins *Acc. Chem. Res.* **1993**, 26, 614-620.

44. De Young, L. R.; Dill, K. A.; Fink, A. L. Aggregation and denaturation of apomyoglobin in aqueous urea solutions. *Biochemistry* **1993**, 32, 3877-3886.
45. Demas, J. N. Excited state lifetime measurements **1983**, Academic Press, New York.
46. Dimcheff, D. E.; Portis, J. L.; Caughey, B. Prion proteins meet protein quality control *Trends Cell Biol*. **2003**, 13, 337-340.
47. Dobson, C. M. Protein folding and misfolding, *Nature* **2003**, 426: 884-890.
48. Dockal, M.; Carter, D. C.; Rüker, F. Conformational transitions of the three recombinant domains of human serum albumin depending on pH. *J. Biol. Chem.*, **2000**, 275, 3042-3050.
49. Dong, D.; Winnik, M. A. The Py scale of solvent polarity. Solvent effects on the vibronic fine structure of pyrene fluorescence and empirical correlations with ET and Y values. *Photochem. Photobiol*. (1982) 35, 17-21.
50. Duma, R. I. ; Thirumalai, D. Exploring the propensities of helices in PrP^{C} to form beta-sheet using NMR structures and sequence alignments. *Biophys. J.* **2002**, 83, 1268-1280.
51. Dumitriu, S. Polysaccharides: Structural diversity and functional versatility, Marcl Dekker Inc., Hong Kong, 1998.
52. Edmond, E.; Ogston, A. G. An approach to the study of phase separation in ternary aqueous systems *Biochem. J.* **1968**, 109, 569-576.
53. Eftink, M. R., "Topics in Fluorescence Spectroscopy-Vol. 6: Protein Fluorescence," ed. by J. R. Lakowicz, Plenum Pub. Corp. New York (2001), pp. 1-15
54. Eigen, M. Prionics or the kinetic basis of prion diseases *Biophys. Chem.***1996** , 63, A1-A18.
55. Ellis, R. J. Macromolecular crowding: an important but neglected aspect of the intracellular environment. *Curr. Opin. Struct. Biol*. **2001b** 11,114-119.
56. Ellis, R. J. Macromolecular crowding: obvious but underappreciated. *Trends Biochem. Sci*. **2001a**,26, 597-604.
57. Elowitz, M. B. ; Surette, M. G. ; Wolf, P. E. ;Stock, J. B. ; Leibler, S. Protein mobility in the cytoplasm of Escherichia coli. *J. Bacteriol*. **2001**,181,197-302.

58. Esler, W. P. ; Felix, A. M., Stimson, E. R. ; Lachenmann, M. J. ; Ghilardi, J. R. ; Lu, Y.-A. ; Vinters, H. V. ; Mantyh, P. W. ; Lee, J. P. ; Maggio, J. E. Activation barriers to structural transition determine deposition rates of Alzheimer's disease *J. Struct. Biol.* **2000**, 130, 174-183.
59. Fasman, G. D. "Practical Handbook of Biochemistry and Molecular Biology" ed by, CRC Press, London, 1992, pp.79-83
60. Fink, A. L., Folding and Design, 3, R9,1998.
61. Fulton, A. B. How crowded is the cytoplasm? *Cell* **1982**, 30, 345-347.
62. Furukawa, R. et al. Macromolecules 1991, 24, 599-605.
63. Georgiou, G.; Valax, P.; Ostermeier, M.; Horowitz, P. M. Folding and aggregation of TEM beta-lactamase: analogies with the formation of inclusion bodies in Escherichia coli. *Protein Sci.,* **1994**, 3, 1953-1960.
64. Gibbons, R. M The scaled particle theory for particles of arbitrary shapes *Mol. Phys.* **1969**,17, 81-86.
65. Gillespie, D. T. A rigorous derivation of the chemical master equation. *Physica A.* **1992**, 188, 404-425.
66. Goldberg, M. E.; Rudolph, R.; Jaenicke, R. A kinetic study of the competition between renaturation and aggregation during the refolding of denatured-reduced egg white lysozyme. *Biochemistry* **1991** 30, 2790- 2797.
67. Goldberg, M. S.; Lansbury, P. T. Jr. Is there a cause-and-effect relationship between alpha-synuclein fibrillization and Parkinson's disease? *Nat. Cell Biol.* **2000**, 2, E115-E119.
68. Gombotz., W. R.; Pankey, S. C.; Phan, D.; Drager, R.; Donaldson, K.; Antonsen, K. P.; SHoffman, A. S.; Raff, H. V. The stabilization of a human IgM monoclonal antibody with poly(vinylpyrrolidone). *Pharm. Res*. **1994**, 11, 624-632.
69. Goodsell, D. S. The machinery of Life; Springer-Verlag: New York, 1992.
70. Goodsell, D. S. Inside a living cell *Trends Biochem. Sci.* **1991**, 16, 203-206.
71. Greenfield, N.; Fasman, G. D. Computed circular dichroism spectra for the evaluation of protein conformation. *Biochemistry* 1969, 8, 4108-4116.
72. Haass, C.; Steiner, H. Protofibrils, the unifying toxic molecule of neurodegenerative disorders? *Nat. Neurosci*. **2001**, 4, 859-860.

73. Hagag, N.; Birnbaum, E. R.; Darnall, D. W. Resonance energy transfer between cysteine-34, tryptophan-214 and tyrosine-411 of human serum albumin *Biochemistry* **1983**, 22, 2420-2427,
74. Hall, D.; Minton, A. P. Macromolecular crowding: qualitative and semiquantitative successes, quantitative challenges *Biochem. Biophys. Acta* **2003**, 1649, 127-139.
75. Hammarström, P.; Jiang, X.; Hurshman, A. R.; Powers, E. T.; Kelly, J. W. Sequence-dependent denaturation energetics: a major determinant in amyloid disease diversity *Proc. Natl. Acad. Sci. U. S. A.* **2002**, 99, 16427-16432.
76. Han, J.; Herzfeld, J. Macromolecular diffusion in crowded solutions *Biophys. J.* **1993**, 65, 1155-1161.
77. Hanabusa, T.; Kubo, K.; Oki, C.; Nakano, Y.; Okai, K.; Sanke, T.; Nanjo, K. Islet amyloid polypeptide (IAPP) secretion from islet cells and its plasma concentration in patients with non-insulin-dependent diabetes mellitus *Diabetes Res. Clin. Pract.* **1992**, 15, 89-96.
78. Hardy, J.; Selkoe, D. J. The amyloid hypothesis of Alzheimer's disease: progress and problems on the road to therapeutics. *Science* **2002**, 297: 353-356.
79. Harper, J. D.; Lansbury, P. T. Jr. Models of amyloid seeding in Alzheimer's disease and Scrapie: Mechanistic truths and physiological consequences of the time-dependent solubility of amyloid proteins *Annu. Rev. Biochem.*, **1997,** 66, 385-407.
80. Hatters, D. M.; Minton, A. P.; Howlett, G. J. Macromolecular crowding accelerates amyloid formation by human apolipoprotein C-II *J. Biol. Chem*. **2002**, 277, 7824-7830.
81. Haugland, R. P. Handbook of Fluorescence Probes and Research Products, ninth edition, 2002, pp 91.
82. Homchaudhuri, L.; Swaminathan, R. Novel absorption and fluorescence of L-lysine *Chem. Lett*. **2001**, 844-845.
83. Howard, M.; Welch, W. J. Manipulating the folding pathway of ΔF508 CFTR using chemical chaperones *Methods Mol. Met.* **2002**, 70: 267-275.

84. Huang, T. H.; Yang, D. S.; Plaskos, N. P.; Go. S.; Yip, C. M.; Fraser, P. E.; Chakrabartty, A. Structural studies of soluble oligomers of the Alzheimer beta-amyloid peptide. *J. Mol. Biol*. **2000**, 297, 73-87.
85. Hull, R. L.; Westermark, G. T.; Westermark, P.; Kahn, S. E., Islet Amyloid: A critical entity in the pathogenesis of type 2 diabetes *J. Endocrinol .Metabol.* **2004**, 89, 3629-3643.
86. Ikeguchi, M.; Kato, S.; Shimizu, A.; Sugai, S. Molten state of equine beta-lactoglobulin *Proteins* **1997**, 27, 567-575.
87. Jackson, M.; Mantsch, H. H. The use and misuse of FTIR spectroscopy in the determination of protein structure. *Crit. Rev. Biochem. Mol. Biol*., **1995**, 30, 95-120.
88. Janson, J.; Ashley, R. H.; Harrisson, D.; McIntyre, S.; Butler, P. C. The mechanism of islet amyloid polypeptide toxicity is membrane disruption by intermediate sized toxic particles. *Diabetes* **1999**, 48, 491-498.
89. Jarrett, J. T. et al., The carboxy terminus of the beta amyloid protein is critical for the seeding of amyloid formation: implications for the pathogenesis of Alzheimer's disease *Biochemistry* **1993**, 32, 4693-4697.
90. Jayakumar, R.; Jeevan, R. G.; Mondal, A. B.; Manoharan, P. T. Aggregation, hydrogen bonding and thermodynamic studies on Boc-Val-Val-Ile-OMe tripeptide micelles in chloroform *J. Chem. Soc., Faraday Trans*., **1994**, 90, 2725-2730
91. Juneja, J.; Bhavesh, N. S.; Udgaonkar, J.; Hosur, R. V. NMR identification and characterization of the flexible regions in the 160 kDa molten globule-like aggregate of barstar at low pH. *Biochemistry* **2002**, 41, 9885-9899.
92. Jung, C. Insight into protein structure and protein-ligand recognition by Fourier transform infra red spectroscopy. *J. Mol. Recognit*., **2000**, 13, 325-351.
93. Kahn, S. E.; Andrikopoulos, S.; Verchere, C. B. Islet amyloid: a long recognized but under-appreciated pathological feature of type-2 diabetes *Diabetes* **1999**, 48, 241-253.
94. Kalyanasundaram, K. Photochemistry in Microheterogeneous systems Academic Press, New York, (1987), p 41

95. (i) Kalyanasundaram, K.; Thomas, J. K. Environmental effects on vibronic band intensities in pyrene monomer fluorescence and their application in studies of micellar systems *J. Am. Chem. Soc*. **1977**, 99, 2039-2044 . (ii)Lower excitation slit width was used to minimize fluorescence contribution from lysine.
96. Kao, H. P.; Abney, J. R.,; Verkman, A. S. Determinants of the translational diffusion of a small solute in cytoplasm *J. Cell Biol.* **1993**,120, 175-184.
97. Katakam, M.; Banga, A. K. Aggregation of proteins and its prevention by carbohydrate excipients: albumins and gamma-globulin *J. Pharm. Pharmacol.* **1995**, 47, 103-107.
98. Kawski, A. Fluorescence anisotropy as a source of information about different photophysical processes, in Progress and Trends in Applied Optical Spcetrscopy, D. Fassler, K.-H. Feller and B. Wilhelmi (eds.), Teubner-Texte zur Physik, Vol. 13, Teubner Verlagsgesellschaft, Leipzig, pp 6-34, 1986
99. Kawski, A. Fluorescence anisotropy: Theory and applications of rotational depolarization, *Crit. Rev. Anal. Chem*. **1993**, 23, 459-529.
100. Kendrick, B. S., Carpenter, J. F.; Cleland, J. L.; Randolph, T. W. A transient expansion of the native state precedes aggregation of recombinant human interferon-γ. *Proc. Natl. Acad. Sci. USA* **1998**, 95, 14142-14146.
101. Kepler, T. B.; Elston, T. C. Stochasticity in transcriptional regulation: origins, consequences and mathematical representations *Biophys. J.* **2001**, 81, 3116-3136.
102. Kocisco, D. A.; Come, J. H.; Priola, S. A.; Chesebro, B.; Raymond, G. J.; Lansbury, P. T. Jr.; Caughey, B. Cell free formation of protease-resistant prion protein *Nature* **1994**, 370, 471-474.
103. Koetzle, T. F.; Lehmann, M. S.; Verbist, J. J.; Hamilton, W. C. Precision neutron diffraction structure determination of protein and nucleic acid components. VII. The crystal and molecular structure of the amino acid L-lysine monohydrochloride dehydrate *Acta Cryst.* **1972**, B28, 3207-3214.
104. Kopelman, R. Rate processes on fractals-theory, simulations, and experiments *J. Stat. Phys*. **1986**, 42, 185-200.

105. Krebs, M. R. H.; Wilkins, D. K.; Chung, E. W.; Pitkeathly, M. C.; Chamberlain, A. K.; Zurdo, J.; Robinson, C. V.; Dobson, C. M. Formation and seeding of amyloid fibrils from wild-type hen lysozyme and a peptide fragment from the beta-domain, *J. Mol. Biol*., **2000**, 300, 541-549.

106. Lai, Z.; Colon, W.; Kelly, J. W. The acid mediated denaturation pathway of transthyretin yields a conformational intermediate that can self assemble into amyloid. *Biochemistry*, **1996**, 35, 6470-6482.

107. Laidler, K. J. Chemical Kinetics; 3rd edition, Pearson education company, 1987.

108. Lakowicz, J.R. Principles of fluorescence spectroscopy, second edition, Kluwer Academic/Plenum Publishers, 1999, New York

109. Lambert, M. P. Diffusible, nonfibrillar ligands from Abeta 1-42 are potent central nervous system neurotoxins *Proc. Natl. Acad. Sci. USA* **1998**, 95, 6448-6453.

110. Lansbury, P. T. Jr. Evolution of amyloid: what normal protein folding may tell us about fibrillogenesis and disease *Proc. Natl. Acad. Sci. USA* **1999**, 96, 3342-3344.

111. Lansbury, P. T. Jr. In pursuit of the molecular structure of amyloid plaque: New technology provides unexpected and critical information, *Biochemistry*, **1992**, 31, 6865-6870.

112. Laurent, T. C. Enzyme reactions in polymer media *Eur. J. Biochem*. **1971**, 21, 498-506.

113. Laurent, T. C. The interaction between polysaccharides and other macromolecules. 5. The solubility of proteins in the presence of dextrans. *Biochem. J.* **1963**, 89, 253-257.

114. Laurent, T. C.; Ogston, A. G. The interaction between polysaccharides and other macromolecules. 4. The osmotic pressure of mixture of serum albumin and hyaluronic acid. *Biochem. J.* **1963**, 89, 249-253.

115. Le Vine, H. I. Thioflavine T interaction with synthetic Alzheimer's disease {beta}-amyloid peptides: Detection of amyloid aggregation in solution. *Protein Science*, **1993**, 2, 404-410.

116. Lebowitz, J. L. ; Helfland, E. ; Praestgaard, E. Scaled particle theory of fluid mixtures *J. Chem. Phys.* **1965**, 43, 774-779.

117. Levi, V.; Recha, F. L. G. Labeling of proteins with fluorescent probes.Photophysical characterization of dansylated bovine serum albumin. *Biochem. Mol. Biol. Educ*. **2003,** 31 333-336

118. Li, G.; Zhou, P.; Shao, Z.; Xie, X.; Chen, X.; Wang, H.; Chunyu, L.; Yu, T. The natural silk spinning process– A nucleation-dependent aggregation mechanism? *Eur. J. Biochem*., **2001**, 268, 6600-6606.

119. Lide, D. R., (1995) CRC Handbook of Chemistry and Physics, 76th Ed., CRC Press, New York

120. Lindgren, M.; Sörgjerd, K.; Hammarström, P. Detection and characterization of aggregates, prefibrillar amyloidogenic oligomers and protofibrils using fluorescence spectroscopy *Biophys. J.* **2005**, 88, 4200-4212.

121. Lindner, R. A.; Ralston, G.B. Macromolecular crowding-effects on actin polymerization *Biophys. Chem*. **1997**, 66, 57-66.

122. Lorimer, G. H. A quantitative assessment of the role of the chaperonin proteins in protein folding invivo. *FASEB J.* **1996**, 10, 5-9

123. Luby-Phelps, K. Cytoarchitecture and physical properties of cytoplasm: volume, viscosity, diffusion, intracellular surface area. *Int. Rev. Cytol*. **2000**, 192,189-221.

124. Luby-Phelps, K.; Castle, P. E.; Taylor, D. L.; Lanni, F. Hindered diffusion of inert tracer particles in the cytoplasm of mouse 3T3 fibroblasts *Proc. Natl. Acad. Sci. USA* **1987**, 84, 4910-4913.

125. Lumry, R.; Eyring, H. Conformation changes of proteins *J. Phys. Chem.* **1954**, 58,110-120.

126. Martin J. Requirement for GroEL/GroE- dependent protein folding under nonpermissive conditions of macromolecular crowding *Biochemistry* **2002**, 41, 5050-5055.

127. Martin, R. B., Introduction to biophysical chemistry 1964, McGraw-Hill Book Company, New York

128. McCarthy, D.; Goddard, D. H.; Pell, B. K.; Holborow, E. J.Intrinsically stable IgG aggregates *J. Immunol. Methods*, **1981**, 41, 63-74.

129. McDonald, I. K.; Thornton, J. M. Satisfying hydrogen bonding potential in proteins *J. Mol. Biol.* **1994**, 238, 777-793.

130. Meireles, M.; Pierre, A.; Sanchez, V. Albumin denaturation during ultrafiltration: Effects of operating conditions and consequences on membrane fouling. *Biotechnol. Bioeng*. **1991**, 38, 528-534.

131. Minton, A. P. Excluded volume as a determinant of macromolecular structure and reactivity *Biopolymers* **1981**, 20, 2093-2120.

132. Minton, A. P.; Wilf, J. Effect of macromolecular crowding upon the structure and function of an enzyme:glyceraldehyde-3-phosphate dehydrogenase. *Biochemistry* **1981**, 20, 4821-4826.

133. Minton, A. P. The effect of volume occupancy upon the thermodynamic activity of proteins: some biochemical consequences *Mol. Cell Biochem*.**1983**, 55, 119-140.

134. Minton, A. P. Holobiochemistry: the effect of local environment upon the equilibria and rates of biochemical reactions *Int. J. Biochem*. **1990**, 22, 1063-1067.

135. Minton, A. P. Confinement as a determinant of macromolecular structure and reactivity *Biophys. J*. **1992**, 63, 1090-1100.

136. Minton, A. P. Influence of excluded volume upon macromolecular structure and associations in 'crowded' media. *Curr. Opin. Biotechnol*. **1997**, 8, 65-69.

137. Minton, A. P. Implications of macromolecular crowding for protein assembly *Curr. Opin. Struct. Biol*. **2000**, 10, 34-49.

138. Minton, A. P. The influence of macromolecular crowding and macromolecular confinement on biochemical reactions in physiological media. *J. Biol. Chem*., **2001**, 276, 10577-10580.

139. Minton, K.W. ; Karmin, P. ; Hahn, G. M. ; Minton, A. P. Non specific stabilization of stress-susceptible proteins by stress-resistant proteins: A model for

the biological role of heat shock proteins *Proc. Natl. Acad. Sci. USA* **1982**, 79, 7107-7111.

140. Mulkerrin, M. G.; Wetzel, R. pH dependence of the reversible and irreversible thermal denaturation of gamma interferons *Biochemistry* **1989**, 28, 6556-6561.

141. Muzammil, S.; Kumar, Y.; Tayyab, S. Molten globule-like state of human serum albumin at low pH. *Eur. J. Biochem.* **1999**, 266, 26-32.

142. Naber, D.; Korte, U.; Krack, K. Content of water-soluble and total proteins in the aging human brain *Exp. Geront*. **1979**, 14, 59-63.

143. Nagy, I. Z. ; Nagy, K. ; Lustyik, G. Protein and water contents of aging brain *Exp. Brain Res. Suppl*. **1982**, 5, 118-122.

144. Nagy, I.; Nagy, K.; Nagy, V.; Kalmar, A.; Nagy, E. Alterations in total content and solubility characteristics of proteins in rat brain and liver during ageing and centrophenoxine treatment. *Exp. Geront*. **1981**, 16, 229-240.

145. Naiki, H.; Higuchi, K.; Hosokawa, M; Takeda, T. Fluorometric determination of amyloid fibrils in vitro using the fluorescent dye, thioflavin T1 *Anal. Biochem*., **1989**, 177, 244-249.

146. Nelson, D. L.; Cox, M. M. Lehninger Principles of Biochemistry, 4th edition, W. H. Freeman and Company, New York, 2005.

147. Nussbaum R. L.; Ellis C. E. Alzheimer's disease and Parkinson's disease *N. Engl. J. Med.* **2003**, 348, 1356-1364.

148. O'Connor, D. V.; Philips, D. Time-correlated single photon counting 1984, Academic Press NY.

149. Ogston, A. G. Some thermodynamic relationships in ternary systems with special reference to the properties of systems containing hyaluronic acid and protein *Arch. Biochem. Biophys*. 1 **1962**, (Suppl.), 39-51.

150. Ogston, A. G.; Phelps, C. F. The partition of solutes between buffer solutions and solutions containing hyaluronic acid *Biochem. J*. **1960**, 78, 827-833.

151. Oliva, A.; Santovena, A.; Llabres, M.; Farina, J. B. Stability study of human serum albumin pharmaceutical preparations. *J. Pharm. Pharmacol*., **1999**, 51, 385-392.

152. Opie, E. L. The relation of diabetes mellitus to lesions of the pancreas: hyaline degeneration of the islets of Langerhans *J. Exp. Med.* **1901**, 5, 527-540.

153. Otzen, D. E. ; Kristensen, O. ; Oliveberg, M. et al. Designed protein tetramer zipped together with a hydrophobic Alzheimer homology: a structural clue to amyloid assembly. *Proc. Natl .Acad. Sci. USA* **2000**, 97, 9907-9912.

154. Otzen, D. E.; Oliveberg, M. Salt-induced detour through compact regions of the protein folding landscape. *Proc. Natl. Acad. Sci. USA* **1999**, 96, 11746-11751.

155. Ovchinnikov, A. A.; Zeldovich, Y. B. Role of density fluctuations in bimolecular reaction kinetics *Chem. Phys*. **1978**, 28, 215-218.

156. Pelton, J. T.; McLean, L. R. Spectroscopic methods for the analysis of protein secondary structure *Anal. Biochem*. **2000**, 277, 167-176.

157. Pepys, M. B.; Hawkins, P. N.; Booth, D. R.; Vigushin, D. M.; Tennent, G. A.; Soutar, A. K.; Totty, N.; Nguyen, O.; Blake, C. C. F.; Terry, C. J.; Feest, T. G.; Zalin, A. M.; Hsuan, J. J. Human lysozyme gene mutations cause hereditary systemic amyloidosis *Nature* **1993,** 362, 553-557.

158. Perrin, F. Mouvement brownien d'un ellipsoide (I). Dispersion diélectrique pour des molécules ellipsoidales, *J. Phys. Radium* **1929**, 10, 497-511.

159. Perrin, F. Diminution de la polarization de la fluorescence des solutions résultant du movement brownien de rotation *Acta Phys. Pol*. **1936**, 5, 335-345.

160. Perrin, F. La fluorescence des solutions. Induction moléculaire-polarisation et durée d'émission-phtochemie, *Ann. Phys*. **1929**, 12, 169-275.

161. Perrin, F. Mouvement brownien d'un ellipsoide (II). Rotation libre et depolarization des fluorescences. Translation et diffusion de molécules ellipsoidales *J. Phys. Radium* **1936**, 1, 1-11.

162. Perutz, M. F. Glutamine repeats and neurodegenerative diseases: molecular aspects *Trends Biochem. Sci*. **1999**, 24, 58-63.

163. Perutz, M. F.; Windle, A. H. Cause of neuronal death in neurodegenerative diseases attributable to expansion of glutamine repeats. *Nature*, **2001**, 412, 143-144.

164. Peters, Jr., T., All about albumin, 1996, Academic Press, San Diego

165. Pitschke, M.; Prior, R.; Haupt, M.; Riesner, D. Detection of single amyloid β–protein aggregates in the cerebrospinal fluid of Alzheimer's patients by fluorescence correlation spectroscopy *Nature Med*., **1998**, 4, 832-834.

166. Poon, J.; Bailey, M.; Winzor, D. J.; Davidson, B. E.; Sawyer, W. H. Effects of molecular crowding on the interaction between DNA and the Escherichia coli regulatory protein TyrR *Biophys. J*. **1997**, 73, 3257-3264.

167. Powell, K.; Zeitlin, P. L. Therapeutic approaches to repair defects in ΔF508 CFTR folding and cellular targeting *Adv. Drug Deliv. Rev*. **2002**, 54, 1395-1408.

168. Pratap, J. V.; Ravishankar, R.; Vijayan, M. X-ray studies on crystalline complexes involving amino acids and peptides. XXXV. Invariance and variability in amino acid aggregation in the complexes of maleic acid with L-histidine and L-lysine. *Acta Crystallogr., Sect. B* **2000**, 56, 690-696.

169. Prusiner, S. Prions. *Proc. Natl. Acad. Sci.* USA **1998**, 95, 12580-12585.

170. Ralston, G. B. Effects of "crowding" in protein solutions. *J. Chem. Educ*. **1990**, 67, 857-860.

171. Reddy, R.C. K. ; Lilie, H.; Rudolph, R.; Lange, C. L-Arginine increases the solubility of unfolded species of hen egg white lysozyme, *Protein Sci*. **2005**, 14, 929-935.

172. Richardson, J. S. ; Richardson, D. C. Natural beta-sheet proteins use negative design to avoid edge-to-edge aggregation. *Proc. Natl. Acad. Sci. USA* **2002**, 99, 2754-2759.

173. Ring, J.; Stephan, W.; Brendel, W. Anaphylactoid reactions to infusions of plasma proteins and human serum albumin. Role of aggregated proteins and of stabilizers added during production *Clin. Allergy* **1979**, 9, 89-97.

174. Rivas, G.; Fernandez, J. A.; Minton, A. P. Direct observation of self-association of dilute proteins in the presence of inert macromolecules at high concentration via tracer sedimentation equilibrium: theory, experiment and biological significance *Biochemistry*, **1999**, 38, 9379-9388.

175. Roberts, A. N.; Leighton, B.; Todd, J. A.; Cockburn, D.; Schofield, P. N.; Sutton, R.; Holt, S.; Boyd, Y.; Day, A. J.; Foot, E. A.; Willis, A. C.; Reid, K. B.

M.; Cooper, G. J. S. Molecular and functional characterization of amylin, a peptide associated with type 2 diabetes mellitus *Proc. Natl. Acad. Sci. USA* **1989**, 86, 9662-9666.

176. Roher, A. E.; Chaney, M. O.; Kuo, Y. M.; Webster, S. D.; Stine, W. B.; Haverkamp, L. J.; Woods, A. S.; Cotter, R. J.; Tuohy, J. M.; Krafft, G. A., Bonnell, B. S.; Emmerling, M. R. Morphology and toxicity of A β–(1-42) dimmer derived from neuritic and vascular amyloid deposits of Alzheimer's disease. *J. Biol. Chem*. **1996**, 271, 20631-20635.

177. Rosenheck, K.; Doty, P. The far ultraviolet spectra of polypeptide and protein solutions and their dependence on conformation *Proc. Natl. Acad. Sci.* USA **1961**, 47, 1775-1785.

178. Rosenqvist, E.; Jossang, T.; Feder, J. Thermal properties of human IgG. *Mol. Immunol*., **1987**, 24, 495-501.

179. Ross, C. A. When more is less: Pathogenesis of glutamine repeat neurodegenerative diseases *Neuron*, **1995**, 15, 493-496.

180. Ross, C. A.; Pickart, C. The ubiquitin proteasome pathway in Parkinson's disease and other neurodegenerative diseases *Trends Cell Biol.* **2004,** 14, 703-711.

181. Ross, C. A.; Poirier, M. A. Protein aggregation and neurodegenerative disease. *Nature Med*. **2004**, S10-S17.

182. Saborio, G. P.; Permanne, B.; Soto, C. Sensitive detection of pathological prion protein by cyclic amplification of protein misfolding *Nature* **2001**, 411, 810-813.

183. Safar, J.; Wille, H.; Itri, V.; Groth, D.; Serban, H.; Torchia, M.; Cohen, F. E.; Prusiner, S. B. Eight prion strains have PrP^{Sc} molecules with different conformations, *Nat Med*, **1998**, 4 1157-1165.

184. Sakurai, K.; Oobatake, M.; Goto, Y. Salt-dependent monomer-dimer equilibrium of bovine beta-lactoglobulin at pH 3. *Protein Sci*. **2001**, 10, 2325-2335.

185. Savageau, M. A. Biochemical systems analysis. I. Some mathematical properties of the rate law for the component enzymatic reactions. *J. Theor. Biol.* **1969**, 25, 365-369.

186. Savageau, M. A. Biochemical systems analysis: A study of function and design in molecular biology. Addison-Wesley, Reading, MA.

187. Schnell, S.; Turner, T. E. Reaction kinetics in intracellular environments with macromolecular crowding: simulations and rate laws. *Prog. Biophys. Mol. Biol.* **2004**, 85, 235-260.

188. Schuler, J.; Frank, J.; Saenger, W.; Georgalis, Y. Thermally induced aggregation of human transferrin receptor studied by light scattering techniques. *Biophys. J.* **1999**, 77, 1117-1125.

189. Selkoe, D. J. Alzheimer's disease: genes, proteins and therapy, *Physiol. Rev.* **2001**, 81, 741-746.

190. Selkoe, D. J. Folding proteins in fatal ways *Nature* **2003**, 426, 900-904.

191. Semisotnov, G. V.; Rodionova, N. A.; Razgulyaev, O. I.; Uversky, V. N.; Gripas, A. F.; Gilmanshin, R. I. Study of the "molten globule" intermediate state in protein folding by a hydrophobic fluorescent probe *Biopolymers*, **1991**, 13, 119-128.

192. Shiraki, K.; Kuduo, M.; Imanaka, T.; Takagi, M. Biophysical effects of amino acids on the prevention of protein aggregation. J. Biochem. 2002, 132, 591-595

193. Shire, S. J.; Shahrokh, Z.; Liu, J. Challenges in the development of high protein concentration formulations *J. Pharm. Sci*. **2004**, 93, 1390-1402.

194. Sian, A. K. ; Frears, E. R. ; El-Agnaf, O. M. ; Patel, B. P. ; Manca, M. F. ; Siligardi, G. Oligomerization of beta-amyloid of the Alzheimer's and the dutch-cerebral-haemorrhage types. *Biochem. J.* **2000**, 349, 299-308.

195. Silveira, J. R.; Raymond, G. J.; Hughson, A. G.; Race, R. E.; Sim, V. L.; Hayes, S. F.; Caughey, B. The most infectious prion protein particles *Nature* **2005**, 437, 257-261.

196. Simopoulos, T. T.; Jencks, W. P. Alkaline phosphatase is an almost prefect enzyme *Biochemistry* **1994**, 33, 10375-10380.

197. Sluzky, V.; Tamada, J. A.; Klibanov, A. M.; Langer, R. Kinetics of insulin aggregation in aqueous solutions upon agitation in the presence of hydrophobic surfaces. *Proc. Natl. Acad. Sci., USA* **1991**, 88, 9377-9381.

198. Small, E. W. and Isenberg, I. Hydrodynamic properties of a rigid molecule: Rotational and linear diffusion and fluorescence anisotropy *Biopolymers* **1977**, 16, 1907-1928.

199. Smith, D. P.; Radford, S. E. Role of the single disulfide bond of beta(2)-microglobulin in amyloidosisin vitro. *Protein Sci*. **2001**, 10, 1775-1784.

200. Soleillet, P. Sur les paramètres caractérisant la polarization partielle de la lumière dans les phénomènes de fluorescence, *Ann. Phys. Biol. Med.* **1929,** 12, 23-97

201. Sophianopoulos, A. J.; van Holde, K. E. Evidence for dimerization of L-lysozyme in alkaline solution, *J. Biol. Chem.*, **1961**, 236, PC82-PC83.

202. Sophianopoulos, A. J.; van Holde, K. E. Physical studies of muramidase (Lysozyme): pH dependent dimerization, *J. Biol. Chem*.,**1964**, 239, 2516-2524.

203. Speed, M. A.; Wang, D. I.; King, J. Multimeric intermediates in the pathway to the aggregated inclusion body state for P22 tailspike polypeptide chains. *Protein Sci*. **1995**, 4, 900-908.

204. Speed, M. A.; Wang, D. I.; King, J. Specific aggregation of partially folded polypeptide chains: the molecular basis of inclusion body composition. *Nat. Biotechnol.* **1996**, 14, 1283-1287.

205. Srisailam, S.; Kumar, T. K. S.; Srimathi, T.; Yu, C. Influence of backbone on protein aggregation *J. Am. Chem. Soc*. **2001**, 124, 1884-1888.

206. Stefani, M. Protein misfoldingand aggregation: new examples in medicine and biology of the darkside of the protein world *Biochem Biophys Acta* **2004**, 1739, 5-25.

207. Steiner, R. F., Fluorescence Anisotropy: Theory and Applications, in Topics in Fluorescence Spectroscopy, Volume 2, Principles, J. R. Lakowicz (ed.), Plenum Press, New York, 1991, pp. 1-52

208. Stine, W. B. Jr.; Snyder, S. W.; Ladror, U. S.; Wade, W. S.; Miller, M. F.; Perun, T. J.; Holzman, T. F.; Krafft, G. A. The nanometer-scale structure of amyloid-beta visualized by atomic force microscopy. *J. Prot. Chem*. **1996**, 15, 193-203.

209. Swaminathan, R.; Krishnamoorthy, G.; Periasamy, N. Similarity of fluorescence lifetime distributions for single tryptophan proteins in the random coil state. *Biophys. J.* **1994b**, 67, 2013-2023.

210. Swaminathan, R.; Nath, U.; Udgaonkar, J. B.; Periasamy, N.; Krishnamoorthy, G. Motional dynamics of a buried tryptophan reveals the presence of partially structured forms during denaturation of barstar. *Biochemistry* **1996**, 35, 9150-9157.

211. Swaminathan, R.; Periasamy, N.; Udgaonkar, J. B.; Krishnamoorthy, G. Molten globule like conformation of barstar: a study by fluorescence dynamics *J. Phys. Chem*. **1994a**, 98, 9270-9278.

212. Tatford, O. C.; Gomme, P. T.; Bertolini, J. Analytical techniques for the evaluation of liquid protein therapeutics *Biotechnol. Appl. Biochem*. **2004**, 40, 67-81.

213. Taylor, J. P.; Fischbeck, K. H. Toxic proteins in neurodegenerative disease. *Science* **2002**, 296, 1991-1995.

214. Terefe, N.S.; Arimi, J. M.; Van Loey, A.; Hendrickx, M. Kinetics of alkaline phosphatase catalysed hydrolysis of disodium p-nitro phenyl phosphate: effects of carbohydrate additives, low temperature and freezing *Biotechnol. Prog*. **2004**, 20, 1467-1478.

215. Thirumalai, D.; Klimov, D. K.; Dima, R. I. Emerging ideas on the molecular basis of protein and peptide aggregation *Curr. Opin. Struct. Biol.* **2003**, 13, 146-159.

216. Tjeruberg, L. O.; Näslund, J.; Lindqvist, F.; Johansson, J.; Karlström, A. R.; Thyberg, J.; Terenius, L.; Nordstedt, C. Arrest of beta-amyloid fibril formation by a penta-peptide ligand, *J. Biol. Chem*. **1996**, 271, 8545-8548.

217. Tokuriki, N.; Kinjo, M.; Negi, S.; Hoshino, M.; Goto, Y.; Urabe, I.; Yomo, T. Protein folding by the effects of macromolecular crowding *Protein Science* **2003**, 13, 125-133.

218. Toussaint, D.; Wilczek Particle-anti particle annihilation in diffusive motion *J. Chem. Phys.* **1983**, 78, 2642-2647.

219. Turner, T. E.; Schnell, S.; Burrage, K. Stochastic approaches for modeling in vivo reactions *Comp. Biol. Chem*., **2004**, 28, 165-178.

220. (i)Turro, N. J. Modern Molecular Photochemistry, University Science Books, Mill Valley California 1991 (ii) We experimented with lysine obtained from multiple sources including the Sigma-Aldrich Company to rule out impurities.

221. Uversky, V. N. ; Cooper, E. M. ; Bower, K. S. ; Li, J. ; Fink A. L. Accelerated alpha-synuclein fibrillation in crowded milieu. *FEBS Lett*. **2003**, 515, 99-103.

222. Uversky, V. N.; Winter, S.; Lober, G. Use of fluorescence decay times of 8-ANS-protein complexes to study the conformational transitions in proteins which unfold through the molten globule state. *Biophys. Chem.* **1996**, 60, 79-88.

223. van den Berg, B.; Ellis, R. J.; Dobson, C. M. Effects of macromolecular crowding on protein folding and aggregation *EMBO J*. **1999**, 18, 6927-6933.

224. van den Berg, B.; Wain, R.; Dobson C. M.; Ellis, R. J. Macromolecular crowding perturbs protein refolding kinetics: Implications for folding inside the cell. *EMBO J*. **2000**, 19, 3870-3875.

225. Venkatraman, J.; Prabu, M. M.; Vijayan, M. X-ray studies on crystalline complexes involving amino acids and peptides. XXXII. Effect of chirality on ionization state, stoichiometry and aggregation in the complexes of oxalic acid with DL and L-lysine. *J. Peptide Res.* **1997**, 50, 77-87.

226. Virchow, R. The Cellulose-Fruge, *Virchows Arch*.**1855**, 8, 140-144.

227. Vos, K.; van Hoek, A.; Visser, A. J. Application of a reference convolution method to tryptophan fluorescence in proteins. A refined description of rotational dynamics, *Eur. J. Biochem*., **1987**, 165, 55-63.

228. Wahl, P. Measurement of the decays of the polarized fluorescence of 5-dimethylaminonaphthalene-1-sulfonyl-gamma globulin. *Biochim. Biophys. Acta* **1969**, 175, 55-64.

229. Walsh, D. M.; Hartley, D. M.; Kusumoto, Y.; Fezoui, Y.; Condron, M. M.; Lomakin, A.; Benedek, G. B.; Selkoe, D. J.; Teplow, D. B. Amyloid

β−protein fibrillogenesis. Structure and Biological activity of protofibrillar intermediates. *J. Biol. Chem*. **1999**, 274, 25945-25952.

230. Walsh, D. M.; Klyubin, I.; Fadeeva, J. V.; Cullen, W. K.; Anwyl, R.; Wolfe, M. S.; Rowan, M. J.; Selkoe, D. J. Naturally secreted oligomers of amyloid beta protein potently inhibit hippocampal long term potentiation *in vivo*, *Nature* **2002**, 416, 535-539.

231. Wang, X.; de Vocht, M. L.; de Jonge, J.; Poolman, B.; Robillard, G. T. Structural changes and molecular interactions of hydrophobin SC3 in solution and on a hydrophobic surface. *Protein Sci.,* **2002**, 11, 1172-1181.

232. Wang, X.; Graveland-Bikker, J. F.; de Kruif, C. G.; Robillard, G. T. Oligomerization of hydrophobin SC3 in solution: from soluble state to self assembly *Protein Sci.* **2004**, 13, 810-821.

233. Ware, W. R. Transient luminescence measurements, in creation and destruction of the excited state, Vol.1A, A. A. Lamola (ed.), Marcel Dekker, New York, **1971**, pp213-302.

234. Wenner, J. R.; Bloomfield, V. A. Crowding effects on EcoRV kinetics and binding. *Biophys. J*. **1999**, 77, 3234-3241.

235. Westermark, P.; Wilander, E. The influence of amyloid deposits on the islet volume in maturity onset diabetes mellitus *Diabetologia* **1978**, 15, 417-421.

236. Wetzel, R.; Becker, M.; Behlke, J.; Billwitz, H.; Bohm, S.; Ebert, B.; Hamann, H.; Krumbiegel, J.; Lassmann, G. Temperature behaviour of human serum albumin *Eur. J. Biochem*. **1980**, 104, 469-478.

237. Wong, P. C.; Cai, H.; Borchelt, D. R.; Price, D. L. Genetically engineered mouse models of neurodegenerative diseases. *Nat. Neurosci*. **2002**, 5, 633-639.

238. Wood, S. J.; MacKenzie, L.; Maleeff, B.; Hurle, M. R.; Wetzel, R. Selective inhibition of Abeta fibril formation *J. Biol. Chem*.**1996**, 271, 4086-4092.

239. Wood, S. J.; Maleeff, B.; Hart, T.; Wetzel, R. Physical, morphological and functional differences between pH 5.8 and 7.4 aggregates of the Alzheimer's amyloid peptide Abeta *J. Mol. Biol.* **1996**, 256, 870-877.

240. Young, L. R. D.; Fink, A. L.; Dill, K. A. Aggregation of globular proteins *Acc. Chem. Res.* **1993**, 26, 614-620.

241. Zimmerman, S. B. Macromolecular crowding effects on macromolecular interactions: some implications for genome structure and function. *Biochim. Biophys. Acta. Gene Struct. Expression*. **1993**, 1216, 175-185.

242. Zimmerman, S. B.; Minton, A.P. Macromolecular crowding: biochemical, biophysical and physiological consequences. *Annu. Rev. Biophys. Biomol. Struct*. **1993**, 22, 27-65.

243. Zimmerman, S. B.; Pheiffer, B. H. Macromolecular crowding allows blunt-end ligation by DNA ligases from rat liver or Escherichia coli *Proc. Natl. Acad. Sci. USA* **1983**, 80, 5852-5856.

244. Zimmerman, S. B.; Trach, S.O. Estimation of macromolecular concentrations and excluded volume effects for the cytoplasm of Escherichia coli. *J. Mol. Biol*. **1991**, 222, 599-620.

245. Zolkiewski, M. ClpB cooperates witj DnaK, DnaJ and GrpE in suppressing protein aggregation *J. Biol. Chem.* **1999**, 274, 28083-28086.

List of Publications:

1. L. Homchaudhuri and R. Swaminathan, Novel Absorption and Fluorescence Characteristics of L-Lysine, *Chem. Lett.*(2001), 844-845
2. L. Homchaudhuri and R. Swaminathan, Near Ultraviolet Absorption Arising from Lysine residues in Close proximity: A probe to Monitor Protein Unfolding and Aggregation in Lysine-Rich Proteins, *Bull. Chem. Soc. Jpn*. (2004) 77: 765-769
3. L. Homchaudhuri, N. Sarma and R. Swaminathan, Effect of Macromolecular Crowding on the Rate of Alkaline Phosphatase Catalyzed Hydrolysis (to be communicated)
4. L. Homchaudhuri, S. Kumar and R. Swaminathan, Slow aggregation of lysozyme in alkaline pH monitored in real time employing the fluorescence anisotropy of covalently labeled dansyl probe. (communicated)

TH-265_004703